Using Novel Stimuli and Alternative Signal Processing Techniques to Enhance BCI Paradigms

by

Simon R. H. Davies

A thesis submitted in fulfilment of the requirements for the degree of Doctor of Philosophy in Engineering

University of Warwick, Warwick Manufacturing Group

August, 2015

Contents

Declaration

I, Simon R. H. Davies

declare that this thesis and the work presented in it are my own and has been generated by me as the result of my own original research.

I confirm that:

1. This work was done wholly or mainly while in candidature for a research degree at this University;

2. Where any part of this thesis has previously been submitted for a degree or any other qualification at this University or any other institution, this has been clearly stated;

3. Where I have consulted the published work of others, this is always clearly attributed;

4. Where I have quoted from the work of others, the source is always given. With the exception of such quotations, this thesis is entirely my own work;

5. I have acknowledged all main sources of help;

6. Where the thesis is based on work done by myself jointly with others, I have made clear exactly what was done by others and what I have contributed myself;

7. Parts of this thesis have been published by the author: Davies and James 2013a [98], Davies and James 2013b [101], Davies and James 2014a [106], Davies and James 2014b [110], and Davies and James 2014c [137].

Signed: 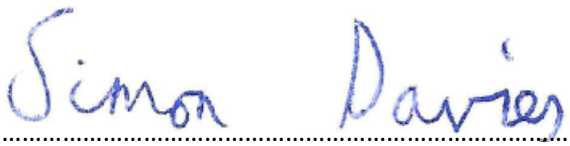 ……

Date:……10/08/2015……

Abstract

A Brain-Computer Interface (BCI) is a device that uses the brain activity of a person as an input to select desired outputs on a computer. BCIs that use surface electroencephalogram (EEG) recordings as their input are the least invasive but also suffer from a very low signal-to-noise ratio (SNR) due to the very low amplitude of the person's brain activity and the presence of many signal artefacts and background noise. This can be compensated for by subjecting the signals to extensive signal processing, and by using stimuli to trigger a large but consistent change in the signal – these changes are called evoked potentials. The method used to stimulate the evoked potential, and introduce an element of conscious selection in order to allow the user's intent to modify the evoked potential produced, is called the BCI paradigm. However, even with these additions the performance of BCIs used for assistive communication and control is still significantly below that of other assistive solutions, such as keypads or eye-tracking devices.

This thesis examines the paradigm and signal processing components of BCIs and puts forward several methods meant to enhance BCIs' performance and efficiency. Firstly, two novel signal processing methods based on Empirical Mode Decomposition (EMD) were developed and evaluated. EMD is a technique that divides any oscillating signal into groups of frequency harmonics, called Intrinsic Mode Functions (IMFs). Furthermore, by using Takens' theorem, a single channel of EEG can be converted into a multi-temporal channel signal by transforming the channel into multiple snapshots of its signal content in time using a series of delay vectors. This signal can then be decomposed into IMFs using a multi-channel variation of EMD, called Multi-variate EMD (MEMD), which uses the spatial information from the signal's neighbouring channels to inform its decomposition. In the case of a multi-temporal channel signal, this allows the temporal dynamics of the signal to

be incorporated into the IMFs. This is called Temporal MEMD (T-MEMD). The second signal processing method based on EMD decomposed both the spatial and temporal channels simultaneously, allowing both spatial and temporal dynamics to be incorporated into the resulting IMFs. This is called Spatio-temporal MEMD (ST-MEMD). Both methods were applied to a large pre-recorded Motor Imagery BCI dataset along with EMD and MEMD for comparison. These results were also compared to those from other studies in the literature that had used the same dataset.

T-MEMD performed with an average classification accuracy of 70.2%, performing on a par with EMD that had an average classification accuracy of 68.9%. Both ST-MEMD and MEMD outperformed them with ST-MEMD having an average classification accuracy of 73.6%, and MEMD having an average classification accuracy of 75.3%. The methods containing spatial dynamics, i.e. MEMD and ST-MEMD, outperformed those with only temporal dynamics, i.e. EMD and T-MEMD. The two methods with temporal dynamics each performed on a par with the non-temporal method that had the same level of spatial dynamics. This shows that only the presence of spatial dynamics resulted in a performance increase. This was concluded to be because the differences between the classes of motor-imagery are inherently spatial in nature, not temporal.

Next a novel BCI paradigm was developed based on the standard Steady-state Somatosensory Evoked Potential (SSSEP) BCI paradigm. This paradigm uses a tactile stimulus applied to the skin at a certain frequency, generating a resonance signal in the brain's activity. If two stimuli of different frequency are applied, two resonance signals will be present. However, if the user attends one stimulus over the other, its corresponding SSSEP will increase in amplitude. Unfortunately these changes in amplitude can be very minute. To counter this, a stimulus generator was constructed that could alter the amplitude and frequency of the vibrotactile stimuli. It was hypothesised that if the stimuli

were of the same frequency, but one's amplitude was just below the user's conscious level of perception and the other was above it, the changes in the SSSEP between classes would be the same as those between an SSSEP being generated and neutral EEG, with differences in α activity between the low-amplitude SSSEP and neutral activity due to the differences in the user's level of concentration from attending the low-amplitude stimulus.

The novel SSSEP BCI paradigm performed on a par with the standard paradigm with an average 61.8% classification accuracy over 16 participants, compared to an average 63.3% classification accuracy respectively, indicating that the hypothesis was false. However, the large presence of electro-magnetic interference (EMI) in the EEG recordings may have compromised the data. Many different noise suppression methods were applied to the stimulus device and the data, and whilst the EMI artefacts were reduced in magnitude they were not eliminated completely. Even with the noise the standard SSSEP stimulus paradigm performed on a par with studies that used the same paradigm, indicating that the results may not have been invalidated by the EMI.

Overall the thesis shows that motor-imagery signals are inherently spatial in difference, and that the novel methods of T-MEMD and ST-MEMD may yet out-perform the existing methods of EMD and MEMD if applied to signals that are temporal in nature, such as functional Magnetic Resonance Imaging (fMRI). Whilst the novel SSSEP paradigm did not result in an increase in performance, it highlighted the impact of EMI from stimulus equipment on EEG recordings and potentially confirmed that the amplitude of SSEP stimuli is a minor factor in a BCI paradigm.

Abbreviations

AAR	Adaptive Auto-regressive
AR	Auto-regressive
ALS	Amyotrophic Lateral Sclerosis
ANN	Artificial Neural Network
ATT	Absolute Tactile Threshold
BAER	Brainstem Auditory Evoked Response
BCI	Brain-Computer Interface
BMI	Brain-Machine Interface
BOLD	Blood-oxygen-level Dependent
BSREC	Biomedical and Scientific Research Ethics Sub-Committee
BSS	Blind Source Separation
C	Central
CSP	Common Spatial Pattern
CWT	Continuous Wavelet Transform
DHWT	Discrete Harmonic Wavelet Transform
ECG	Electrocardiogram
ECoG	Electrocortiogram
EEG	Electroencephalogram
EMD	Empirical Mode Decomposition
EMG	Electromyogram
EMI	Electromagnetic Interference
ERD	Event-related Desynchronisation
ERS	Event-related Synchronisation
F	Frontal
FFT	Fast Fourier Transforms

Fp	Frontal Pole
FT	Fourier Transform
fMRI	functional Magnetic Resonance Imaging
HCA	Hierarchical Clustering Analysis
ICA	Independent Component Analysis
IMF	Intrinsic Mode Function
IMT	Intrinsic Mode Type
ITR	Information Transfer Rate
LAS	Lock-in Analyser System
LDA	Linear Discriminant Analysis
LOO	Leave One Out
MEMD	Multi-variate Empirical Mode Decomposition
MI	Motor Imagery
NLMS	Normalised Least Mean Squares
O	Occipital
P	Parietal
PCA	Principal Component Analysis
PLS	Primary Lateral Sclerosis
PPDA	Pre-processing Discriminant Analysis
PSD	Power Spectral Density
SCP	Slow Cortical Potential
SNR	Signal-to-Noise Ratio
SSEP	Steady-State Evoked Potential
SSSEP	Steady-State Somatosensory Evoked Potential
SSVEP	Steady-State Visual Evoked Potential
STFT	Short-time Fourier Transform
ST-MEMD	Spatio-temporal Multi-variate Empirical Mode Decomposition

SVM	Support Vector Machine
SWT	Synchrosqueezed Wavelet Transform
T-MEMD	Temporal Multi-variate Empirical Mode Decomposition
USAF	United States Air Force
WT	Wavelet Transform

List of Figures

List of Tables

CHAPTER 1

Introduction

1.1 Motivation

The human body is controlled by the brain, a large interconnected structure primarily made up of cells called neurons. These neurons can communicate with each other and send commands to other parts of the body using electrical excitation, either in response to an external stimulus or consciously generated actions [1]. Brain activity is the combined result of these electrical excitations and it can be measured using several different devices, such as an electroencephalogram (EEG) [2]. However damage to the brain, either through physical trauma or disease, can result in a person being unable to control parts or all of their body [3]. In the most serious cases they suffer total paralysis and are left with no means of communication. Using EEG recordings to identify a person's intent from their brain activity can offer a limited but vital form of communication in the form of a Brain-Computer Interface (BCI) that results in an increased quality of life.

A BCI is a device that uses the brain activity of a person as an input to select desired outputs on a computer [4]. Due to their current low information-throughput and requirement of specialist technology, BCIs are predominantly only used by patients with severe paralysis who are unable to operate muscle-based communication devices. This PhD examines the current state of the field of non-invasive BCIs and puts forward several novel methods applied to key components of BCIs in order to try and enhance them. Different components of BCI systems, such as the stimuli applied to participants and the processing

of their brain activity, are examined individually and changes to them are proposed and evaluated.

1.2 Background

Damage to the brain may never be fully healed, depending on the nature and location of the damage, and a person can find certain bodily functions permanently stripped away from them. Damage to the spinal cord can also result in a fully functioning brain with the inability to transmit its commands to the rest of the body. In order to observe a person's brain activity the EEG was developed [2]. Using electrodes to detect the brain's electrical emissions resulting from mental actions, it could represent them in the form of a signal recording. Conscious changes in a person's brain activity that result in a consistent, identifiable change in their EEG recording can also be used to bridge the gap between mental command and physical action. This is called a BCI, also known as a Brain-Machine Interface (BMI).

There are three types of BCI: invasive, partially invasive, and non-invasive. Invasive BCIs involve implanting electrodes inside the blood-brain barrier [5]. Partially invasive BCIs require electrodes to be placed inside the skull, but outside the blood-brain barrier [5]. Non-invasive BCIs rely on electrodes placed on the surface of the scalp [5]. Whilst invasive and partially invasive BCIs receive a much clearer signal due to being closer the signal source and are less prone to signal contamination, their use requires undergoing surgery. With non-invasive BCIs, brain activity is obtained as an input using an EEG amplifier connected to surface electrodes. EEG signals have a very low signal-to-noise ratio as brain activity is measured in microvolts and is distorted by dense bone, cerebrospinal fluid and the skull [6] before being measured by the electrodes. As a result many BCIs rely on the generation of so-called evoked potentials [7].

Evoked potentials are significant changes in amplitude or frequency induced as a result of a stimulus. Stimuli can be visual, auditory, or tactile, or any combination thereof so long as it results in providing a stimulus to the brain. That nature of the stimuli dictates what area or combination of areas of the brain will be stimulated, e.g. the source of an evoked potential in response to receiving visual stimuli would be located in the brain's vision centre, known to be in the occipital cortex, under the rear of the scalp. The "paradigm" behind a BCI is the method it uses to map information onto an evoked potential. Some evoked potentials can be self-generated, i.e. the brain activity is consciously modulated by the user. These have the advantage of the BCI needing a very simple paradigm to ascribe intent, e.g. the user consciously generates an evoked potential every time they want to select an option highlighted on a computer screen. In contrast reflexive evoked potentials often need complex paradigms to convey the intent of the evoked potential, e.g. a P300 word grid using sequences of flashing letters to generate an evoked potential when the desired letter appears [8].

1.3 Aims and Objectives

The goal of this PhD was to improve the performance of BCI systems, primarily through the increase of classification accuracy, by examining the components of BCIs and developing novel variations of them in order to make them more practical as assistive communications devices, and thereby raise their users' quality of life. The components in question were the signal processing component and the BCI paradigm component that is responsible for generating evoked potentials, and are detailed in the next subsections. Due to the highly limited access to patients with sub-dermal implants in the UK and at the University of Warwick specifically, this work focuses exclusively on non-invasive BCIs when it comes to applied research.

1.3.1 Development and Application of Novel Signal Processing Techniques

Even after an evoked potential is generated it still requires processing before it can be accurately classified. There are many signal and pattern processing techniques that are applicable to EEG, such as filtering, the Wavelet Transform (WT), Independent Component Analysis (ICA), *etc.*, each with their own advantages and disadvantages. Once processed, the signals can be submitted to a classifier, an algorithm that will separate the signals into a pre-selected number of groups based on their properties. Insufficient processing can lead to a classifier being unable to correctly sort the inputted signals into their respective groups, causing false positives and negatives. If a BCI is being used for real-time communication then being able to complete the signal processing and classifying techniques within a short amount of time becomes an important factor.

The work presented here, covered in Chapter 4, focuses on a method called Empirical Mode Decomposition (EMD) as it is a purely data-driven method and adapts itself to the data rather than the user tailoring the process to the signal. Like many signal processing methods, such as the WT, it divides a signal into time-frequency components but it also preserves the morphology of the underlying signals masked by other sources and external noise. EMD is an iterative sifting process that splits a signal into statistically important frequency bands and residual noise called Intrinsic Mode Functions (IMFs). Novel variations of EMD were researched and evaluated in this work. As it can be applied to any non-linear and non-stationary signal, and as frequency is a key component of many evoked potentials, it is readily applicable to EEG which can be viewed as non-stationary due to its frequency content changing over time periods usually longer than 0.25 seconds [9]. In this case it was applied to Motor Imagery (MI). MI is a very common BCI paradigm. In terms of brain activity, imagining moving a limb and physically moving a limb are identical [10]. The brain

has a strict left-right divide for limbs depending on their lateral location, i.e. the right hemisphere of the brain controls the limbs on the left side of the body and vice versa, giving a clear spatial distribution for evoked potentials. The most significant component of MI evoked potentials is the suppression of a rhythmic wave, called the μ-rhythm, localised in the 8-13 Hz band in the hemisphere controlling the limb. This frequency-centric evoked potential made MI ideal for the application of techniques such as EMD.

After evaluating the performance of EMD, novel versions were developed with the goal of improving its performance. An enhanced version of EMD called Multi-variate EMD (MEMD) was obtained from the literature that can decompose all channels simultaneously [11]. This allows each channel to produce the same number of IMFs and for each order of IMF to occupy the same frequency bands, allowing direct comparisons of each channel's IMFs for signal processing. This method was then used to modify single-channel EMD to incorporate temporal dynamics into the decomposition process - information on how aspects of the signal such as variance and frequency content change over time. This method was called Temporal Multi-variate EMD (T-MEMD).

A further enhanced version of T-MEMD, called Spatio-temporal Multi-variate EMD (ST-MEMD), was also devised. This method was very similar to T-MEMD except that MEMD was applied to all dynamically embedded channels simultaneously, allowing the process to incorporate both spatial and temporal information.

The contribution to knowledge from this work was the development of the novel signal processing method T-MEMD, the development of the novel ST-MEMD signal processing method, and the discovery of further evidence that the key differences between different classes of MI are inherently spatial during the evaluation of the aforementioned signal processing methods.

1.3.2 Development and Evaluation of Novel Stimulus of Evoked Potentials

In Chapter 5, after the extensive novel work on signal processing through the use of EMD, focus moved to development of the paradigm side of the BCI field. BCIs using tactile stimuli were investigated due to them being more practical as they leave the visual and auditory channels clear, and because it is a promising area of research compared to the other types of stimuli. Conventional tactile BCIs use a vibrotactile transducer on each hand, operating at different frequencies. Both stimuli produce resonance frequencies visible in the user's brain activity. When the user attends to one transducer over the other, its resonant frequency comes to dominate over the other one in terms of amplitude.

The novel tactile BCI devised here worked similarly, except that the transducers operated at the same frequency but significantly different vibrational amplitudes in an attempt to have one transducer vibrate at such low amplitude that it was similar to no stimulus being applied at all, but still distinctive compared to neutral EEG recordings. This was so as to try and produce evoked potentials from each hand that had same ease of differentiation as a single evoked potential from one hand and no evoked potential from the other, rather than differentiating between two similar evoked potentials.

The contribution to knowledge from this work was the strong indication that the hypothesised changes to the BCI paradigm did not result in an increase in performance. The study is not conclusive due to the potential compromising of the data by an electromagnetic artefact. Several counters to this artefact were implemented with varying degrees of success, indicating that other tactile BCI studies in the literature could potentially have been affected by the same artefact unknowingly as it occupies the same frequency and temporal domains as the evoked potential resulting from the BCI paradigm.

1.4 Thesis Structure

Following this introductory chapter a review of the literature is carried out, beginning in Chapter 2 with a background on brain activity, the recording of these biosignals, and the development of BCIs and their associative paradigms. In Chapter 3 an overview of the most prominent signal processing techniques used in BCI and their respective performances is provided. Next the development of the novel signal processing methods T-MEMD and ST-MEMD is detailed and the methods are evaluated alongside existing forms of EMD in Chapter 4. Chapter 5 covers the design and implementation of a novel tactile BCI paradigm and its resulting performance in comparison with the standard tactile BCI paradigm. Chapter 6 deals with the conclusions drawn from the work in this thesis and how well its objectives were met. Following that are the references and relevant appendices.

1.5 Publications

S.R.H. Davies, and C.J. James, "*Multi-Channel Empirical Mode Decomposition in Brain-Computer Interfaces*," 7th IEEE EMBS UK and RI Postgraduate Conference in Biomedical Engineering and Medical Physics, pp. 21, July 2013.

S.R.H. Davies, and C.J. James, "*Novel use of empirical mode decomposition in single-trial classification of motor imagery for use in Brain-Computer Interfaces*," 35th Annual International Conference of the IEEE EMBS, pp. 5610-5613, July 2013.

S.R.H. Davies, and C.J. James, "*Including Temporal Dynamics in Single Trial Motor Imagery Classification using Empirical Mode Decomposition*," 6th International Brain-Computer Interface Conference, pp. 52-55, September 2014.

S.R.H. Davies, and C.J. James, "*Using Empirical Mode Decomposition with Spatio-Temporal Dynamics to Classify Single-Trial Motor Imagery in BCI*," 36th Annual International Conference of the IEEE EMBS, pp. 4631-4634, September 2014.

S.R.H. Davies, and C.J. James, "*Exploiting the Absolute Threshold of Vibrotactile Stimulation to Generate Evoked Potentials in EEG*," 8th IEEE EMBS UK and RI Postgraduate Conference in Biomedical Engineering and Medical Physics, pp. 15-16, July 2014.

CHAPTER 2

Origins and Physiology behind EEG and BCI

This chapter will cover the origins and physiology behind EEG signals, such as the basic components and functions of the brain and the more common signals it generates. EEG is an accessible technology that allows the recording of these brain signals. The accurate interpretation of consistently occurring changes in brain activity allows us to successfully classify mental states and tasks. These could then be mapped to assistive control systems, be used to help diagnose the conscious state of a person suffering trauma to the brain, or used to provide feedback to a patient going through physical rehabilitation.

2.1 The Brain

The brain is the most complex organ in the human body. The primary component of the brain is the neuron, depicted in Figure 2.1, with 100 billion of them present and each connected up to 1000 of its neighbours. They are made up of three parts:

- Soma – the main cell body responsible for keeping the neuron alive.
- Axon – a long thread capable of transmitting an electrical excitation.
- Dendrites – small branches of nerve endings that allow the neuron to communicate with other cells and receive inputs themselves.

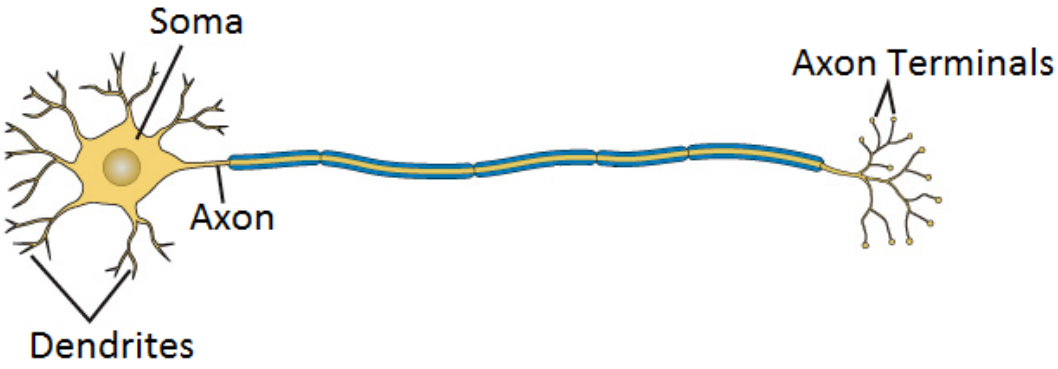

Fig. 2.1: A neuron consists of a cell body or "soma", dendrites and an axon that ends at a terminal [1].

Neurons can transmit information through electrical excitation. It is this transmission of information that allows the brain to carry out functions such as storing memories or controlling limbs. There are specialised types of neurons such as sensory neurons for receiving stimuli and motor neurons that activate muscles in response to a command from the brain. Neurotransmission occurs when the neuron's electrical membrane potential rapidly changes [1]. Membrane potential is the difference between the electric potentials outside the cell and inside it. A sudden inflow of Sodium ions causes this change, resulting in the emission of Potassium ions afterwards to equalise the membrane potential. This neuronal firing results in the sending of neurotransmitters to other neurons.

Like all vertebrate brains, it is divided into a forebrain, midbrain and hindbrain. The forebrain makes up the majority of the brain and consists of the cerebrum, which itself can be divided into several lobes. Figure 2.2 shows how the cerebrum is split into two hemispheres and is comprised of four lobes that bisect both hemispheres:

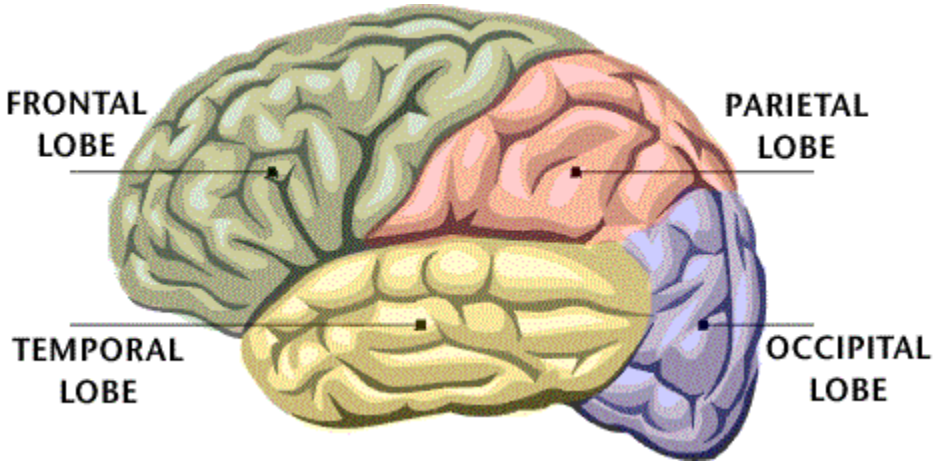

Fig. 2.2: The human brain divided into four lobes, each with unique functions [12].

- the Frontal lobe, which is associated with activities such as planning and reasoning. At the rear of the Frontal lobe lies the sensorimotor area that controls conscious limb movement.
- the Parietal lobe, which is used to process many sensory inputs such as touch, taste and heat.
- the Occipital lobe, which is responsible for processing visual input.
- the Temporal lobe, which is associated with memory and emotion. At the top of the Temporal lobe lies an area responsible for processing auditory input.

2.1.1 Brain Disorders

Damage to the brain can result in various neurological disorders; these can arise due to disease or trauma. There are many types of neurological disorders, with epilepsy being the most common, including Alzheimer's, Cerebral Palsy, Huntington's, Multiple Sclerosis, Narcolepsy, and Tourette's, all with a wide array of symptoms and causes. Some disorders result in semantic and motor impairments, despite the appropriate biological apparatus being intact [3]. These types of dysfunction include:

- Apraxia – the inability to execute conscious movements despite the appropriate muscles being intact.
- Dysarthria – the inability to properly execute movements specifically involving the muscles used in speech despite them being intact.
- Dysgraphia – the inability to express language in its written form.

There are also disorders that specifically affect motor neurons, which can lead to several forms of paralysis:

- Amyotrophic lateral sclerosis (ALS) – the degeneration of upper and lower motor neurons leading to the loss of all control over voluntary movements.
- Primary lateral sclerosis (PLS) – the degeneration of lower motor neurons leading to the loss of all control over voluntary movements.

In the case of initiating movement, upper motor neurons in the cerebrum transmit information to lower motor neurons in the brain stem and spinal cord. All of the above disorders would result in impairment in the patient's ability to communicate, and for the more extreme cases even specialist communication equipment such as eye-gaze detection [13], a device that tracks where a person's pupils are pointing in relation to a screen for the purposes of selecting control inputs, would be unusable. Brain disorders are an issue that can seriously impact the quality of life of those who suffer from them. For the detection and diagnosis of brain functions, tools are needed that are able to detect brain activity.

2.2 Electroencephalography

The EEG is the recording of the brain's electrical activity at the scalp and was first achieved by Hans Berger in 1924 [2]. The energy of the ions resulting from groups of pyramidal neurons firing [7] can be detected when they impact on electrodes. There are several methods of recording EEG activity, with EEG measured from the surface of the scalp being

the most common. EEG measured from the cortical surface but outside the blood-brain barrier is called an electrocortiogram (ECoG) [14]; whilst EEG measured from within the brain using depth electrodes is called an electrogram [15]. Both of the latter forms of EEG require removal of a section of the skull and invasive surgery, and are therefore tightly regulated to protect the patients' health, despite the improved signal quality that comes from being closer to the source and having fewer obstructions. Modern EEGs tend to use chlorided silver electrodes placed on the scalp to record the changes. Surface EEGs can use passive or active electrodes, with active electrodes having an amplifier placed within the electrode to eliminate noise from skin impedance, and cable and connector movements [16].

EEGs measure the changes in voltage potential in respect to a reference channel. The reference channel should ideally be affected by voltage changes that impact all other channels, but not impacted by any localised changes. It should also not be affected by external noise from non-neurological sources. This allows it to act as a baseline that highlights localised changes in the other channels. Early EEGs produced an analogue output by tracing the signal on paper. Modern EEGs tend to produce a digital output that needs a set sampling frequency, *Fs*, which refers to how many samples per second the EEG is recording. Typically the sampling frequency should be at least twice the highest frequency of interest to prevent aliasing [17]. An example of an EEG cap and an EEG amplifier can be seen in Figures 2.3 and 2.4.

Fig. 2.3: gtec g.GAMMAcap for fitting electrodes on a person's scalp with g.LADYbird electrodes applied [18].

Fig. 2.4: gtec g.HIamp EEG amplifier [19].

Berger [2] discovered a rhythmic wave in the 8 – 13 Hz frequency band that he named the α wave. This is regarded as the brain's "idle" signal, present when no significant action is taking place, and is strongest around the occipital lobe. There is also a variant centred on the motor cortex called the μ-rhythm. This rhythm is also strongest when no motor actions are being performed.

A large proportion of the brain's activity is made up of several rhythmic waves centred on specific frequency bands. Overall these are:

- α/Alpha waves lie within the 8 – 13 Hz range and occur during relaxation when no significant activity is occurring.
- β/Beta waves occur between 13 – 40 Hz, are produced during concentration and heightened alertness.
- ϑ/Theta waves are produced during light sleep and dreaming, they occur between 4 – 7 Hz.
- δ/Delta waves are the slowest of the brain waves occurring between 0.5 – 4 Hz during deep sleep or unconsciousness.

Due to the sensitivity of EEG, many non-neuronal signals can be detected. These are called artefacts and can range from electrocardiographic (ECG) activity from the user's heart to large electrical devices operating nearby. Artefacts make up a large proportion of EEG readings. Muscle movements can easily generate ten times the amplitude of any neural activity. Small actions such as blinking, frowning or clenching one's jaw can cause large spikes of electromyographic (EMG) activity to occur in EEG readings, obscuring the brain activity it is meant to detect. Small movements from unsecured electrodes will also cause large artefacts in EEG readings. The combination of being placed outside the skull, neural activity's low amplitude and the amount of artefact contamination means that EEG recordings have a very low signal-to-noise ratio (SNR).

2.2.1 Electrode Locations for EEG Recording

Herbert Jasper was appointed by the First International EEG Congress in 1947 to develop a standardised way of placing electrodes [20]. The criteria for such a method were as follows:

1. Electrode locations must be proportional to the size of the person's head.
2. The possible electrode locations should adequately cover all areas of the head.
3. Location names must use biological references instead of purely arbitrary labels.
4. Electrode locations should try to be over a single cortical area of the brain.

In 1949 Jasper proposed the 10-20 system to the Second International EEG Congress. This system used the distance between the subject's nasion and inion as a reference for longitudinal measurements, and the distance between the subject's Central coronal plane for lateral measurements, as shown in Figure 2.5. Along the nasion-inion line, five points were identified that marked out the position of imaginary lines that divided the brain into lateral segments. These were called the Frontal Pole (Fp), the Frontal (F), the Central (C), the Parietal (P), and the Occipital (O). Crucially, these positions were spaced out 20% of the nasion-inion distance from their neighbour. The lateral co-ordinates increased numerically every 20% of the Central coronal line, with the letter *'z'* representing zero, even numbers representing the right-hand side and odd numbers the left-hand side.

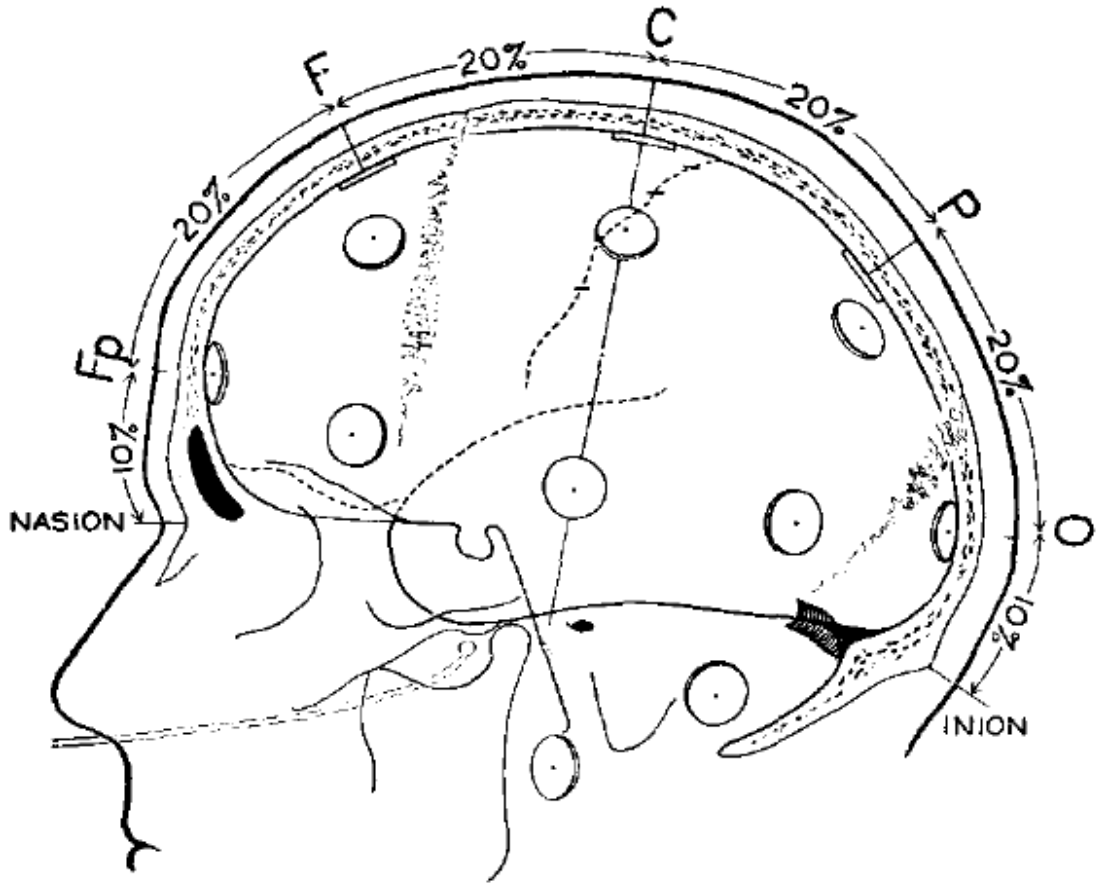

Fig. 2.5: A side-view of a person's head with the 10-20 coordinates overlaid, demonstrating how electrode sites are spaced using percentage values of the length of the person's scalp [20].

For example, the position Cz is exactly 50% of the nasion-inion distance, making it equidistant from the nasion and inion. The *'z'* indicates that it is offset laterally 0% of the Central coronal line, making Cz the exact centre-point of the scalp.

In 1985, as EEG amplifiers advanced and studies were using more electrodes for greater spatial resolution, a 10-10 system was proposed [21], shown in Figure 2.6. It functioned much in the same way as the 10-20 system except it used 10% increases in distance, creating four new points along both the nasion-inion and Central coronal lines, allowing for denser electrode coverage.

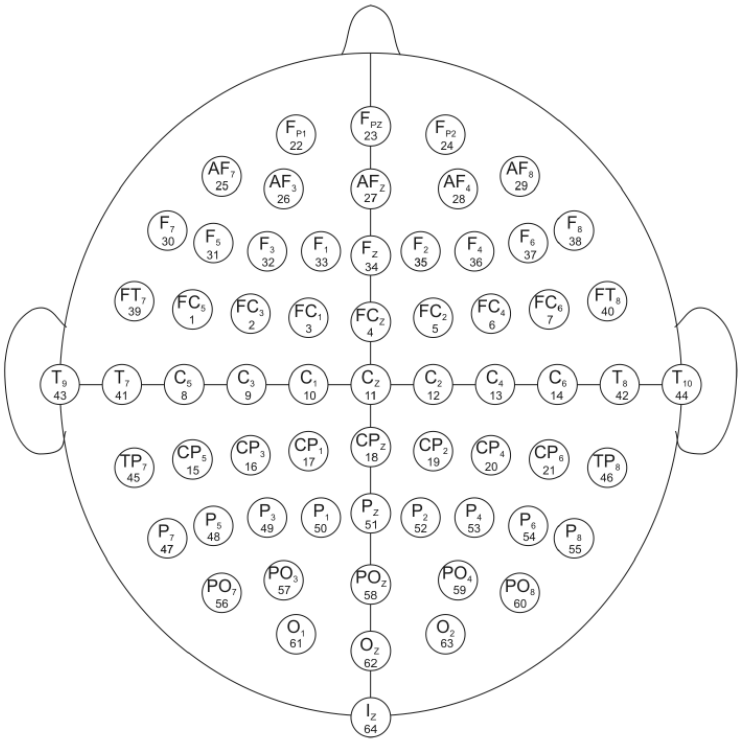

Fig. 2.6: A top-down view of a person's head with the 10-10 coordinates overlaid. This allows for up to 64 electrodes to be placed on a person's scalp [22].

With surface EEGs becoming more practical and being shown to be able to robustly detect identifiable brain activity it was considered if they might be able to bridge the gap between thought and action for those suffering motor neuron damage [23].

2.3 Brain-Computer Interfaces

A BCI, also called a Brain-Machine Interface, is a device that uses the brain-activity of a person as an input to select desired outputs on a computer [4]. The concept of a BCI was first proposed in 1973 by Vidal [23] who suggested that consistent responses to stimuli in brain activity, called evoked potentials, could be used to convey information or intent that could then be used to control other devices.

An evoked potential, also called an evoked response or event-related response, can be triggered by any sensory input. Aside from BCI, they are typically used in the diagnosis of

neurological conditions that result in the demyelination of neural pathways, such as Multiple Sclerosis [24]. Evoked potentials still have very small potentials, but their consistent morphology and time of appearance allow them to be isolated. Vidal's pilot study used a stimulus that could provoke a consistent evoked potential that was distinctive in EEG readings regardless of the brain's current state, and had a voluntary attention component so that the user could select which evoked potential to generate at will.

Vidal suggested complementary images for a stimulus. These images consist of two distinct features that could be combined to form a new image and viewed individually. In this case he suggested using a grid comprised of vertical and horizontal lines. The user would focus on either the vertical or horizontal lines, perceptually bringing the lines into their foreground and pushing the other into the background. He also noted that the local origin of the evoked potential in the brain would need to be identified for the purposes of electrode placement. Fortunately neurophysiology has helped map the areas of the brain primarily responsible for processing the different forms of external stimuli. If a stimulus is visual, it will generate an evoked potential over the Occipital lobe, where the O band on the 10-20 system is located. If it is auditory the evoked potential will be centred on the auditory cortex on the sides of the head, located at T7 and T8. A tactile stimulus will generate an evoked potential that can be best detected over the sensorimotor cortex, located at the central C and CP band on the 10-20 system. Vidal also noted the low SNR of EEG due to artefacts and background noise and the need for intensive signal processing before attempting to classify the signal.

Since then all BCIs have had the same basic structure of triggering an evoked potential in the user, either with an external stimulus or self-modulation, recording these evoked potentials using an EEG, signal processing to extract a set of features representing the uniqueness of the evoked potentials, and finally classification of these features. Once that

is done the possible classification groups can be mapped to any arbitrary set of controls that have the same class of choice.

2.3.1 BCI Paradigms

There are several paradigms used in BCIs to ascribe intent to an evoked potential. These can be divided into a) Self-modulated evoked potentials, and b) Reflexive evoked potentials [25]. Self-modulated evoked potentials are those that are generated by the conscious mental actions of the user. It is much easier to ascribe intent as they are only meant to appear when the user wants them to, e.g. when their desired selection option is highlighted on a computer screen. They are much less prone to causing false positives as they will not be accidentally triggered by external stimuli. However they require a much longer training period so that users can consistently cause the change on demand. They are also slower as a user may need up to several seconds lead time before the change in brain activity is fully realised. A BCI that uses self-modulated evoked potentials is also known as an asynchronous BCI, as the inputs are not spaced regularly by the arbitrary display time of a stimulus [25].

By contrast a BCI that uses reflexive evoked potentials needs little to no training as the changes are automatic. There has to be some method that allows the changes to be associated with an intent, such as having an option presented with an accompanying visual stimulus that triggers an evoked potential when the user looks directly at it. They typically have a much lower specificity rating as they can be unintentionally triggered by external stimuli. A BCI that uses reflexive evoked potentials is also known as a synchronous BCI, as the inputs and outputs are synched to the pacing of the application of the stimulus [25].

A. Self-modulated

- Motor Imagery (MI): this paradigm exploits the left-right divide of the brain and limb control. Imagining moving a limb and physically moving a limb produces the same brain activity. When a person imagines moving a limb on the left side of their body there is heavily localised activity on the right side of their sensorimotor cortex and vice-versa [26]. This activity also occurs within specific frequency bands. A rhythmic signal in the 8-13 Hz band called the μ-rhythm will be suppressed on the contralateral side of the motor cortex. This may also result in resonance activity in the 20 Hz band. At the onset of MI there will be a large event-related desynchronisation (ERD) and event-related synchronisation (ERS) of brain activity that takes approximately one second as depicted in Figure 2.7 [27].

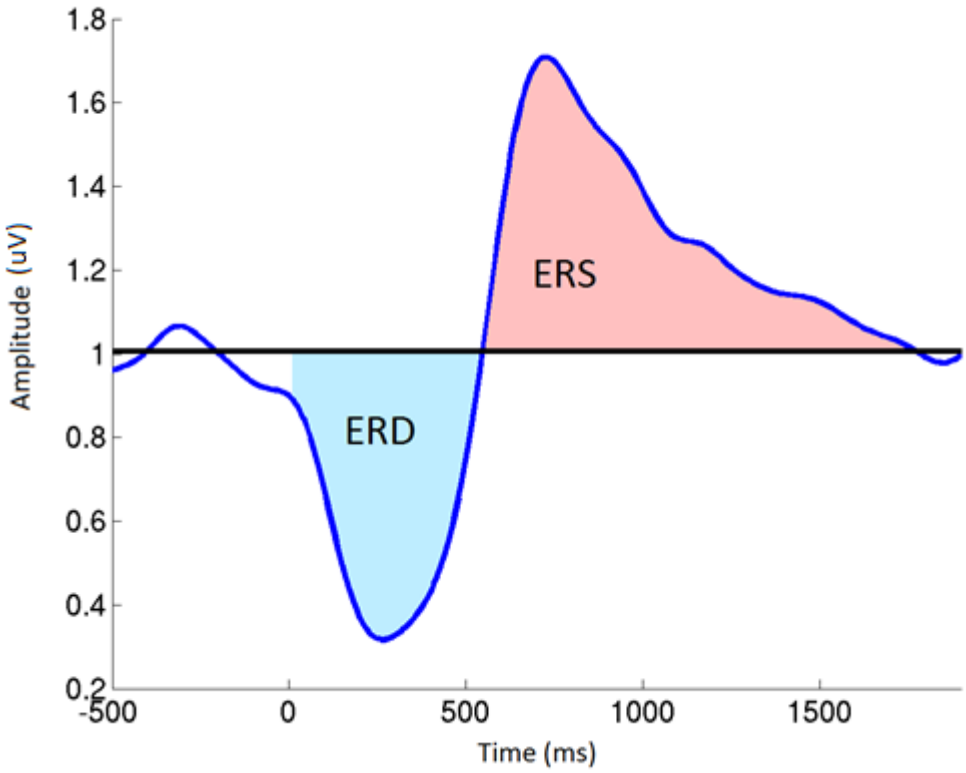

Fig. 2.7: A plot showing the distinctive waveform caused by ERD/ERS just after the user consciously initiates MI at time 0 milliseconds [28].

MI was first used as the basis of a BCI paradigm by Wolpaw *et al.* [29] in 1990. To show that people could modulate their own μ-rhythms reliably and rapidly enough to be used to give commands to a computer, they constructed an experiment where a mouse cursor on a screen moved up in response to an increase in amplitude in the μ-rhythm and down in response to a decrease. Five participants were recruited and told to guide the cursor to a target on a screen. They used the strategies of relaxation to make the cursor move upwards, and imagined physical activities to make the cursor move downwards, corresponding to the knowledge that the μ-rhythm is suppressed during imagined movements. One participant was unable to master the concept and dropped out, but the remaining four achieved an average of 89.5% accuracy.

In 1996 the Graz BCI group expanded the idea to make use of multiple parts of the body [30]. Instead of choosing between imagined movement and no imagined movements, they created a three-class paradigm that differentiated between the imagined movement of the left index finger, the imagined movement of the right index finger, and the imagined movement of the right foot. Their four participants only achieved an average accuracy of 60%, highlighting the difficulty of distinguishing between the different μ-rhythm responses to imagined movements, as well as the decrease in accuracy that comes from the classifier having more states to choose from.

Pfurtscheller and Neuper 2001 [25] improved on their work at Graz with a new MI BCI that used algorithms to objectively select the statistically most relevant frequencies and electrode channels, as well as reducing the imagined movement selection to the two opposing actions of left hand movements vs right hand

movements. This BCI was used by a tetraplegic patient for four months, who achieved 60% accuracy at the outset before progressing to an average of 90%.

- Slow Cortical Potentials (SCPs): this paradigm is based on detecting an overall decrease or increase in the voltage of the EEG due to a decrease or increase respectively in the excitability thresholds of large groups of neurons [31], shown in Figure 2.8. Users can train themselves to focus their attention to trigger a negative SCP or train themselves to relax in order to trigger a positive SCP. This can take several months of training and SCPs can take up to 3 seconds to present in EEG readings, making them slow in comparison to other evoked potentials. As SCPs are an overall change in the brain's state it can be detected universally throughout the scalp.

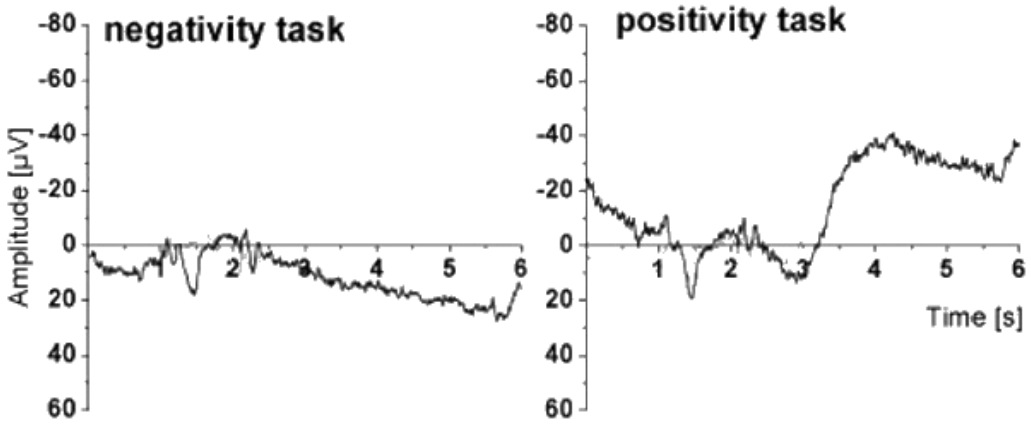

Fig. 2.8: Plots showing negative and positive SCPs, distinguished by the overall negative or positive change in amplitude of the EEG activity [32].

SCPs were pioneered by Birbaumer's group in 2000 [33] as an assistive communications device for ALS patients with the detection of an SCP being used to select letters from within groups. Of the five patients, three achieved reliable self-control of the SCP BCI. Each achieved an average accuracy of at least 75%, but on

average it took 28 trials to select a single letter, with one letter being selected every two minutes. The inefficiency of the paradigm has led to very little follow-up research.

B. Reflexive

- P300: The P300 is a positive change in amplitude that peaks on average around 300ms after the stimulus that triggered it was received, as shown in Figure 2.9, and is associated with recognition and categorisation [8]. It is triggered upon the reception of a rare but expected stimulus, e.g. a low pitched tone played during a group of high-pitched tones, and can be detected along the central-parietal area of the brain. Intent can be ascribed to its occurrence using a P300 Speller. A word grid is displayed on a computer screen with each row and column flashing individually in a random order. The user focuses on the letter they would like to select. When the row or column containing that letter flashes it triggers a P300 response. Knowing what row and column was flashing at the time of the P300 waves allows one to identify the letter the user was focusing on.

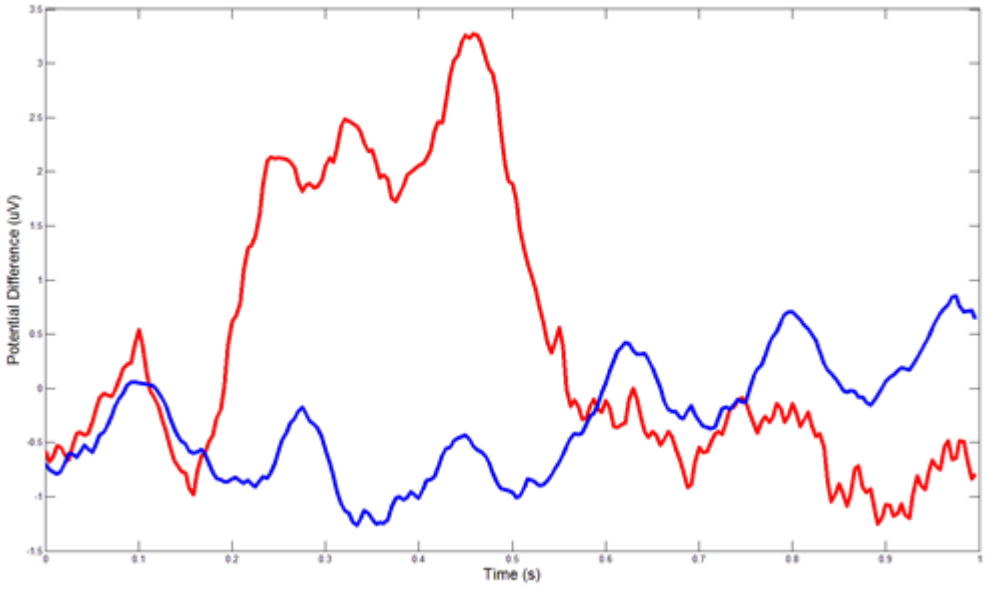

Fig. 2.9: A plot in red of the P300 evoked potential triggered in response to recognising a rarely occurring but

expected stimulus. It is characterised by a large positive change in amplitude that peaks approximately 300 ms after the stimulus occurred at time point 0 seconds. The blue represents neutral EEG.

The P300 Speller was first proposed by Donchin's research group [34] in 1988. Four volunteers were tested to see how long on average the Speller had to cycle through its 6 x 6 word grid for the participants to achieve 85% accuracy. These times varied between 15 and 36 seconds. This work was continued by Donchin's group with a larger-scale test involving ALS patients [35]. Beforehand it was concluded that the word grid needed to be reduced in size, to 4 x 4, to improve accuracy by reducing the number of classes that the classifier had to distinguish between. Nine of the fifteen patients were able to achieve accuracy rates of 75% or greater.

There is a large amount of research on P300 Spellers due to the BCIs' immediate practical applications in assistive communication. Its performance is also highly dependent on the structure of the paradigm. Decreases in the inter-stimulus time means the Speller can cycle through all the possible options faster, but may result in a weaker P300 being elicited. A smaller word grid means a decrease in the amount of options to choose from but also a smaller number of groups to be correctly classified. Letters adjacent to the letter being attended to can generate weak P300s when they are highlighted, leading to false positives. Townsend *et al.* 2010 [36] tested a paradigm where instead of flashing rows and columns, an algorithm selected six squares on an 8 x 9 word grid in such a way that it ensured no two adjacent sqaures would flash at the same time. After testing both a standard and their novel P300 Spellers, they found their novel method resulted in a marked increase in classification accuracy, from 77% up to 92%, and the amount of letters selected per minute, from 17 to 23.

- Steady-State Evoked Potential (SSEP): An SSEP is a resonance-based signal generated in response to a frequency-based stimulus [37], e.g. staring at a light flashing at 10 Hz will induce a resonance signal at 10 Hz and 20 Hz, as shown in Figure 2.10. Its location in the brain is predicated on what type of stimulus is being used. A visual based stimulus means the SSEP will be detected over the occipital lobe, whilst a tactile based stimulus means it will occur over the sensorimotor cortex. Intent can be ascribed by mapping specific frequencies to specific actions, such as making a button flash at 15 Hz and executing the function mapped to it when a 15 Hz SSEP is detected, as that means the user must be looking at the button.

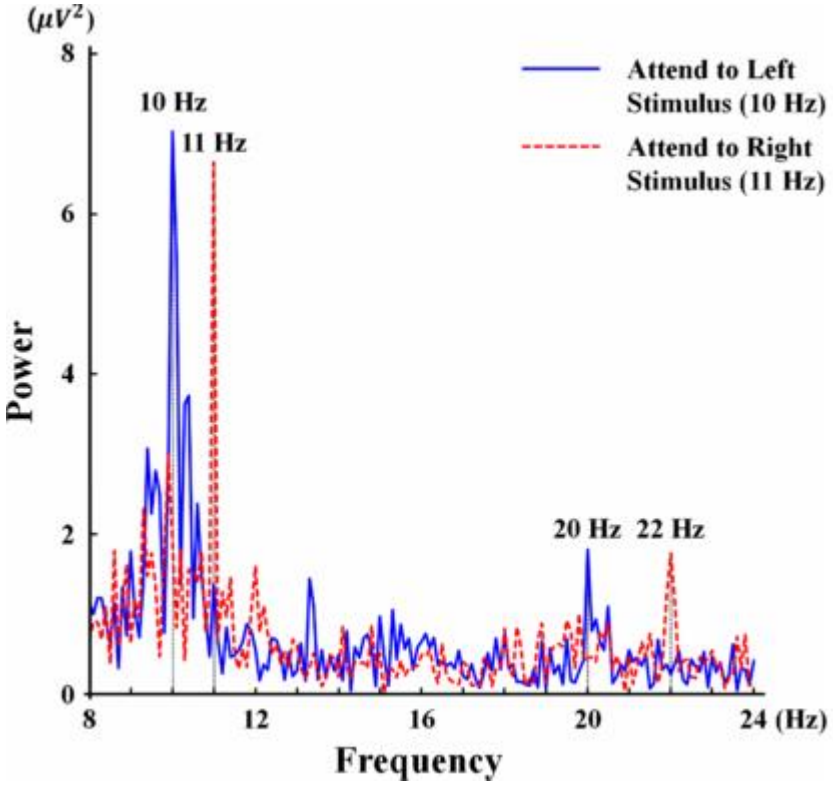

Fig.2.10: A plot showing SSEPs of two different frequencies and their accompanying resonance frequencies. Attending to different stimuli will result in SSEPs of different frequencies allowing the user's current area of focus to be identified [38].

SSEPs were first used as a diagnostic tool. For example, new-born infants are unable to give vocal feedback on auditory tests, so a Brainstem Auditory Evoked Response (BAER) test can be performed to test the function of their nervous system [39]. If a tone is played and its corresponding SSEP is present in the infant's EEG recordings, then it can be concluded that the pathways from the ear to the auditory cortex are functioning.

Using them as a method of control in the form of a BCI was first proposed as part of the United States Air Force's (USAF) Alternative Control Technology research programme in 1995 [40]. Lights behind the screen of a flight simulator flashed at a rate of 13.25 Hz. If the resulting Steady-State Visual Evoked Potential (SSVEP) increased in magnitude the simulator would bank to the right, if it decreased it banked to the left. Participants were able to achieve over 80% accuracy.

The USAF's research continued with an SSVEP BCI being developed in 2000 [41]. This BCI paradigm made use of two virtual buttons on the left and right sides of a computer screen flashing at different frequencies with participants required to fixate on the button indicated. Out of 200 trials participants achieved an average of 92% accuracy.

As mentioned beforehand, SSEPs can be generated by any form of constant stimuli. Pfurtscheller's group evaluated an SSEP BCI that relied on a tactile stimulus to generate Steady-State Somatosensory Evoked Potentials (SSSEPs) [42]. Vibrotactile stimulators applying vibrations of different frequencies to each hand produced two SSSEPs of different frequency in the EEG recordings. By focusing on one hand over the other, the user could increase the amplitude of the SSSEP produced by the

vibrations being applied to the hand they were focusing on, with eight participants achieving an average of 70% accuracy.

- N200: The N200 is related to cognitive processing and is a negative change in amplitude that on average peaks 200ms post-stimulus, as shown in Figure 2.11. The most common stimulus that triggers it is incongruent groupings as shown in the Eriksen flanker task [43]. The Eriksen flanker task is when a target stimulus is flanked by either matching or mismatching stimuli. For example, with "<<<<<", the centre target stimuli of "<" is flanked by matching stimuli, but in ">><>>" it is flanked by mismatching stimuli. This incongruent grouping triggers an N200 response around the central anterior area of the scalp. Intent can be ascribed by mapping congruent and incongruent stimuli to different selections similar to SSEPs.

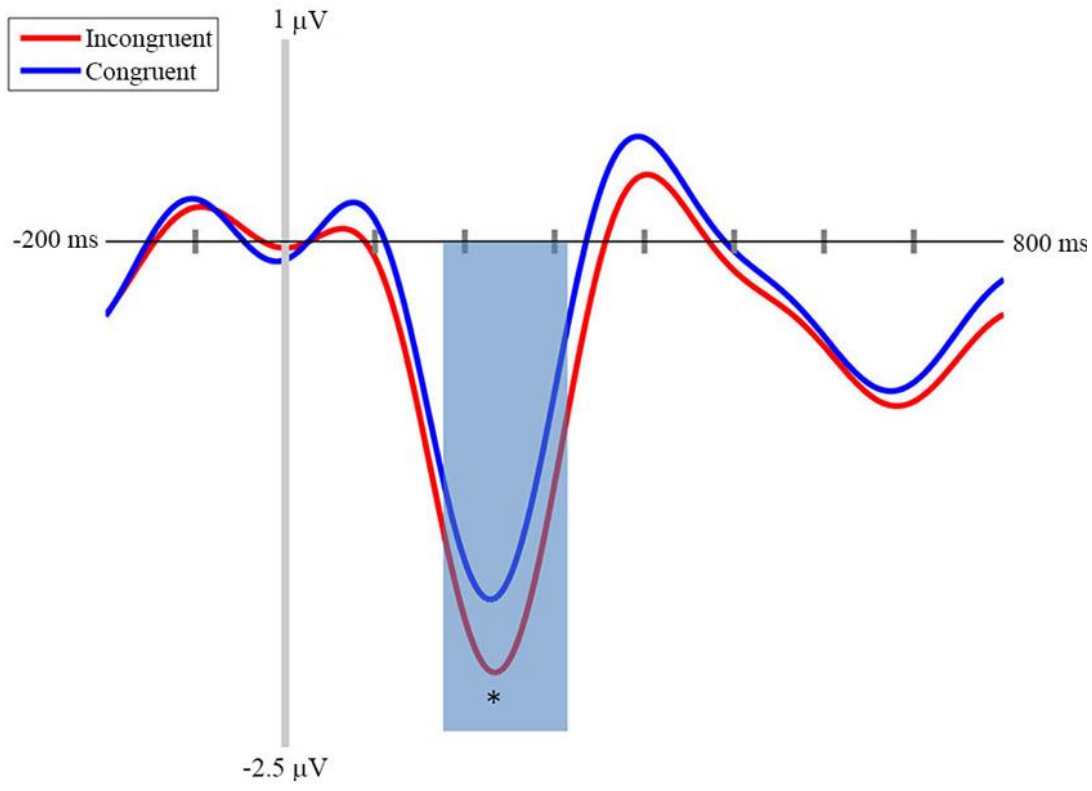

Fig.2.11: A plot showing an N200 wave occurring approximately 200ms after stimulus at time point 0 ms [44].

- N400: The N400 is similar to the N200 in that it is triggered by incongruent stimuli, however the key difference is that the stimuli must be semantically incongruent, e.g. “I take coffee with cream and dog” instead of “I take coffee with cream and sugar” [45]. The dissimilarity of the word from the rest of the sentence, both in phonics and in context, will increase the change in amplitude of the N400 response. The N400 peaks around 400ms post-stimulus. The N400 evoked potentials’ and the above N200 evoked potentials’ lack of distinctness compared to other “oddball paradigm” responses such as the P300 means that few BCIs used them as the basis of their paradigm.

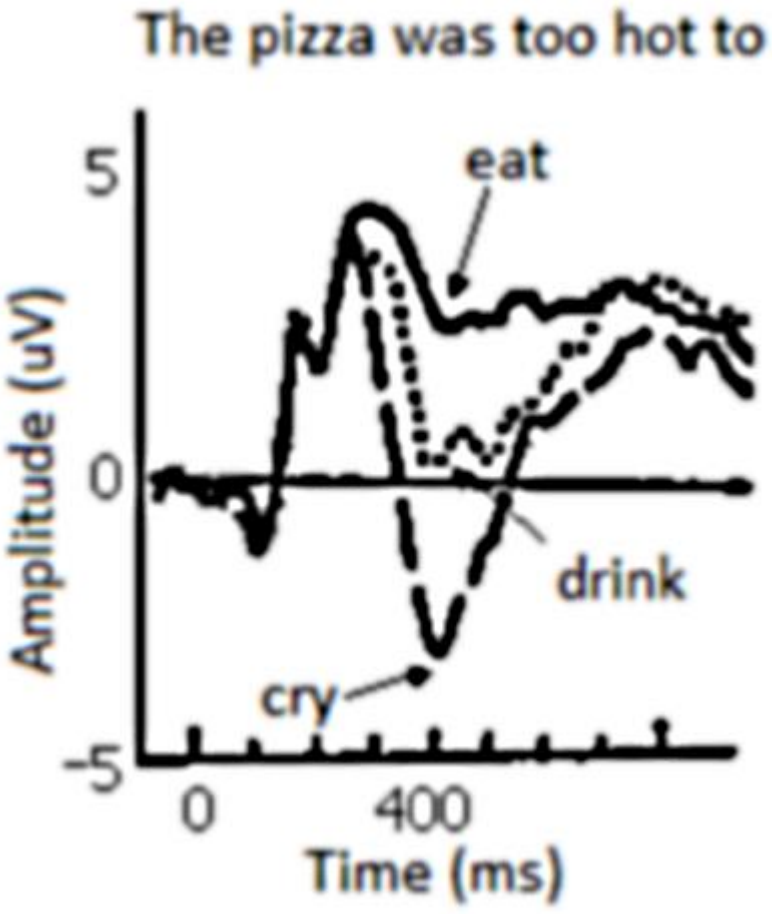

Fig.2.12: A plot showing several different N400 waves occurring approximately 400 ms after different semantic congruity stimuli were presented at time point 0 [46].

These paradigms show how evoked potentials can be triggered at will via conscious effort by the user. However, EEG's low SNR mean that they are still difficult to detect in raw EEG readings.

2.4 Summary

The brain is a complex organ that is still not entirely understood. Repairing damage can be beyond the abilities of the body and medicine. This can lead to deficiencies in the brain's processes, resulting in the loss of certain bodily functions such as speech or muscle control. EEG can be a tool to diagnose a person's brain functions and act as a bridge between mental commands and their corresponding actions if the recorded brain activity can be correctly interpreted with a BCI.

BCI research is still in its infancy, hampered by the technology and the resulting noisy signals. Ingenuity has to be employed in order to exploit changes in brain activity to convey information from mental actions to the outside world. Reflexive evoked potentials have the advantage in that there is no uncertainty over whether the user is performing the task correctly, as the mechanism of generating the evoked potential is not within their control, only the choice of when to experience the stimulus that triggers the evoked potential is. However, even the most distinct evoked potential is still relatively weak and masked by a multitude of a noise and other signal sources. Intensive processing of the EEG recordings is needed before they can be correctly classified, which is discussed in the next chapter.

CHAPTER 3

Signal Processing in EEG for BCI

Signal processing, in the context of digital signals, is the application of mathematical functions and operations on vectors of data points recorded electronically from a source. This can include transforming the signal from its amplitude-time domain to a new domain to better represent its properties, or the identification of thresholds which can be used to separate desirable data from undesirable data. This chapter covers a multitude of prominent signal processing techniques in the literature that are usually applied to EEG in this context.

EEG recordings are the combined result of multiple underlying sources and artefacts. As mentioned in Chapter 2, artefacts are signals produced by non-neurological sources. There are physiological artefacts that are generated within the body, such as energy from muscle movements, and there are extra-physiological artefacts that come from external sources, such as the electrical mains powering the EEG amplifier. The beating of the heart, the person's pulse, eye blinks, poor electrode contact, electrode lead movement, and electrical devices in the vicinity of the electrodes can all be sources of artefacts [47]. These artefacts' comparatively high amplitude relative to EEG is the reason why EEG has a very low SNR.

This mix of signals is referred to as the "cocktail party problem" [48], the analogy being that identifying one neurological signal out of the mixed signals found in EEG is similar to identifying one speaker over the background conversation of a party. Applications of signal processing techniques in EEG encompass a range of methods that can be used to suppress artefacts, simplify the data, or extract signals buried in the mix. The focus of BCIs on

generating evoked potentials is in part because it results in the EEG containing a consistent, distinct signal. Once a set of features representing these evoked potentials has been extracted using signal processing, they can then be classified to form the final output in a BCI control system, shown in Figure 3.1. These classifiers sort the trials from BCI systems into pre-designated groups. A BCI system with adequate signal processing should perform with a high degree of classification accuracy.

Fig 3.1: The fundamental components of a BCI. The recorded EEG data must be processed in order to highlight the unique features of the evoked potential and then classified.

There are two approaches to signal processing: removing or extracting signal data based on known quantities, and removing or extracting signal data based on unknown quantities. The former relies on knowing the properties unique to the signal you wish to extract, such as frequency or morphology. The latter is based on maximising statistical differences between each class of signal. This is called Blind Source Separation (BSS) and has the advantage of forgoing any *a priori* knowledge of the signals recorded. Due to EEG's non-stationary manner and it being the result of multiple unknown underlying sources, BSS is a field of signal processing that is highly applicable in processing EEG.

Depending on the EEG's sampling frequency, signals of frequencies in the hundreds of Hz can be recorded. However the vast majority of neurological signals are below 50 Hz in terms of frequency. Filters make a good starting point for removing large quantities of unwanted data identified in the frequency domain from the signal.

3.1 Filters

With the multitude of signals that make up a person's brain activity, such as the ever-present α rhythms, muscle artefacts, *etc.,* it makes sense to initially apply a filter to excise data not immediately at the frequency domain the desired evoked potential is located in, though there is the danger of accidentally discarding subtle signals relevant to the evoked potential [49]. Filters can be applied to signals in several ways:

- High Pass filter – Frequencies below a specified level are attenuated and frequencies above a certain level are passed over.
- Low Pass filter – Frequencies above a specified level are attenuated and frequencies below a certain level are passed over.
- Band Pass filter – Frequencies within a specified, contiguous range are passed and frequencies above or below that range are attenuated.
- Band Stop filter – Frequencies within a specified, contiguous range are attenuated and frequencies above or below that range are passed over. A Notch filter is a Band Stop filter with a very narrow specified frequency band.

The cut-off point of the frequencies is not instantaneous. The slope of the frequency plot determines how fast the transition is and is influenced by the order of the filter [49]. The order of the filter refers to the order of polynomial the filter can be written as. Having too high an order filter will warp the phase of the original signal. However, filtering by itself is usually insufficient to prepare a signal for classification as even a narrow frequency range will contain a multitude of signals. Frequency content needs a more detailed representation for the signal to be properly analysed along this variable, which leads to the application of Fourier Transforms (FTs).

3.2 Fourier Transforms

An FT converts a signal from the time domain to its frequency domain, so instead of a standard signal plot of time versus amplitude it produces a frequency versus power plot. Squaring the magnitude of the FT obtains the signal's Power Spectral Density (PSD), providing an estimation of the power per Hz for each frequency component of the signal [50]. This is extremely useful for seeing which frequencies are most prominent in the signal epoch the FT was calculated from. For example, to confirm the presence of an SSVEP you would expect to see a peak in the FT at the same frequency as the stimulus.

There are different types of FT, with the FFT finding much use in signal processing due to how much faster it is to calculate than the original FT. The FFT's assumption that the signal is periodic allows the calculation of the FT to be factorised, resulting in a decrease in the number of operations by several orders of magnitude [51]. Short-time Fourier Transforms (STFTs) can be used when an increased temporal resolution is required. It is similar to an FT except that it is applied to individual parts of a signal after it has been divided into segments small enough that they can be treated as stationary signals [52].However the length of the segments can limit the STFT's frequency resolution if they are too short, and limit the STFT's temporal resolution if they are too long.

STFTs are a key component of spectrograms, a useful tool for analysing EEG signals. Spectrograms are a 3D plot of time vs PSD vs frequency. This can be useful in BCI paradigms that rely on a stimulus as we can see the change in power of rhythmic waves over time, such as how we would see the power in the μ-rhythm decreasing in certain channels after the onset of MI [26]. However, spectrograms and FTs in general are still limited by their low temporal resolution. A method that could have a high temporal resolution without sacrificing the frequency resolution would be an improvement.

3.3 Wavelet Transform

The Wavelet Transform (WT) is a very powerful signal processing tool that has been used in many high performance BCIs in the literature [53]. The WT is similar to an STFT, except instead of using sines and cosines to represent the segments of data in the frequency domain, it uses dilations and translations of a pre-selected mother wavelet to represent all the data in a frequency-time domain. This is advantageous compared to an FT that only represents the data in the frequency domain and advantageous specifically compared to STFTs as instead of a fixed temporal resolution the WT has a variable resolution. The WT can be expressed as

$$F(s,\tau) = \int_{-\infty}^{\infty} f(x)\varphi^{*}_{(s,\tau)}(x)dx \tag{3.1}$$

where s is the scale, τ is the translation, φ is the mother wavelet and * is the complex conjugate [53]. As the scale value increases the length of the mother wavelet increases and the window of data it is multiplied with also increases. This leads to an increased frequency resolution for lower frequencies. When the scale value decreases, only high frequencies are detected but with an increased temporal resolution due to the short length of the signal segment. This results in increased temporal resolution at higher frequencies and increased frequency resolution at low frequencies, precisely where it is needed, giving it a much better resolution compared to an STFT [53]. The wavelet function must be carefully selected to fit the data at hand as that strongly influences the temporal and frequency resolution. Choosing an incorrect mother wavelet will produce an inaccurate representation of the signal in the transform. There are several mother wavelets to choose from [54]:

- Haar wavelet – a sequence of square waves, the simplest possible wavelet.

- Daubechies wavelet – characterised by having the highest number of vanishing moments, i.e. the number of coefficients it can be scaled to.
- Symlet wavelet – similar to the Daubechies wavelet but with a high degree of symmetry.
- Coiflet wavelet – similar to the Symlet wavelet but both the wavelet and scaling functions have vanishing moments.
- Morlet wavelet – a complex exponential multiplied by a Gaussian window

There are several variations of WT. The Continuous Wavelet Transform (CWT) uses arbitrary, non-orthogonal wavelets and can be written as

$$CWT_x^{\varphi}(s,\tau) = \frac{1}{\sqrt{|s|}} \int x(t)\varphi^*\left(\frac{t-\tau}{s}\right) dt \tag{3.2}$$

The CWT acts as a measurement of correlation between the mother wavelet at various scales and the signal, with the scale being used as a measure of similarity [55]. With the CWT no phase information from the signal is obtained and the coefficients are too abstracted to be used to reconstruct the original signal. Guo *et al.* 2012 [56] applied the CWT to the P300 paradigm and achieved a minimum classification accuracy of 85% with an average of 90% across five participants, though they did not specify the mother wavelet used. Ting *et al.* 2008 [57] applied WT using a Daubechies wavelet to two public pre-recorded SCP datasets consisting of six participants each performing 300 trials and a single ALS patient performing 200 trials. In both cases they out-performed the other existing methods applied to the same data. Khalid *et al.* 2009 [58] applied the CWT to the MI paradigm with a single participant performing 280 trials using a wavelet adapted from features of the input signal, resulting in an average classification rate of 86% that outperformed the majority of methods applied to the same dataset.

The Synchrosqueezed Wavelet Transform (SWT) is based on CWT and attempts to emulate EMD, a signal processing method described later in this chapter. SWT decomposes a signal into a group of Intrinsic Mode Type (IMT) functions, coefficients grouped by frequency, by first extracting the instantaneous frequencies of the coefficients produced by the CWT, $w_x(s,\tau)$ [59]. This can be defined as

$$w_x(s,\tau) = -i(CWT_x^{\varphi}(s,\tau))^{-1} \times \frac{\partial}{\partial t} CWT_x^{\varphi}(s,\tau) \tag{3.3}$$

for a signal $x(t)$. This can then be used to perform frequency binning of the CWT coefficients using synchrosqueezing,

$$T_x(w_l,t) = \sum_{s_k:\, |w(s_k,\tau)-w_l| \le \Delta w/2} CWT_x^{\varphi}(s_k,\tau)\, {s_k}^{-3/2} \Delta s_k \tag{3.4}$$

where w_l is the central frequency of a selected frequency bin, $\Delta s_k$is the difference of successive discrete scales, and Δw the difference between successive frequency bin centres.

Rutkowski and Mori 2015 [60] present a study where a SWT is applied to a P300 BCI using the Morlet wavelet. With the option of six different cells in the word grid to attend to, the paradigm would give a performance of 16.6% accuracy if random selection was used as a classifier. Their results varied from 20% to 76%. They note that the SWT is more than 50 times faster computationally than EMD but make no mention of its comparative accuracy. Muller-Putz *et al.* 2006 [42] on the other hand compare both the CWT and the SWT for the same datasets using the Morlet wavelet in both cases. With 10 different participants, each having performed 90 trials of binary-class MI, they reported that the CWT outperformed the SWT with a classification accuracy of 72.3% versus 64.9% respectively.

The Discrete Harmonic Wavelet Transform (DHWT) is another variation of WTs that uses harmonic wavelets, i.e. wavelets that are multiples of a given frequency [61]. The main

advantage of DHFT is that it's resulting time-frequency coefficients do not overlap and are therefore more precise. Its implementation is based on the FFT algorithm for increased speed. The DHWT can be represented as

$$w_\tau^s(x) = \frac{e^{4\pi i(2^s x-\tau)} - e^{2\pi i(2^s x-\tau)}}{2\pi i(2^s x-\tau)} \tag{3.5}$$

There are no studies where this was used in the context of a BCI, but it has been applied to EEG in the context of identifying epileptic episodes by Adeli *et al.* 2003 [62]. CWT with a Daubechies wavelet and DHWT were applied to patients' EEG with qualitative conclusions about the nature of epileptic EEG drawn as a result. The authors do not comment on the methods individual performance but state that both methods were very appropriate for the wavelet analysis of spike and wave EEG signals.

3.4 Blind Source Separation

As mentioned earlier, another approach to signal processing is to not use known quantities to identify signals buried in the data and instead learn those quantities from the data itself. BSS is a field of signal processing where techniques are focused on separating a signal into multiple sources with very little information about said sources [63]. BSS techniques tend to assume that the signal sources are statistically independent or uncorrelated with each other. Due to their placement on the surface of the scalp, EEG electrodes have a very low spatial resolution and pick up signals from different parts of the brain as well as the signals from the part of the brain directly underneath the electrode. Physiological and extra-physiological artefacts generated from outside of the brain can also be mixed into the EEG signal, and the underlying systems that produce neurological signals are not fully understood. With so many unknown quantities this makes EEG a prime application for BSS.

3.4.1 Principal Component Analysis

The goal of Principal Component Analysis (PCA) is to reduce the number of dimensions in a dataset so that all that remains is a linear combinations of the dimensions that account for the greatest variation in the data [64], making it a useful pre-processing technique to help simplify the data. Mathematically it is an orthogonal linear transform that projects the data onto a new coordinate system. First the data are standardised by subtracting the mean and dividing by the standard deviation so that the average of all the data are zero, i.e. if these data were plotted on an *n*-dimensional graph the data points would be orientated around the origin point. The first principal component axis is the one that displays the greatest variance. This is done by finding the coordinates of an axis that travels through the origin and has the shortest cumulative distance to all the data points plotted making it as close to as many data points as possible. The second principal component axis obeys the same rules except that it must be perpendicular to the first principal component axis. Ideally if the data were then re-plotted with respect to these new axes we would see a strong linear relationship.

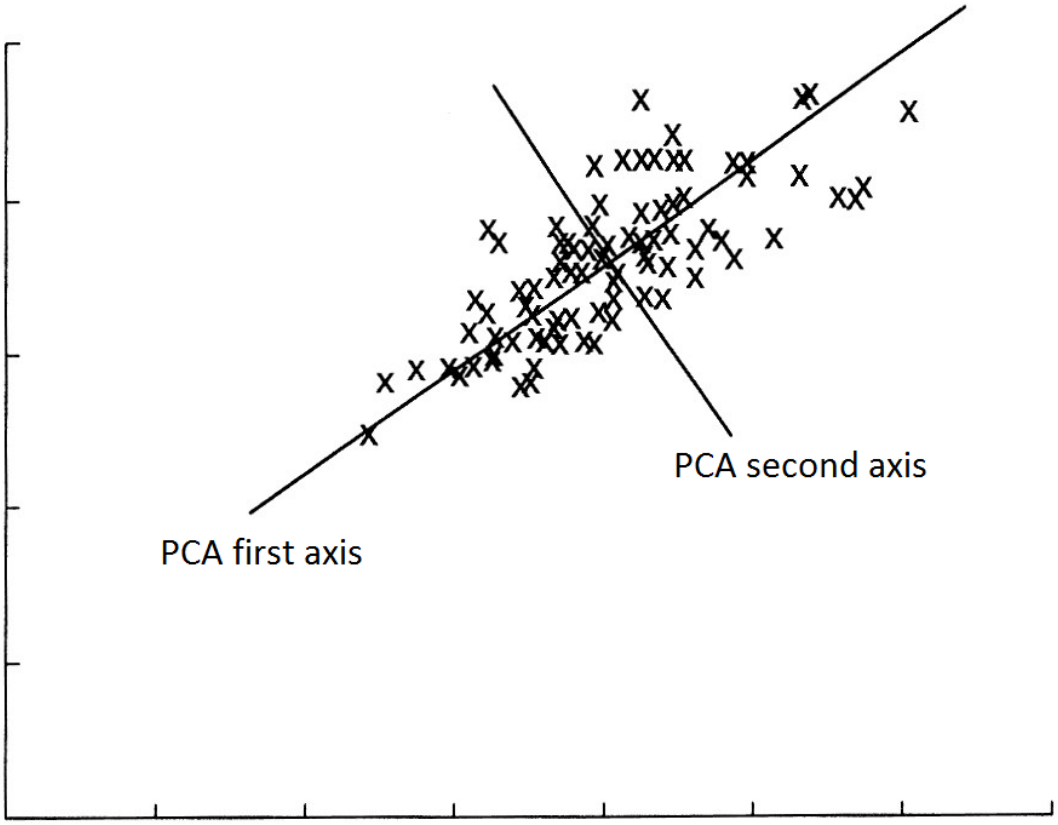

Fig. 3.2: An example of axis selection using PCA [65].

The eigenvalues of the covariance matrix of the data represent how much variance they account for. An eigenvalue whose magnitude is four fifths of the sum total of the eigenvalues accounts for 80% of the data variance. Data suitable for PCA application should have the vast majority of its variance accounted for in the first two or three axes. PCA is non-parametric, requiring no *a priori* knowledge about the data to be inputted into the function, and has the added benefit of compressing the data, increasing the speed of any subsequent processing.

Kottaimalai *et al.* 2013 [66] show how PCA as a pre-processing method improved the performance of an Artificial Neural Network (ANN) classifier when applied to an EEG dataset of mental tasks. Seven participants performed five different mental tasks for ten trials each. These tasks consisted of the simple mental actions of relaxation, simple multiplication of numbers, visualising a rotating geometric shape, mentally composing a

letter to a friend, and visualising counting numbers on a blackboard. Without PCA applied the ANN only classified 28% of the trials correctly, but with PCA it achieved 100% accuracy.

Guan *et al.* 2004 [67] applied PCA to a P300 BCI dataset along with three other pre-processing methods, where six subjects performed 42 trials each. On average, in comparison to the other methods and in the case where no method was applied, PCA had the second highest performance with 94.2% classification accuracy.

As PCA is typically used as a pre-processing method, it is useful for simplifying the data so that it can maximise the performance of a subsequent signal processing method but is not enough by itself to remove the noise and superfluous signals from the EEG recordings.

3.4.2 Independent Component Analysis

Independent Component Analysis (ICA) separates a multivariate signal into statistically independent components [68]. ICA assumes that the underlying sources are independent of each other and are linearly mixed, making it useful for artefact removal in EEG as sources of noise are typically independent of each other. It also assumes that there are fewer sources than observed signals or channels. If the signal data are represented as the vector

$$x(t) = [x_1(t), x_2(t), \dots, x_m(t)]^T, \tag{3.5}$$

where t is the sample number and x_i is the i^{th} out of m observed signals resulting from the sources, s,

$$s(t) = [s_1(t), s_2(t), \dots, s_n(t)]^T, \tag{3.6}$$

where n is the number of signal sources, then the m by n mixing matrix A would take the sources in s and produce the observed signal x,

$$x(t) = As(t) \tag{3.7}$$

ICA tries to find the pseudo-inverse of matrix A, the unmixing matrix W, and use it with the observed signals to find an estimate of the signal sources, $\hat{s}^t$,

$$\hat{s}^t = Wx(t) \tag{3.8}$$

The first step in obtaining W is to whiten the data to remove any existing correlations to ensure the obtained unmixing matrix is for independent signals. An ICA model will try to obtain an unmixing matrix that minimises the Gaussianity of the variables. This means that ICA will not work on variables that have only Gaussian sources.

ICA is another common method used in the processing of EEG signals. Hung *et al.* 2005 [69] used ICA to extract features from trials from a MI based BCI. Four participants each performed 200 trials of left and right hand MI. Four different classifiers were applied to the data, with and without ICA applied beforehand. Without ICA classification accuracies were at near-random levels, whilst with ICA each classifier saw on average a 20% increase in accuracy.

Naeem *et al.* 2006 [70] applied ICA to a more complex four-class MI BCI and compared them to Common Spatial Patterns (CSPs). Eight participants performed 72 trials for each of the four MI tasks. On average ICA achieved 59.8% accuracy compared to CSP's 64.6%. Whilst it did not out-perform CSP, it is a marginal difference in classification accuracies.

Piccione *et al.* 2006 [71] applied ICA to a four-class P300 dataset. Seven healthy and five tetraplegic participants performed 300 trials each. The healthy participants achieved an average classification accuracy of 76.2% with them selecting 7.59 characters per minute, whilst the tetraplegic participants achieved an average classification accuracy of 68.6% with them selecting 7.77 characters per minute. Kamousi *et al.* 2005 [72] applied ICA to another binary-class MI dataset of four subjects performing 180 trials each. They reported an overall classification accuracy of 80%.

3.4.3 Common Spatial Patterns

Common Spatial Patterns (CSPs) is a technique that finds spatial patterns that maximise the variance between the binary classes of a set of multivariate data to help improve classification performance [73]. This is especially useful in regards to EEG due to its low spatial resolution. As it focuses on the statistical measure of variance with no knowledge as to how the underlying EEG sources contributed to the signal it is considered another BSS technique. CSPs first require the normalised spatial covariance matrix, *C*, for each trial in the dataset. Each trial, consisting of an $N \times M$ matrix where N is the number of channels and *M* the number of samples, is represented by *X*,

$$C = \frac{XX^T}{tr(XX^T)}, \tag{3.9}$$

where T is the transpose of the matrix it is applied to and tr is the trace of the matrix it is applied to. A trace is the sum of the elements along the main diagonal of the matrix. C is then used to calculate the composite spatial covariance matrix, C_C,

$$C_C = \bar{C}_A + \bar{C}_B \tag{3.10}$$

where $\bar{C}_A$ is the average of the normalised spatial covariance matrices for class A and $\bar{C}_B$ is the average of the normalised spatial covariance matrices for class B. As C_C can be factorised into $U_C \lambda_C U_C^T$, where U_C is the matrix of eigenvectors and λ_C the diagonal matrix of eigenvalues, it can used to calculate the whitening transformation. The whitening transformation is a decorrelation transform of a covariance matrix into a set of variables whose covariance is an identity matrix. The whitening transformation, P, can be found by

$$P = U_C^T \times \sqrt{\lambda_C^{-1}} \tag{3.11}$$

As the eigenvalues of PC_CP^T would give an identity matrix, and the $\bar{C}_A$ and $\bar{C}_B$ are components of C_C, it can be concluded that $P\bar{C}_AP^T$ and $P\bar{C}_BP^T$ share a common eigenvector

matrix. Their corresponding eigenvalues, once sorted in descending order as matrix *B,* can be used to create the set of spatial filters, W^T,

$$W^T = B^T P \tag{3.12}$$

This can now be applied to the trials in the dataset to extract a set of features, f_p, using the variance of the spatially filtered signal, Z,

$$Z = W^T X, \tag{3.13}$$

$$f_p = \log \frac{var(Z_p)}{\sum_{i=1,\ldots,m \text{ and } N-m+1,\ldots,N} var(Z_i)}, \tag{3.14}$$

where p is the sample index of Z. The sample indexes that maximise the difference in variance between the two classes are the first and last samples. The variance difference decreases the further you are from the borders of vector Z, as does their usefulness in enhancing the difference between the two classes of the dataset.

As mentioned earlier in this chapter, Naeem *et al.* 2006 [70] compared CSP performance with that of ICA in the context of a four-class MI dataset, and reported that CSPs performed better with 64.6% classification accuracy. Samek *et al.* 2011 [74] applied CSPs to two large binary-class MI datasets, with a total of 14 participants performing 280 trials each. On average they achieved 77.9% classification accuracy.

Wang *et al.* 2006 [75] show how CSPs can be used to identify the most significant EEG channels by finding the two channels corresponding to the maximal coefficients of *Z*. The channel selections corresponded with the known neurophysiology of MI when applied to an MI dataset.

CSPs can make a good post-processing technique, taking a processed signal and reducing it to a handful of variables that maximise the variance between the different classes of signal. Some supervised classifiers that rely on training data respond well to this compression of

the data, with the number of observations being more critical to their performance than the resolution of these observations [76].

3.4.4 Empirical Mode Decomposition

EMD is a data-driven mathematical process developed by N. E. Huang *et al.* [77] in 1998, making it a relatively "young" method. It shares some similarities with SWT in that it splits a signal into a group of time-frequency components except that EMD is purely data-driven instead of making any assumptions about the data, making it more adaptive to the signal it is applied to as it has to learn the different properties from the data themselves. It is also completely objective as it does not require the selection of a mother wavelet like the WT or any other choices by the user to inform its outputs.

EMD applies an iterative sifting process to a signal in order to decompose it into a group of Intrinsic Mode Functions (IMFs) and residual noise, depicted in Figure 3.3 [77]. An IMF is defined as a signal that is symmetrical with respect to the amplitude and has at least two extrema, i.e. it is comprised completely of sinusoids. EMD can be applied to any non-linear and non-stationary signal as its decomposition is based on the local characteristic time scale of the data, allowing it to be used in many different fields, from analysing mortgage rate data [78] to characterising non-linear water waves [79]. It functions by subtracting the mean envelope of the signal repeatedly until it produces a signal with symmetrical oscillations. This is stored as an IMF and the envelope subtraction continues until no peaks or troughs are left, leaving the remainder of the signal to be classified as residual noise.

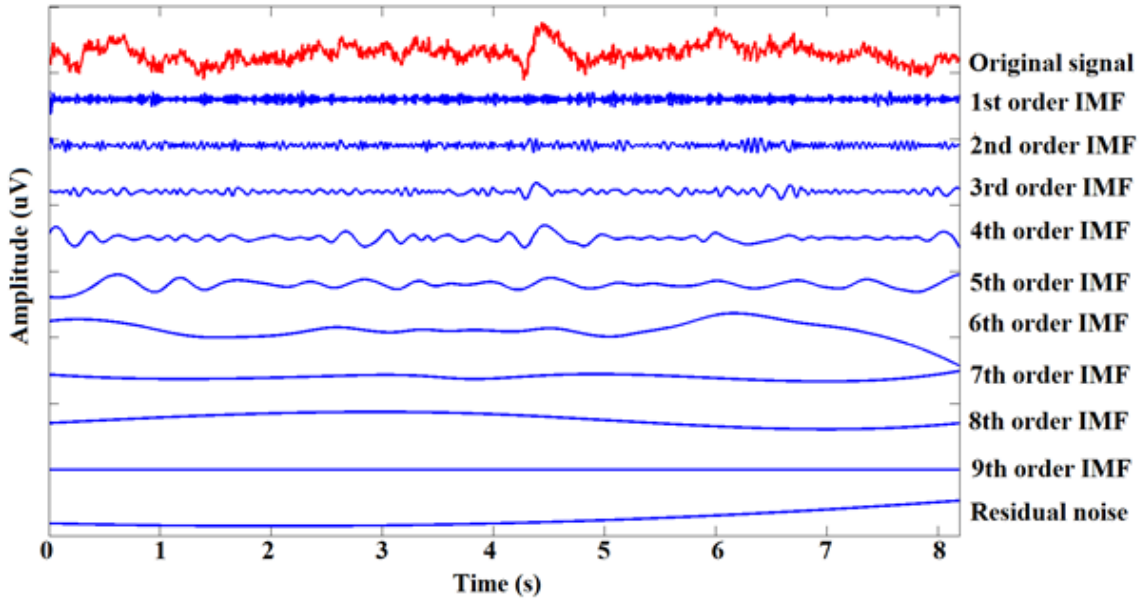

Fig. 3.3: A decomposed channel from a single trial of a BCI MI experiment, with the stimulus cue appearing at 4.1 seconds. The IMFs are sorted by frequency in a descending order until only the residual noise is left. Should all the IMFs and noise be summed together they will reform the original signal. This process is useful for extracting features from a signal that are composed of a narrow range of frequencies, such as MI's rhythmic 8-13Hz μ-rhythm.

A signal decomposed by EMD can be defined as

$$x(t) = \sum_{j=1}^{n} c_j + r_n, \tag{3.15}$$

where c_j is the j^{th} IMF, r_n is the residual and $x(t)$ is the original signal. IMFs are obtained by applying an iterative sifting process using the following steps to the signal, $x(t)$:

1. Identify the maxima and minima of the signal.
2. Interpolate between the maxima and minima to create upper and lower envelopes.
3. Calculate the mean between the two envelopes, $m(t)$.
4. Subtract the mean from the signal to get an IMF candidate, $x_{n+1}(t) = x_n(t) - m(t)$.
5. Check if $x_{n+1}(t)$ is an IMF by calculating if it is symmetrical with respect to zero.

6. If $x_{n+1}(t)$ is an IMF then store the IMF and return to step 1.) with the signal $x(t) = x_n(t) - x_{n+1}(t)$, else discard and return to step 1.) with the signal $x(t) = x_n(t) - x_{n+1}(t)$.
7. When there are less than two extrema left in the signal the remaining data are classified as the residual.

These IMFs give us the ability to localise any signal event by time, frequency, and morphology, compared to just frequency in an FFT or frequency and time in a spectrogram.

Diez *et al.* 2009 [80] applied EMD to the same mental task dataset Kottaimalai *et al.* 2013 [66] used in their study on PCA and ANNs. Diez *et al.* 2009 [80] found that EMD performed well with classification accuracies ranging from 80.9% to 97.4%. Wei *et al.* 2009 [81] applied EMD to a binary-class MI dataset consisting of four subjects. The tasks were performed un-cued, meaning there were no delineated trials, making it more similar to the EEG signals that would be produced in a practical setting. IMFs with frequency content within a range of 6 – 30 Hz were selected, and an average classification accuracy of 85.9% was reported.

Williams *et al.* 2009 [82] applied EMD to a dataset of artificial EEG signals. A 1000 trial dataset consisting of synthetic P300 evoked potentials mixed with simulated EEG signals at different SNR levels was constructed. The two lowest frequency IMFs were always chosen and summed to form the processed signal. At every SNR level the classifier combined with EMD outperformed the classifier on its own. It may have performed better if IMFs were not chosen based on their numerical index when sorted by frequency, as the number of IMFs produced by EMD varies depending on the signal content. This is because the more content a signal has the more unique components there are to be separated into IMFs. For example, if the user blinks enough times the consistent changes in amplitude and

frequency could be interpreted as its own unique IMF instead of part of an IMF of similar frequency. Whilst artefact removal is an application of EMD, it can lead to a higher number of IMFs being produced which is why using the absolute indexes of IMFs to select them is not preferable.

He *et al.* 2012 [83] applied EMD and CSPs to a pre-recorded binary-class MI BCI dataset consisting of five subjects performing 200 trials each. Again, the IMFs were selected by their index, with IMF 1, IMF 2, IMFs 1 and 2 summed together, and IMFs 1, 2, and 3 summed together evaluated. Classifiers using individual IMFs had the lowest performance with approximately 70% classification accuracy. CSPs achieved a classification accuracy of 79.2% but the summed IMFs both produced a performance of 82% classification accuracy. This is a negligible difference between the two methods, but it does show EMD is applicable in the processing of MI EEG signals.

Wu *et al.* 2011 [84] used EMD to extract SSVEPs in a BCI. They constructed a six-class SSVEP control system that used icons flashing on a screen at the frequencies of 30, 31, 32, 33, 34, and 35 Hz to control a mouse cursor. Five subjects each attempted to perform a sequence of commands, totalling 20 commands altogether. The percentage of correct commands out of total commands executed varied from 77% to 95%, with an average of 84.6%. The average time to complete the sequence was 66.5 seconds, giving an average of 37 commands per minute. This is a relatively high performance for a BCI. As SSEPs in general are sinusoids of a constant frequency they match the properties of an IMF precisely, meaning EMD is very robust at separating them from a mix of signal sources.

3.5 Classifiers

After processing has obtained a set of features from a signal it needs to be classified into one of a selection of pre-defined groups. Whilst a classifier can be as simple as comparing

the magnitudes of a certain aspect such as PSD, with BCI the low SNR means that more complex classifiers are needed to identify the subtle, and at times inconsistent, differences between classes with residual extraneous signals and artefacts still present. There are several signal classifiers that make use of pattern recognition and machine learning in their construction. These classifiers rely on supervised learning, where a set of data already correctly classified ahead of time is used to train the classifier [85].

BCI classifiers can also be online or offline [86]: online classifiers classify a BCI task as soon as it is performed and before the next task occurs, i.e. in real time, and provide feedback that can be used by the user to adjust their performance. Offline classifiers are classifiers executed after the BCI has ceased being used, usually on a large amount of pre-recorded tasks. Online analysis is important for BCIs being used for assistive communication as in practice any control system must select its outputs within a reasonable amount of time. For medical diagnosis, however, the response does not need to be so immediate.

3.5.1 Linear Discriminant Analysis

Linear Discriminant Analysis (LDA) attempts to find the best linear combination of features that can be used to separate two or more classes [87]. LDA shares some similarities with PCA in that it is a linear transformation that can be used for dimension reduction. LDA is a supervised classifier compared to PCA as it does not ignore the data's class labels. It also assumes the data has a Gaussian distribution. The goal of LDA is to find the axis that maximises $J(w)$, the ratio of total sample variance to the sum of variances for each class,

$$J(w) = \frac{w^T(\sum_i(x_i - \mu)^T(x_i - \mu))\,w}{w^T(\sum_c \sum_{i \subset c}(x_i - \mu_c)^T(x_i - \mu_c))w} \tag{3.16}$$

where w is a vector, c is the class, Σ_c is the summation for class c, μ is the sample mean, and μ_c is the mean for class c. Whilst the threshold vector can still function properly even if

the class boundaries overlap, it cannot be an effective classifier if the centroids are too close.

3.5.2 Support Vector Machines

Support Vector Machines (SVMs) are classifiers that focus on identifying the patterns and structure of the data in each class to create a hyperplane to separate the two groups of data [76]. The optimum hyperplane will maximise the distance between it and the two groups of data. This is called the maximum-margin hyperplane. The hyperplane, $f(x)$, can be defined as

$$f(x) = \beta_0 + \beta_x^T = 1, \tag{3.17}$$

where β is the weight vector, β_0 is the bias and x are the training samples for each class closest to the hyperplane, known as support vectors. If the Euclidean distance between the support vectors and the hyperplane can be represented as

$$\frac{|\beta_0 + \beta_x^T|}{\|\beta\|}, \tag{3.18}$$

then by using equation 3.17 it can also be represented as

$$\frac{1}{\|\beta\|} \tag{3.19}$$

The distance between the support vectors for each class, M, must be at least twice the distance between the support vector and the hyperplane, therefore

$$M = \frac{2}{\|\beta\|} \tag{3.20}$$

As the issue of maximising M is the equivalent of minimising the Lagrangian function $L(\beta)$, then the model of the hyperplane that correctly classifies all the training samples can be written as

$$\min_{\beta,\beta_0} L(\beta) = \frac{1}{2}\|\beta\|^2 \text{ subject to } y_i(\beta^T x_i + \beta_0) \geq 1 \; \forall i \quad (3.21)$$

where x_i are the training samples and y_i are their corresponding class labels. After the hyperplane has been created, new unlabelled samples can be classified using a function called a kernel that measures the similarity between the new sample and the training samples. Kernel types can be selected based on previous knowledge of the data, allowing the classifier to be customised.

3.5.3 Artificial Neural Networks

Artificial Neural Networks (ANNs) take their inspiration from the brain. They are comprised of many layers of inter-connected nodes, the software-equivalent of neurons, to classify data, bordered by layers comprised of the input data and possible outputs [88]. Each neuron is comprised of a set of input values, a set of weights, and a function that sums the weights and maps the result of applying them to the input data to an output.

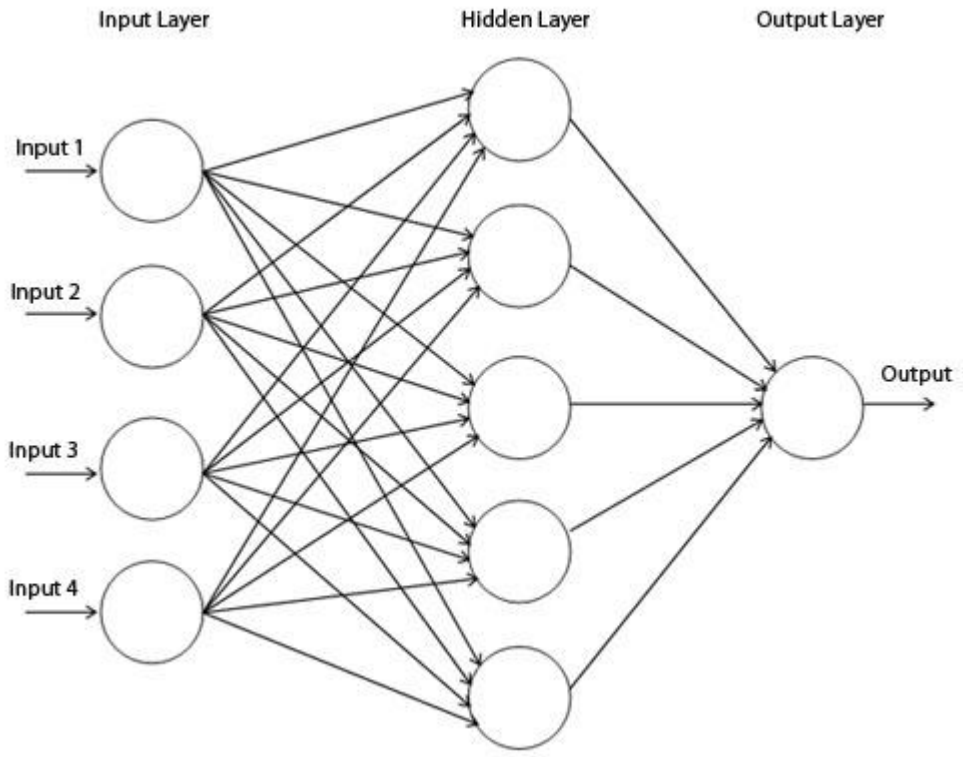

Fig. 3.4: A diagram of a neural network showing the interconnected nodes where weights are applied to the inputs [89].

A set of random weights is initially applied to the data and the network uses them to assign a value to each output node. The data are assigned to the class whose corresponding node has the higher value. Each time the network compares the classification with the labels to see if it was correct. Incorrect outcomes cause the sets of weights in the hidden layers to be adjusted, usually by applying the Delta rule. The Delta rule uses the difference between the desired outcome and the actual outcome combined with a scaling factor to ensure the weights change in proportion to the size of the error. This process is repeated iteratively until enough of the training set is classified correctly. The number of layers must be selected by the user.

ANNs are usually applied when the data have a high diversity and the relationships between the samples are not fully understood. It is also not limited by pre-conditions or assumptions on the data, such as if it is or is not Gaussian, correlated or linear like other methods do [88]. However as the learning relationship cannot be extracted from the

hidden layers, no information on how or why the data are related can be discovered, making it unsuitable for academic applications where the knowledge of why the data are behaving as they do and what separates the different classes is of importance.

Garrett *et al.* 2003 [90] applied LDA, SVMs and ANNs to the same extracted features from the mental task dataset used by Kottaimalai *et al.* 2013 [66] and Diez *et al.* 2009 [80]. They reported that SVMs performed best, followed by ANNs and then LDA. There was only a 3% difference in classification accuracy between each method. It should be noted that LDA performed the fastest and SVMs the slowest. Time can be a factor in the practicality of a BCI if it is being used for real-time communication.

Zhou *et al.* 2008 [91] also applied LDA, SVMs and ANNs to the same extracted features of a binary-class MI BCI dataset that Khalid *et al.* 2009 [58] applied CWT to in their study. SVMs and ANNs both resulted in 90% classification accuracy whilst LDA gave an 89.3% classification accuracy, a negligible difference. However SVMs again took the most computational time to produce a result.

Hung *et al.* 2005 [69] applied LDA, SVMs and ANNs to a different binary-class MI BCI dataset. Four participants performed 200 trials each using a 64 electrode EEG. As in [90], they reported that SVMs had the highest classification accuracy with 77.3%, followed closely by ANNs with 75.5% and LDA performing the worst again with 69.8%. They make no mention of the processing duration.

3.6 Measuring BCI Performance

Once the BCI system is functional, there needs to be a way of quantitatively measuring its performance so that it can be evaluated and compared to different systems. There are several different metrics used in the literature. The most obvious one is accuracy in terms of the number of trials correctly classified, but there are others that take into account other

relevant variables, such as time and specifically what aspects of the classifier are the most accurate. In the role of an assistive communications device, the time it takes to process an EEG signal is an important factor in facilitating real-time communication.

3.6.1 Sensitivity and Specificity

Sensitivity and specificity are complimentary metrics used in the statistical evaluation of binary classification systems. Sensitivity measures the percentage of trials belonging to Class A correctly identified as Class A, whilst specificity measures the percentage of trials not belonging to Class A correctly identified as a class other than A [92]. A classifier with high sensitivity and low specificity will correctly identify every instance of Class A, but also misidentify many other trials as Class A as it is so sensitive to features resembling those of Class A. A classifier with low sensitivity and high specificity will correctly exclude all the non-Class A trials but will only correctly identify the Class A trials that most closely match the features of Class A and contain little to no extraneous information such as noise.

Sensitivity can be calculated as

$$\frac{number\ of\ true\ positives}{number\ of\ true\ positives + number\ of\ false\ negatives} \times 100 \tag{3.22}$$

Specificity can be calculated as

$$\frac{number\ of\ true\ negatives}{number\ of\ true\ negatives + number\ of\ false\ positives} \times 100 \tag{3.23}$$

Sensitivity and specificity can be used as measures to show the specific type of proficiency or deficiency in a classifier's accuracy.

3.6.2 Information Throughput

Another metric is the Information Transfer Rate (ITR) which provides a measure of the system's speed versus its accuracy [93]. It can be calculated as

$$B = \log_2 N + P \log_2 P + (1 - P) \log_2 \left(\frac{1 - P}{N - 1}\right) \tag{3.24}$$

where *B* is the ITR in bits per unit time, *N* is the number of classes, and *P* is the accuracy of the classifier. A communicative BCI of any practical use must have a high ITR in order to provide real-time control of a system by the user. This highlights the response time of the system as an important factor.

P300 Spellers especially make use of ITRs as the system is designed specifically for text communication rather than a vague class-selection that can be mapped to any control system. In Chapter 2 several P300 studies were referenced. Farwell and Donchin 1988 [34] and Townsend *et al.* 2010 [36] achieved very similar classification accuracies of 75 – 80%, but Townsend *et al.* 2010 [36] reported an ITR of 17 bpm compared to Farwell *et al.* 1988's [34] ITR of 2.3 bpm, highlighting the difference between the two BCI systems.

An SCP BCI study by Birbaumer *et al.* 2000 [31] was also referenced in Chapter 2 with the remark that very little follow-up research was performed on this paradigm, in part due to its slowness. Its ITR of 0.5 bpm highlights this.

In [94] by Cheng *et al.* 2002, they explicitly set out to maximise the ITR of an SSVEP BCI in order to increase its practicality. Out of seven subjects they reported an average ITR of 29 bpm.

In terms of evaluating a BCI for assistive communication ITR is the superior measure as it combines both the BCIs' speed and accuracy, whilst sensitivity and specificity only use accuracy. For an offline BCI used in diagnoses, speed is less important than accuracy as identifying the patient's condition is critical in diagnoses so long as it occurs in such a

timeframe that a patient backlog forms or the patient's condition will deteriorate before the result is known. However, many BCI studies use only classification accuracy simply because achieving high accuracy is difficult enough without having to introduce a time factor. This reflects the limits faced by BCI research due to the technology of surface EEG.

3.7 Summary

There are a large variety of signal processing techniques, many with origins outside of biosignals. Their application to BCI is a necessity due to the large mix of signals and artefacts present in EEG recordings. With BCI it is important to choose the technique that will maximise the features unique to the different signals and classes of the desired signals, whilst balancing practical concerns such as computational overhead and the number of channels required. BCI paradigms that produce evoked potentials with clearly defined properties may benefit from knowledge-based signal processing methods that work to extract known features, but with other evoked potentials and the number of unknown factors underpinning the biological system that produces these signals it can be more prudent to try and adapt the signal processing technique to the data itself, by identifying features unique to the dataset in question. In the case of a BCI being used for real-time communication, the time required to process the signal will be a significant factor in the system's practicality. As well as influencing the choice of BCI paradigm, this can influence the choice of classifier in an effort to avoid performing redundant computational operations on the feature set extracted from the signals.

The volume of research into EMD in the context of BCI does not appear to be as large as some other techniques. The criteria for its decomposed outputs, a constant frequency and rhythmic morphology, match the properties of several evoked potentials, e.g. the μ-rhythm and SSEPs, suggesting it is well-suited to the processing of EEG signals. Its data-driven approach allows it to adapt to different types of signals, whilst the lack of abstraction of its

outputs means they are easy to interpret in the context of signals and can still undergo post-processing prior to classification. These properties make it a personally interesting signal processing technique for further investigation.

CHAPTER 4

Novel applications of Empirical Mode Decomposition in BCI

This chapter will cover the implementation and evaluation of EMD and novel variations thereof in the context of processing EEG signals. First, the original EMD algorithm was applied as a signal processing component in a BCI as a proof-of-concept that the method is relevant in conjunction with EEG and to compare its performance alongside other signal processing methods. Next, an already-existing variation of EMD in the literature called Multi-variate EMD (MEMD) [11] is detailed as it forms the basis for two novel variations of EMD: Temporal MEMD and Spatio-temporal MEMD. T-MEMD's performance was compared with that of standard EMD's as T-MEMD contains the same information as EMD as well as added temporal dynamics. ST-MEMD was compared with MEMD as both make use of the same amount of new spatial information but ST-MEMD also uses temporal dynamics to inform the decomposition of the signals.

4.1 Proof-of-concept

The original EMD algorithm was first applied to the MI paradigm to test the hypothesis that this method could be used to process and extract features from EEG signals. As mentioned in Chapter 2, the onset of MI that involves limbs that are located laterally left or right is denoted by the suppression of the μ-rhythm in the contralateral cortex. As the μ-rhythm occupies a specific frequency band this makes EMD ideal for finding it embedded in a noisy raw EEG signal.

A key part of the processing is how to determine which IMFs should be kept and which should be discarded after decomposition. The goal here was to make the process as objective as possible, with selection by algorithm used where possible as opposed to subjective selection by the user. This process will be detailed later in the next section where EMD, the selection criteria and its resulting classifier was applied to two different pre-recorded MI datasets.

4.1.1 Dataset 1

The first dataset was provided by the Graz BCI group for use in BCI Competition II, Dataset III [95]. A 25 year old female participant sat in a chair whilst an EEG recorded brain activity from electrode positions C3, Cz and C4. As shown in Figure 4.1, each trial of the MI experiment consisted of a two second pause, followed by an audio cue to signify the start of the test and a fixation cross displayed for one second. At three seconds into the trial a left or right arrow was displayed for six seconds to indicate which hand to imagine moving. A feedback bar was also displayed to the user during this time to help indicate the success of the imagined movements. The trial lasted nine seconds in total, with 280 trials recorded on the same day with several minutes rest every 70 trials. The trials were then randomly sorted into training and test groups, with 70 trials of imagining left and 70 trials of imagining right forming the training data group, and the remaining 140 trials forming the test data group. The EEG was sampled at 128 Hz and band-pass filtered to between 0.5 and 30 Hz.

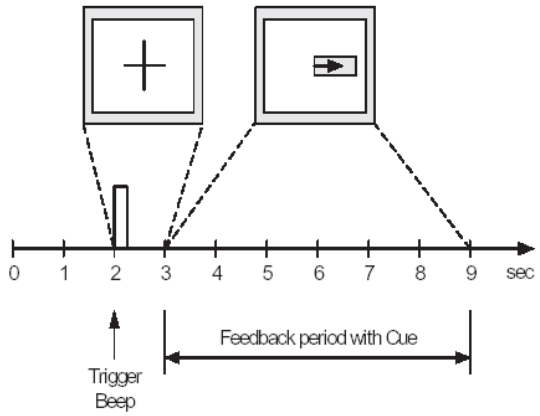

Fig. 4.1: At 2 seconds into the trial a fixation cross appears and an audio cue is sounded. At 3 seconds into the trial a randomly selected left or right arrow is displayed and at this point the participant imagines moving the hand on the side of their body that corresponds with the direction of the arrow. At 9 seconds the trial ends and the next trial begins [95].

For each trial EMD was applied to channels C3 and C4 at the onset of MI until one second before the end of the trial (3 – 8 seconds), with Cz ignored due to its central location with regards to the motor cortex. The residual noise was immediately discarded as it has no rhythmic properties, meaning no μ-rhythm components could be present, and the IMFs of both electrodes were grouped together so that the data from more than one channel was included. FFTs were calculated for each IMF and the peak frequency of each IMF and its corresponding amplitude were identified. These peak frequencies were grouped into clusters using Hierarchical Clustering Analysis (HCA), ensuring that IMFs spanning similar frequency bands would be grouped together.

HCA calculates the Euclidean distance between every possible pair of data points and constructs a binary hierarchical cluster tree with the pair of elements with the smallest distance between them forming the next link [96]. The tree is then partitioned into separate clusters when there is a sudden increase in the distance between links. This algorithm ensures that the grouping by peak frequency values is done objectively.

The cluster that occupied the same frequency band as the μ-rhythm was identified, with the initial boundaries being set at 9 – 11 Hz. Should excessive artefacts or noise distort the signal to the extent that no clusters spanning 9 – 11 Hz were detected, the frequency band was expanded by 1 Hz in both directions until a cluster fell within it. This was so that trials which had had their μ-rhythm obscured by noise still could contribute some data that could be used to classify them, rather than be discarded completely. The channel of each IMF in the μ-rhythm cluster was identified and the amplitudes of the peak frequencies of IMFs from the same channel summed together, producing a single value for each channel. This value represents the power in the μ band for an individual electrode, giving us amplitude, frequency and spatial data. After that a simple comparison of the values' magnitudes was enough to determine which hand the participant was imagining moving, with greater power in C3 meaning the participant was imagining moving their left hand and greater power in C4 meaning the participant was imagining moving their right hand. This difference in magnitudes corresponds to the theory of μ-rhythm suppression on the contralateral side of the motor cortex during a MI task. This process can be seen in Figures 4.2, 4.3 and 4.4.

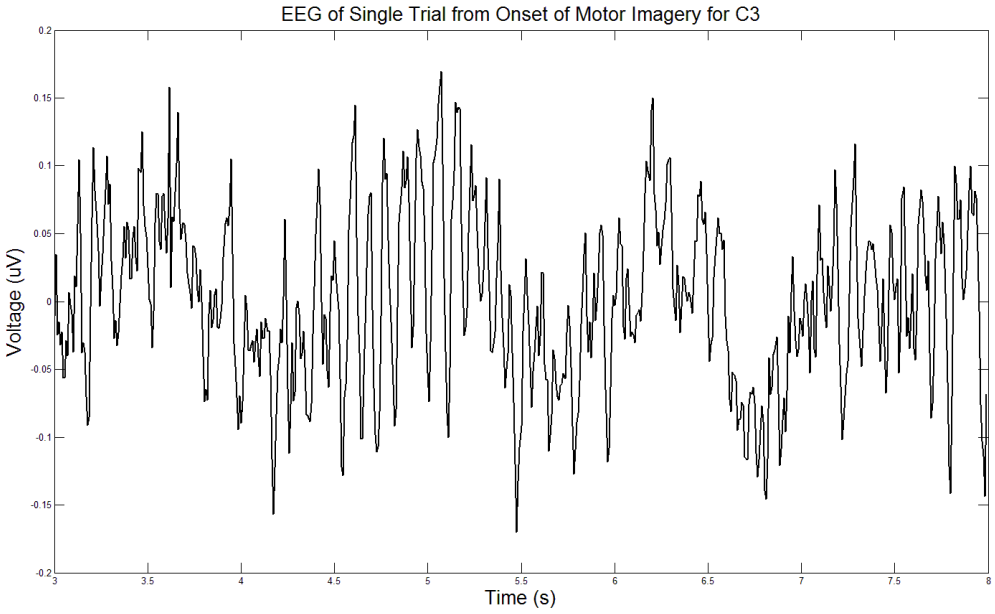

Fig. 4.2: The raw EEG data from a single trial from channel C3 at the onset of MI.

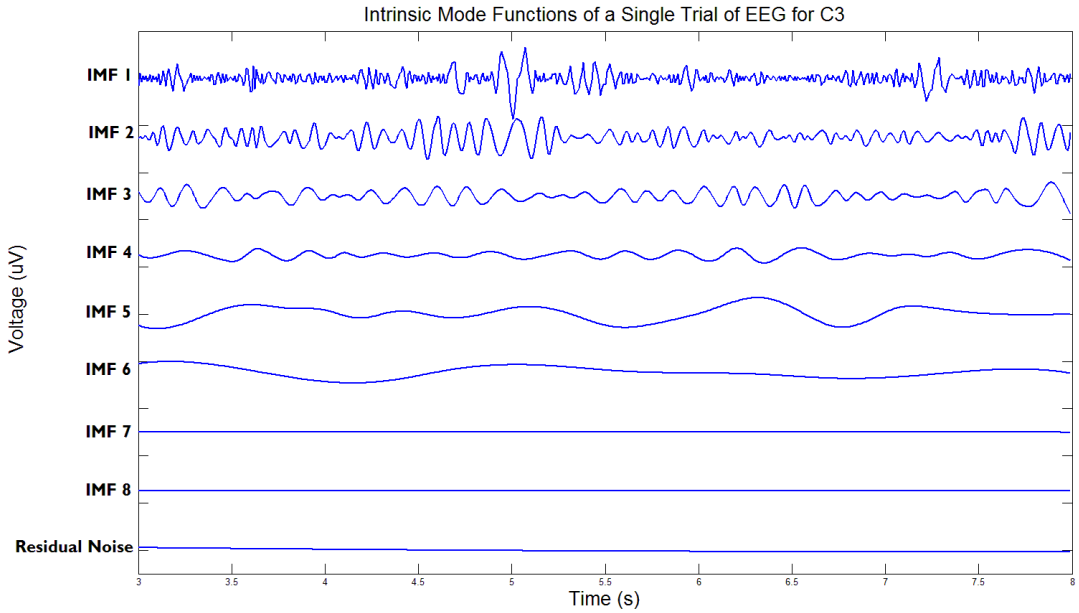

Fig. 4.3: The IMFs and residual noise produced from applying EMD to the data shown in Figure 4.2.

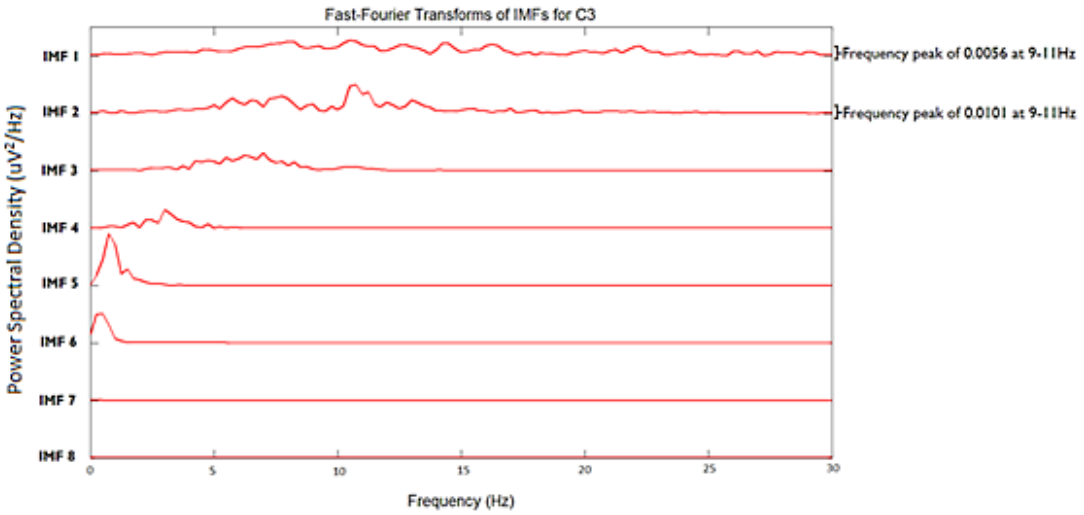

Fig. 4.4: The FFTs calculated from the IMFs in Figure 4.3. The peak frequencies of the IMFs have been clustered to determine which peak frequencies, and by extension which IMFs, are most similar to each other. Then the cluster that consists of peak frequencies within the μ-rhythm *is identified. The amplitudes of the peak frequencies in the IMFs from each electrode are summed and compared, e.g. 0.0157 (0.0056 + 0.0101) in channel C3 vs whatever the value is in channel C4 for this trial. If the magnitude is less in C3 than C4 then the trial is classified as "think Right".*

4.1.2 Analysis

Table 4.1 lists a selection of methods in the literature applied to this dataset sorted by accuracy, with the method described in the above section coming third, demonstrating comparable performance to existing methods.

TABLE 4.1. COMPARISON OF MINIMUM ERROR RATES SUBMITTED BY DIFFERENT GROUPS FOR THE SAME DATA*

Authors	Method	Error Rate (%)
Xu and Song 2008	Wavelet Transform	7.90
Schäfer and Lemm 2003	Wavelet Transform	10.57
Davies and James 2013a	EMD	11.53
Xiaorong *et al.* 2003	ERD	13.57
Xiaorong *et al.* 2003	ERD	15.00
Narayana *et al.* 2003	AR Modelling	15.71
Saffari *et al.* 2003	AAR Modelling	17.14
Sadashivaiah *et al.* 2003	AR Modelling	17.14
Zander *et al.* 2003	AAR Modelling	17.14
Rissacher 2003	Spectral Entropy	23.57
del Rio Vera 2003	PCA	32.14
Mbwana and Laubach 2003	PPDA	49.29

**Results, excluding Xu and Song 2008 [97] and Davies and James 2013a [98], aggregated by Jia et al. 2004 [99]. Error rate is calculated by applying the group's selected processing method to a training set and test set. A moving window of one sample's length is swept across the processed data. For each window an LDA classifier is trained using the training data within the window and applied to the test data that falls within the moving window. The window that produces the lowest error rate is selected as the optimum sample point.*

EMD performs well compared to alternative signal processing methods. Being able to function with a low number of EEG channels also increases its practicality in the field. Requiring no training trials at all in order to construct a classifier is a distinct advantage in ease of use and reducing processing time. Figure 4.5 shows a clear left-right distribution, demonstrating visually in this case the redundancy of a trained classifier such LDA or SVM.

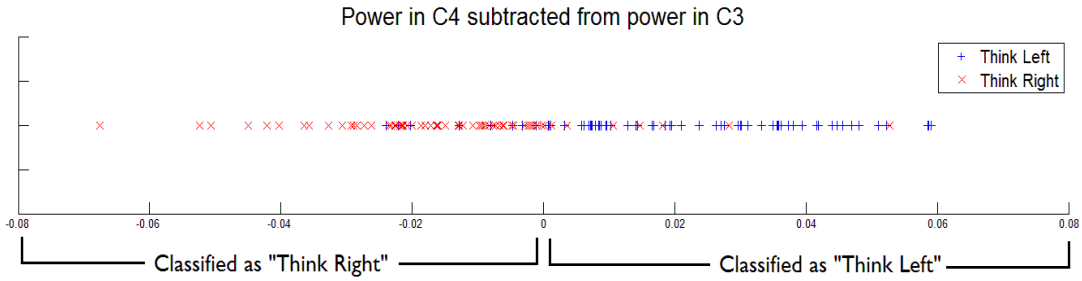

Fig. 4.5: Difference in calculated power between channels C3 and C4. After the power in the μ-rhythm for each electrode has been calculated the two values are compared, with the channel with less power being the one that is contralateral to the imagined movement. Were you to subtract the value in C4 from the value in C3, any trials where the μ-rhythm power was less in C3 would give a negative result and trials where the μ-rhythm power was less in C4 would give a positive result. Therefore any subtraction that gave a negative result would be identified as "Think Right" by the classifier and any subtraction that gave a positive result would be identified as "Think Left". The correct direction the user was thinking of is denoted by the different coloured markers. The spread of the markers has a strong left-right divide over the threshold point (zero).

For the sake of completeness, the processed data from the training and test sets were processed through an LDA classifier and it returned the same accuracy as the simplified threshold classifier, thus showing that a non-complex classifier is sufficient due to efficient feature extraction of the data. The frequency boundaries of the μ-rhythm do need to be defined before executing the process and they may vary slightly between participants. Though it was only tested on the data from one participant, it works well as a proof-of-concept that EMD can be used in the processing of EEG data. An attempt was made to also include IMFs containing resonance activity in the beta frequency band, a component of MI described in Chapter 2, but it resulted in a decrease in performance, indicating that the resonance effect was not pronounced enough to be distinguished from background noise.

4.1.3 Dataset 2

The second dataset was also provided by the Graz BCI group, this time for BCI Competition III, Dataset IIIa [100].

A participant sat in a chair whilst a 60 channel EEG recorded brain activity. As shown in Figure 4.6, each trial of the MI experiment consisted of a two second pause, followed by an audio cue to signify the start of the test and a fixation cross displayed for one second. At three seconds into the trial a left or right arrow was displayed for one second to indicate which hand to imagine moving. The trial lasted seven seconds in total and 120 trials were recorded in sessions of 40 trials, with half the trials being of the class imagining left and the other half imagining right. The trials were then randomly sorted into training and test groups, with 15 trials of imagining left and 15 trials of imagining right forming the training data group, and the remaining 90 trials forming the test data group. The EEG was sampled at 250 Hz and band-pass filtered to between 1 and 50 Hz. Though these values are different to those of the dataset in section 4.1.1, the sampling rates of both are still high enough to prevent aliasing on the signals with the highest possible frequency of interest as prescribed by the Nyquist theorem [17]. The values of the band-pass filters are also both outside the frequency domains of any brain activity of interest.

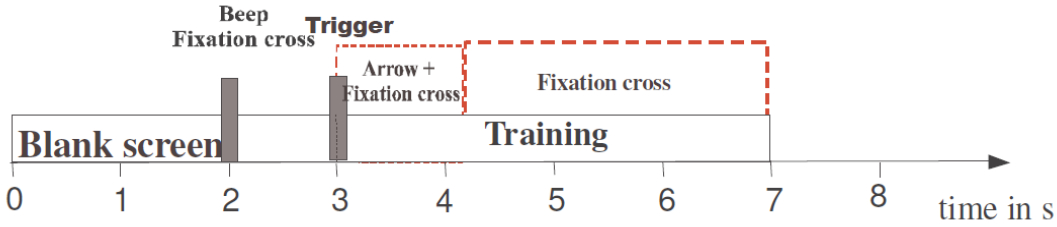

Fig. 4.6: At 2 seconds into the trial a fixation cross appears and an audio cue is sounded. At 3 seconds into the trial a randomly selected left or right arrow is displayed and at this point the participant imagines moving the hand on the side of their body that corresponds with the direction of the arrow. At 7 seconds the trial ends and the next trial begins [100].

The same processing method used on Dataset 1 in 4.1.1 was used on Dataset 2 with a few changes. As before, standard EMD was applied to each channel in turn. FFTs of each IMF were calculated and the peak frequencies and their amplitudes noted. HCA was then used to group the IMFs by peak frequency into clusters. However, in this case, for each trial CSPs were used to extract the top three significant channels for each class.

Wang *et al.* 2006 [75] describe how CSPs can be used to select the optimal channels for classification as part of a BCI, in this case MI. The pseudo-inverse projection matrix resulting from CSPs as described in Chapter 3, W^T, can be considered to be a set of EEG source distribution vectors. Assuming only the first and last spatial patterns are related with the specific sources of the two tasks, then the two channels corresponding to the maximal coefficients of spatial pattern vectors should be the channels most correlated with the task specific sources.

Typically for the class of Left the channels selected were C3 and its adjacent channels. For the class of Right it was C4 and its adjacent electrodes. This corresponds to the theory that the μ-rhythm is suppressed on the hemisphere of the brain contralateral to the position of the limb being imagined moved. Another change to the process compared to Dataset 1 was the use of a supervised LDA classifier. Using the comparison in magnitude as before gave near-random results.

4.1.4 Analysis

For this dataset EMD classified 64.4% of the 90 test trials correctly using LDA. By comparison, Jia *et al.* 2004 [99], who used a bandpass filter of 10 – 12 Hz to find the ERD/ERS evoked potential and calculated the power of it in channels C3 and C4, classified 55% of the test set correctly.

These studies were published in the paper "*Novel use of Empirical Mode Decomposition in single-trial classification of Motor Imagery for use in Brain-Computer Interfaces*" as part of the conference proceedings for the 2013 Annual International of the IEEE Engineering in Medicine and Biology Society [101], and in the paper "*Multi-Channel Empirical Mode Decomposition in Brain-Computer Interfaces*" as part of the conference proceedings for the 7th UK and RI Postgraduate Conference in Biomedical Engineering and Medical Physics [98].

4.2 Multi-variate Empirical Mode Decomposition

MEMD is an enhanced version of EMD created by Park *et al.* 2013 [11] that can decompose multiple channels simultaneously, allowing the neighbouring channel's data to inform the envelopes used in decomposition. MEMD solves the problem of uniqueness, which refers to how different channels can produce a different number of IMFs from each other and no IMFs are guaranteed to share the same frequency bands as its neighbouring channel's IMFs, hindering the analysis of multi-channel signals. Decomposing more than one channel at a time does however lead to an increase by up to ten times the computing time needed, possibly precluding the option to have a BCI system that provides real-time feedback to the user.

Regular EMD calculates the local mean for each sampling point of the signal using its envelopes. MEMD calculates the local mean by generating *n*-dimensional envelopes along different directions through *n*-dimensional space and averaging them, where *n* is the number of channels [11]. Choosing the set of direction vectors is done by using uniform angular sampling of a sphere in an *n*-dimensional hyperspherical coordinate system. To ensure the coordinates are uniformly spaced a Hammersley sequence [102] is employed to generate multi-dimensional sequences with strong uniformity. Stoppage criteria for the sifting process is similar to that of EMD, with the difference that the number of extrema and zero crossings do not have to be equal as extrema cannot be defined in multi-dimensional signals [11].

The final MEMD algorithm is given as thus:

1. Choose a suitable point set for sampling on an $(n-1)$ sphere.

2. Calculate a projection, denoted by $\{p^{\theta k}(t)\}_{t=1}^{T}$, of the input signal $\{\boldsymbol{v}(t)\}_{t=1}^{T}$ along the direction vector $\boldsymbol{x}^{\theta k}$, for all k (the whole set of direction vectors), giving $\{p^{\theta k}(t)\}_{k=1}^{K}$, as the set of projections.

3. Find the time instants $t_j^{\theta k}$ corresponding to the maxima of the set of projected signals $\{p^{\theta k}(t)\}_{k=1}^{K}$.

4. Interpolate $[t_j^{\theta k}, \boldsymbol{v}(t_j^{\theta k})]$ to obtain multivariate envelope curves $\{p^{\theta k}(t)\}_{k=1}^{K}$.

5. For a set of K direction vectors, the mean $\boldsymbol{m}(t)$ of the envelope curves is calculated as $\boldsymbol{m}(t) = 1/K\Sigma_{k=1}^{K} e\theta k(t)$.

6. Extract the "detail" $\boldsymbol{c_i}(t)$ using $\boldsymbol{c_i}(t) = \boldsymbol{v}(t) - \boldsymbol{m}(t)$ (i is an order of IMF). If the "detail" $\boldsymbol{c_i}(t)$ fulfills the stoppage criterion for a multivariate IMF, apply the above procedure to $\boldsymbol{v}(t) - \boldsymbol{c_i}(t)$, otherwise apply it to $\boldsymbol{c_i}(t)$.

4.3 MEMD Performance

MEMD was applied to MI classification by Park *et al.* 2013 [11] in order to compare its performance to other signal processing methods. They used two datasets, BCI Competition IV, Dataset I [103] and the PhysioNet Motor/Mental Imagery database [22].

4.3.1 Dataset 1

A 59 channel amplifier sampling at 1000 Hz recorded 200 trials each for four different participants. Each participant picked a combination of two MI movements: left hand, right hand, and feet. Each trial consisted of the participant imagining one of the two tasks they had picked for four seconds. The task for each trial was randomly selected but overall each task was performed for 100 of the 200 trials. Before undergoing processing for Park *et al.* 2013's [11] study , each trial was downsampled to 100 Hz and channels FC3, FC4, Cz, C3,

C4, C5, C6, T7, T8, CCP3, and CCP4 were selected. The data then had an 8 – 30 Hz bandpass filter applied. CWT, SWT, EMD, and MEMD were all individually applied to the dataset. For EMD and MEMD, IMF selection was done by choosing those that gave the best classification performance with the 140 training trials and then applying the same selection to the remaining 60 test trials. The IMFs for each channel were then summed back together. CSPs were used with each signal processing method to extract four features, with two of the spatial patterns being those that gave the greatest variance within a class and the other two being those that gave the least variance within the other class. These features were then input into an SVM with a Gaussian kernel. Their results are shown in Table 4.2.

4.3.2 Analysis

TABLE 4.2. COMPARISON OF CLASSIFICATION RATES BETWEEN MEMD AND OTHER SIGNAL PROCESSING METHODS FOR BCI COMPETITION DATASET [11]

Participant	Processing Method	Trials correctly classified (%)
a	None	82.3
	CWT	84.5
	SWT	84.0
	EMD	62.6
	MEMD	85.9
b	None	58.6
	CWT	71.0
	SWT	70.5
	EMD	57.3
	MEMD	73.9
c	None	60.2
	CWT	58.5
	SWT	72.2
	EMD	57.2
	MEMD	77.8
d	None	85.6
	CWT	88.1
	SWT	90.5
	EMD	72.3
	MEMD	91.5

Mean	None	71.7
	CWT	75.5
	SWT	79.3
	EMD	62.3
	MEMD	82.3

As shown by the results, MEMD outperforms all the other methods making it a marked improvement compared to the original EMD method. Standard EMD significantly underperforms compared to the other methods, even when no processing between the application of the Butterworth filter and the extraction of features using CSP occurs.

4.3.3 Dataset 2

The PhysioNet dataset recorded data from ten different participants using a 64 channel EEG cap sampling at 160 Hz. Each participant performed 45 trials of each imagined movement, with each trial involving four seconds of MI. The imagined movements were opening and closing the left fist and opening and closing the right fist. Channels FC3, FC4, Cz, C3, C4, C5, C6, T7, T8, CP3, and CP4 were selected for processing. Again, an 8 – 30 Hz bandpass filter was applied and then CWT, SWT, MEMD, but not EMD were all individually applied to the dataset. For MEMD, IMF selection was done by choosing those that gave the best classification performance with the 32 training trials per participant per class and then applying the same selection to the remaining 13 test trials. The IMFs for each channel were then summed back together. CSPs were used with each signal processing method to extract four features, with two of the spatial patterns being those that gave the greatest variance within a class and the other two being those that gave the least variance within the other class. These features were then input into an SVM with a Gaussian kernel. Their results are shown in Table 4.3.

4.3.4 Analysis

TABLE 4.3. COMPARISON OF CLASSIFICATION RATES BETWEEN MEMD AND OTHER SIGNAL PROCESSING METHODS FOR PHYSIONET DATASET [11]

Participant	Processing Method	Trials correctly classified (%)
1	None	74.2
	CWT	73.2
	SWT	65.1
	MEMD	77.2
2	None	86.1
	CWT	86.1
	SWT	73.0
	MEMD	86.0
4	None	61.2
	CWT	50.6
	SWT	54.6
	MEMD	66.4
7	None	96.0
	CWT	96.5
	SWT	78.1
	MEMD	97.1
12	None	62.7
	CWT	62.9
	SWT	54.6
	MEMD	64.0
13	None	65.6
	CWT	64.3
	SWT	59.1
	MEMD	65.5
15	None	69.5
	CWT	70.9
	SWT	64.2
	MEMD	71.2
25	None	61.9
	CWT	51.4
	SWT	60.1
	MEMD	77.6
26	None	74.3
	CWT	70.8
	SWT	57.9
	MEMD	74.2
29	None	96.6

	CWT	95.9
	SWT	81.9
	MEMD	97.4
Mean	None	74.8
	CWT	72.3
	SWT	64.9
	MEMD	77.7

Again, MEMD outperforms all the other methods though only by a few percentage points. In the three datasets it was not the highest performing, there was only a 0.1% difference between its performance and the highest performing method. SWT consistently performed worse than the other methods, even in comparison to no signal processing at all, highlighting how the wrong method can actually decrease the data's feature content. It is not specified why these specific participants' datasets were selected.

4.4 Temporal Multi-variate Empirical Mode Decomposition

T-MEMD is a variation of EMD that uses dynamical embedding and MEMD to extract temporal dynamics from a signal. The temporal dynamics of a signal refer to how the signal's properties, such as frequency and variance, change over time. In [104], James and Lowe 2003 were able to create an ICA method that could be applied to a single channel using dynamical embedding. As an ICA can only usually be applied to multi-channel signals and EEG has a high temporal resolution, when there is only one electrode source a possible workaround is to convert it into a multi-temporal channel signal. It makes the assumption that underlying segments of the measured brain activity is a system of a few degrees of freedom which are non-linearly interacting.

Dynamical embedding can be achieved using Takens' theorem [105], a delayed embedding algorithm that can separate a signal into a sequence of observations and preserves the system's properties. Takens' theorem is applied to each signal channel and this converts a

single channel of data into multiple snapshots of the signal in time using a series of delay vectors,

$$x(t) = [x(t - \tau), x(t - 2\tau), \dots, x(t - (m - 1)\tau)] \in R, \quad (4.1)$$

where τ is the lag and m is the embedding dimension. This new temporal multi-channel signal can now have multi-channel processing methods like ICA applied to it. Afterwards, the processed channels must be un-embedded using the inverse of the Equation 4.1 to return it to its original form,

$$s(t) = \frac{1}{m}\sum_1^m [s(t - \tau), s(t - 2\tau), \dots, s(t - (m - 1)\tau)] \in R, \quad (4.2)$$

This method generates new information in the form of added temporal dynamics with the aim of improving performance. T-MEMD is a similar method to single-channel ICA where MEMD is the multi-channel processing technique applied. The aim of this is to use temporal data to form more accurate and consistent IMFs from an individual channel.

This study was published in the paper "*Including Temporal Dynamics in Single Trial Motor Imagery Classification using Empirical Mode Decomposition*" as part of the conference proceedings for the 6th International Brain-Computer Interface Conference [106].

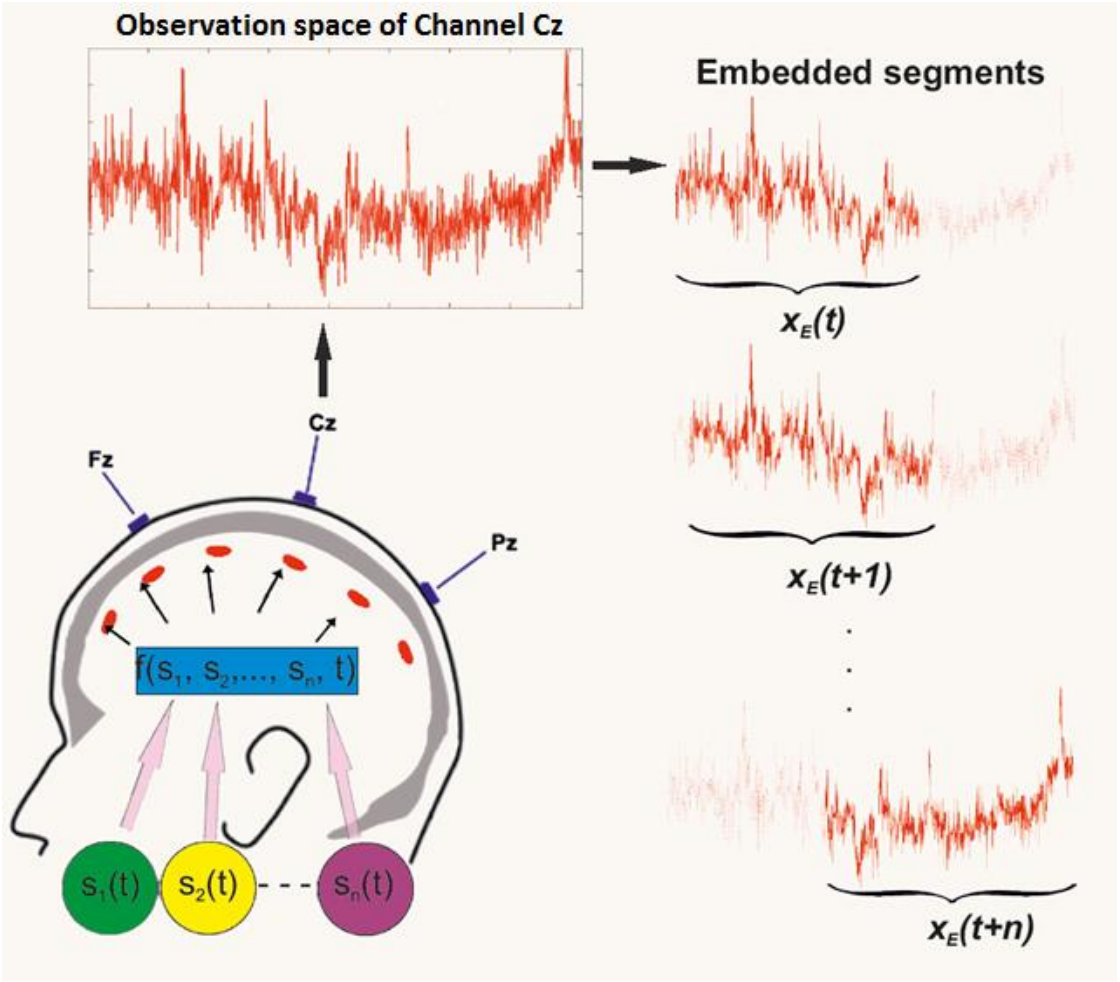

Fig. 4.7: The mixed signal sources that contribute to the overall non-linear EEG signal form a single observation space for each channel. Creating a matrix of delays helps to extract the underlying temporal correlations or structures from the signal.

4.5 T-MEMD Performance

In order to evaluate the performance of T-MEMD, it was applied to the same PhysioNet MI dataset as in section 4.3.3, albeit using a far greater number of trials in order to increase the results' robustness, so that the previous MEMD results could be used as a baseline. EMD was also applied to the same dataset to provide comparative results, as EMD contains the same spatial information as T-MEMD but not the extra temporal dynamics. Overall T-MEMD performed on a par with EMD, both achieving an average of 69% sensitivity and 70% specificity, indicating that the new temporal information was not contributing to the classifier's performance. This was theorised to be because the differences in the MI classes are inherently spatial.

4.5.1 Dataset 1

T-MEMD was applied to 11 participants, each having performed 90 trials, from the same PhysioNet MI dataset as in section 4.3.3, with the same 11 channels of FC3, FC4, Cz, C3, C4, C5, C6, T7, T8, CP3, and CP4 selected for processing for each trial. Some datasets were not of equal length, having +/- 200 samples difference before and after the stimulus cue. Therefore only participants with trials of equal sample length were selected. The data from the signal channels were dynamically embedded using Takens' theorem and MEMD applied to each channel's resulting multi-temporal channel signal. Previous literature on dynamical embedding states that the embedding dimension, *m*, should be greater than *2D + 1* in order to sufficiently capture the information content necessary [104], where *D* is the number of signal sources contributing to the overall signal. In the case of MI EEG, we know that left motor cortex activity, right motor cortex activity, α occipital activity, and high-amplitude muscle activity will be significant contributors, with a myriad of other sources making up background noise. To ensure sufficient embedding for a sampling rate of 160 Hz, an embedding dimension of *m = 30* was selected as it will be significantly higher than the possible number of signal sources. The smaller the lag, τ, the higher the resolution of the embedding window, therefore a lag of $\tau = 1$ was selected in order to provide the best possible resolution. This is in line with the dimension used by James and Lowe 2003 [104].

The resulting IMFs for each trial, for either EMD or T-MEMD, were un-embedded using Equation 4.2 and then selected or discarded based on two different methods, one knowledge-based and one performance-based. The knowledge-based method attempts to select relevant IMFs based on previous knowledge of the features of MI, i.e. changes in amplitude of a continuous 8 – 13 Hz signal called the μ-rhythm. An FFT was calculated for the duration of the signal that was recorded whilst MI activity was being performed. IMFs with at least 5% of their PSD between 8-13 Hz, the frequency range of the μ-rhythm, were

considered to have possible MI relevant data and are kept. This level of 5% was reached by evaluating the algorithm with changes to the level in steps of 5%. 5% was found to give the highest overall performance.

A method similar to the one used by Park *et al.* 2013 [11] in section 4.3.3 was tested in order to provide a more accurate comparison. This performance-based selection approach used a "brute force" method to identify the combination of IMFs that gives the best result per participant in terms of the number of trials correctly classified. Rather than selecting IMFs to use based on their content, this method simply processes every possible combination of IMFs and identifies the one that gave the best performance overall. Due to the number of IMFs per channel in this particular dataset never exceeding 13 and the number of IMFs containing useful information never exceeding five, it means that every classifier resulting from every possible combination of IMFs (maximum number of combinations: 2379) can be tested in a practical amount of time.

The selected IMFs were summed to form the processed signal and features were created for each trial using CSPs, with the first and last indexes of the feature set selected as they maximise the difference in variances between the two classes. The features were then input into an SVM with a linear kernel. As there were only 90 trials per user it was decided to use the Leave One Out method (LOO) [107]. The LOO method is a way to compensate for a small dataset by creating a training set with *1:n-1* trials and using the n^{th} trial as a test set. The result is recorded and then the n^{th} trial is swapped with one of the trials in the training set. This continues until all trials have been used as the test set and the cumulative result of their classification is used as the overall result of the classifier. No trial is used simultaneously in the training and test sets. The results are shown in Table 4.4.

4.5.2 Analysis

TABLE 4.4. COMPARISON OF PERFORMANCE BETWEEN EMD AND T-MEMD SIGNAL PROCESSING METHODS FOR PHYSIONET DATASET

Participant	Processing Method	Sensitivity (%)	Specificity (%)
8	EMD Knowledge-based	45.5	69.6
	T-MEMD Knowledge-based	50.0	45.7
	EMD Brute Force	65.9	67.4
	T-MEMD Brute Force	63.6	67.4
9	EMD Knowledge-based	38.3	23.3
	T-MEMD Knowledge-based	48.9	32.6
	EMD Brute Force	78.7	60.5
	T-MEMD Brute Force	74.5	67.4
10	EMD Knowledge-based	43.8	50.0
	T-MEMD Knowledge-based	75.0	59.5
	EMD Brute Force	75.0	69.0
	T-MEMD Brute Force	72.9	64.3
11	EMD Knowledge-based	62.2	53.3
	T-MEMD Knowledge-based	35.6	37.8
	EMD Brute Force	73.3	75.6
	T-MEMD Brute Force	62.2	71.1
12	EMD Knowledge-based	48.9	51.1
	T-MEMD Knowledge-based	51.1	53.3
	EMD Brute Force	66.7	66.7
	T-MEMD Brute Force	75.6	68.9
13	EMD Knowledge-based	53.2	53.5
	T-MEMD Knowledge-based	55.3	46.5
	EMD Brute Force	68.1	65.1
	T-MEMD Brute Force	74.5	76.7
14	EMD Knowledge-based	43.2	43.5
	T-MEMD Knowledge-based	50.0	52.2
	EMD Brute Force	63.6	67.4
	T-MEMD Brute Force	75.0	63.0
15	EMD Knowledge-based	53.3	53.3
	T-MEMD Knowledge-based	73.3	66.7
	EMD Brute Force	75.6	77.8
	T-MEMD Brute Force	82.2	84.4
16	EMD Knowledge-based	57.8	57.8
	T-MEMD Knowledge-based	57.8	53.3
	EMD Brute Force	64.4	71.1

	T-MEMD Brute Force	73.3	71.1
17	EMD Knowledge-based	41.3	34.1
	T-MEMD Knowledge-based	58.7	47.7
	EMD Brute Force	60.9	68.2
	T-MEMD Brute Force	67.4	65.9
18	EMD Knowledge-based	65.9	52.2
	T-MEMD Knowledge-based	29.5	43.5
	EMD Brute Force	65.9	69.6
	T-MEMD Brute Force	56.8	65.2
Mean	EMD Knowledge-based	50.3	49.2
	T-MEMD Knowledge-based	53.2	49.0
	EMD Brute Force	68.9	68.9
	T-MEMD Brute Force	70.7	69.6
Standard Deviation	EMD Knowledge-based	9.0	12.2
	T-MEMD Knowledge-based	13.6	9.6
	EMD Brute Force	5.8	4.7
	T-MEMD Brute Force	7.4	6.2

EMD and T-MEMD both achieved very similar performance with the difference between the two being well within their respective standard deviations in every case. The brute force method returned significantly higher performance than the knowledge based method for both decomposition methods. 50% in both sensitivity and specificity is the same performance random chance has in a binary-class system, implying that the knowledge-based method is not selecting the correct IMFs. Logically, as IMFs between trials are not consistent, the knowledge-based method has the potential to perform the highest as the brute force method selects the same IMFs for each trial by their index, regardless of their content. This means that the knowledge-based method's criterion for selecting IMFs is flawed; indicating that the composition of MI evoked potentials is more subtle beyond fluctuations in the μ-rhythm. Whilst the IMFs chosen with the brute force method were not consistent between users or decomposition methods, they did focus on the frequency bands known to contain MI information.

As Table 4.4 shows, there is negligible difference in performance between the current EMD method and the novel T-MEMD one, indicating that the added temporal dynamics do not contain any new information. In part, this may be due to the fact that the underlying processes for MI affect all channels, and whilst ERD/ERS and the μ-rhythm are expected to be stronger on one side of the brain versus the other, the changes still occur simultaneously for both hemispheres. This implies that the information content for MI is inherent in the lateralisation of the changes - i.e. spatially. In James and Lowe 2003 [104] adding temporal dynamics to ICA had a greater impact than with EMD because ICA contains zero temporal information, whilst EMD still uses the data laid out in chronological order. EMD can also only discard background noise if it is unstructured due to its criteria for identifying IMFs. IMFs are identified by whether if they are symmetrical with respect to zero across the entire duration of the original signal, meaning any artefact must be present throughout the signal for it to be separated into its own IMF. An artefact that does not have a rhythmic structure and has a short duration will be grouped into an IMF with signal data of the same frequency.

A single channel analysis of the method was carried out to see if embedding temporal data improved the robustness of the process. Channels C3 and C4 were selected as the literature and previous work in section 4.1.2 show them to be key when distinguishing between left limb MI and right limb MI. As CSPs need multiple channels to function the variance of each processed trial was used as the input of the SVM. These results are shown in Table 4.5.

TABLE 4.5. COMPARISON OF PERFORMANCE BETWEEN SINGLE CHANNEL EMD AND T-MEMD SIGNAL PROCESSING METHODS FOR PHYSIONET DATASET

Participant	Processing Method	Sensitivity using channel C3 (%)	Specificity using channel C3 (%)	Sensitivity using channel C4 (%)	Specificity using channel C4 (%)
8	EMD Knowledge-based	25.0	73.9	27.3	78.3
	T-MEMD Knowledge-based	29.5	76.1	31.8	71.7
	EMD Brute Force	47.7	73.9	36.4	82.6
	T-MEMD Brute Force	20.5	73.9	47.7	80.4

9	EMD Knowledge-based	76.6	18.6	87.2	0.0
	T-MEMD Knowledge-based	70.2	25.6	87.2	0.0
	EMD Brute Force	63.8	62.8	85.1	37.2
	T-MEMD Brute Force	78.7	0.0	87.2	27.9
10	EMD Knowledge-based	79.2	0.0	87.5	0.0
	T-MEMD Knowledge-based	97.9	0.0	77.1	19.0
	EMD Brute Force	87.5	35.7	81.3	45.2
	T-MEMD Brute Force	79.2	40.5	81.3	33.3
11	EMD Knowledge-based	53.3	42.2	48.9	37.8
	T-MEMD Knowledge-based	0.0	0.0	0.0	0.0
	EMD Brute Force	66.7	46.7	80.0	48.9
	T-MEMD Brute Force	71.1	40.0	75.6	46.7
12	EMD Knowledge-based	37.8	24.4	0.0	0.0
	T-MEMD Knowledge-based	33.3	64.4	0.0	0.0
	EMD Brute Force	73.3	46.7	68.9	42.2
	T-MEMD Brute Force	55.6	46.7	68.9	51.1
13	EMD Knowledge-based	46.8	62.8	95.7	0.0
	T-MEMD Knowledge-based	46.8	51.2	63.8	7.0
	EMD Brute Force	61.7	69.8	59.6	51.2
	T-MEMD Brute Force	55.3	67.4	53.2	55.8
14	EMD Knowledge-based	0.0	67.4	0.0	56.5
	T-MEMD Knowledge-based	4.5	58.7	43.2	58.7
	EMD Brute Force	70.5	54.3	70.5	54.3
	T-MEMD Brute Force	79.5	47.8	70.5	63.0
15	EMD Knowledge-based	51.1	15.6	62.2	31.1
	T-MEMD Knowledge-based	55.6	37.8	66.7	46.7
	EMD Brute Force	88.9	35.6	66.7	48.9
	T-MEMD Brute Force	84.4	42.2	71.1	51.1
16	EMD Knowledge-based	46.7	62.2	46.7	26.7
	T-MEMD Knowledge-based	35.6	53.3	35.6	60.0
	EMD Brute Force	48.9	82.2	48.9	66.7
	T-MEMD Brute Force	46.7	71.1	46.7	64.4
17	EMD Knowledge-based	52.2	0.0	71.7	25.0
	T-MEMD Knowledge-based	39.1	47.7	71.7	11.4
	EMD Brute Force	89.1	25.0	91.3	29.5

	T-MEMD Brute Force	82.6	29.5	78.3	43.2
18	EMD Knowledge-based	43.2	58.7	45.5	63.0
	T-MEMD Knowledge-based	0.0	71.7	25.0	56.5
	EMD Brute Force	61.4	52.2	63.6	50.0
	T-MEMD Brute Force	61.4	52.2	54.5	54.3
Mean	EMD Knowledge-based	46.5	38.7	52.1	28.9
	T-MEMD Knowledge-based	37.5	44.2	45.6	30.1
	EMD Brute Force	69.0	53.2	68.4	50.6
	T-MEMD Brute Force	65.0	46.5	66.8	51.9
Standard Deviation	EMD Knowledge-based	21.9	27.8	33.2	27.9
	T-MEMD Knowledge-based	30.2	26.1	30.1	28.5
	EMD Brute Force	14.7	17.7	16.2	14.2
	T-MEMD Brute Force	19.6	20.9	14.1	14.6

As before the brute force method significantly outperforms the knowledge-based method and EMD and T-MEMD perform on a par with each other. Compared to the 11 channel performance the single channel method preserves its sensitivity for the most part, but sees a substantial drop in specificity indicating that the classifier is not as robust with less channels and their corresponding spatial information as class difference in MI is predominantly spatial. Figure 4.8 shows a spectrogram of the average signals for each processing and classification method.

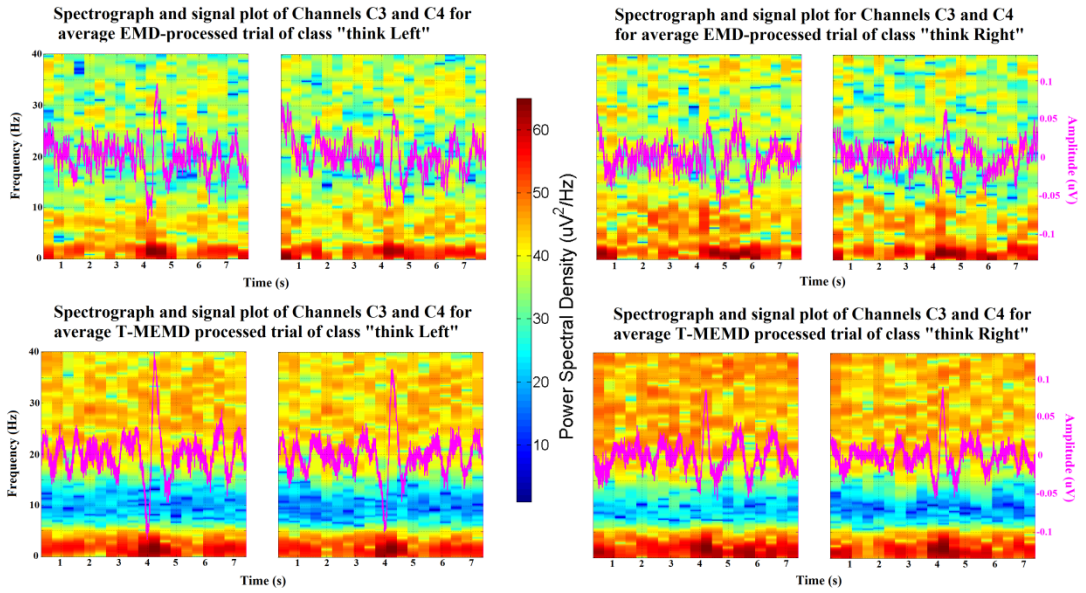

Fig. 4.8: This figure shows the spectrograms for the average processed signal obtained with the brute force method with the waveform itself superimposed in purple. The plots are for electrodes C3 and C4, for the classes "think Left" and "think Right" respectively for the EEG data of User 11. The first row is the original EMD method and the bottom row is the enhanced T-MEMD method with the direction stimulus occurring exactly half way across the x-axis. In this case, T-MEMD has created visibly clearer ERD/ERS peaks at the 4 second mark when motor imagery is initiated.

Ultimately the added temporal dynamics did not significantly improve the classification performance. However it might still have some effect on performance if applied to an EEG signal with significant temporally independent features, which is not the case in MI. Another way to enhance the method could be to incorporate both spatial and temporal information by decomposing all channels in their multi-temporal form simultaneously using MEMD.

4.6 Spatio-Temporal Multi-variate Empirical Mode Decomposition

ST-MEMD is the second novel variation of EMD that is built on the work done with T-MEMD. The process is very similar to T-MEMD in that each channel is dynamically embedded using Takens' theorem and then has MEMD applied to it before being un-embedded, except instead of applying MEMD to each embedded channel individually, all

the embedded channels are decomposed simultaneously. The difference is highlighted in the equations below.

$$Cz = [x_1, x_2, \dots, x_n] \tag{4.3}$$

$$Takens'(Cz) = \begin{bmatrix} x_1, x_2, \dots, x_{n-m} \\ x_{1+\tau}, x_{2+\tau}, \dots, x_{n-m+\tau} \\ . \\ . \\ . \\ x_{1+m\tau}, x_{2+m\tau}, \dots, x_{n+m\tau} \end{bmatrix}^T \tag{4.4}$$

A single EEG channel, Cz, is converted into a matrix of delay vectors, $Takens'(Cz)$, with embedding *m* and lag τ using Takens' theorem.

$$T\text{-}MEMD(Cz) = MEMD \begin{bmatrix} x_1, x_{1+\tau}, \dots, x_{1+m\tau} \\ x_2, x_{2+\tau}, \dots, x_{2+m\tau} \\ . \\ . \\ . \\ x_{n-m}, x_{n-m+\tau}, \dots, x_{n+m\tau} \end{bmatrix} \tag{4.5}$$

T-MEMD decomposes each embedded channel individually, using only the information from each observation's temporal neighbours to inform their decomposition.

$$ST\text{-}MEMD = MEMD\begin{bmatrix} Cz\begin{Bmatrix} x_1, x_{1+\tau}, \dots, x_{1+m\tau} \\ x_2, x_{2+\tau}, \dots, x_{2+m\tau} \\ . \\ . \\ . \\ x_{n-m}, x_{n-m+\tau}, \dots, x_{n+m\tau} \end{Bmatrix} \\ Fpz\begin{Bmatrix} x_1, x_{1+\tau}, \dots, x_{1+m\tau} \\ x_2, x_{2+\tau}, \dots, x_{2+m\tau} \\ . \\ . \\ . \\ x_{n-m}, x_{n-m+\tau}, \dots, x_{n+m\tau} \end{Bmatrix} \\ . \\ . \\ . \\ Oz\begin{Bmatrix} x_1, x_{1+\tau}, \dots, x_{1+m\tau} \\ x_2, x_{2+\tau}, \dots, x_{2+m\tau} \\ . \\ . \\ . \\ x_{n-m}, x_{n-m+\tau}, \dots, x_{n+m\tau} \end{Bmatrix} \end{bmatrix} \quad (4.6)$$

ST-MEMD decomposes all embedded channels simultaneously, using the information from each observation's temporal and spatial neighbours to inform their decomposition. This allows both temporal and spatial dynamics to be incorporated into each IMF.

4.7 ST-MEMD Performance

As with T-MEMD, in order to evaluate the performance of ST-MEMD, it was applied to the same PhysioNet MI dataset as in 4.5.1 so that the previous MEMD results could be used as a baseline. MEMD was also applied to the same dataset to provide comparative results, as MEMD contains the same spatial information as ST-MEMD but not the extra temporal dynamics.

4.7.1 Dataset 1

ST-MEMD followed the same methodology as T-MEMD as detailed in 4.3.1.1. The same 11 channels of FC3, FC4, Cz, C3, C4, C5, C6, T7, T8, CP3, and CP4 were selected for processing. An embedding dimension of $m = 30$ was selected and a lag of $\tau = 1$ was selected. The same two methods for selecting or discarding a channel's IMFS were used: one knowledge-based

and one performance-based. For the knowledge-based method an FFT was calculated for the duration of the signal that was recorded after the stimulus cue and IMFs with at least 5% of their total PSD between 8-13 Hz, the frequency range of the μ-rhythm, were kept. The performance-based method used a brute force method to identify the combination of IMFs that gave the best result per participant in terms of the number of trials correctly classified. As with this dataset the number of IMFs per channel never exceeds 13 and the IMFs containing useful information never exceeds 5 in number, it means that the classifiers resulting from all possible combinations of IMFs (maximum number of combinations: 2379) can be tested in a practical amount of time.

The selected IMFs were summed to form the processed signal and features were created for each trial using CSPs. The features were then input into an SVM with a linear kernel and again the LOO method was used to create a set of test sets. The results are shown in Table 4.6.

4.7.2 Analysis

TABLE 4.6. COMPARISON OF PERFORMANCE BETWEEN MEMD AND ST-MEMD SIGNAL PROCESSING METHODS FOR PHYSIONET DATASET

Participant	Processing Method	Sensitivity (%)	Specificity (%)
8	MEMD Knowledge-based	56.8	52.2
	ST-MEMD Knowledge-based	27.3	26.1
	MEMD Brute Force	77.3	78.3
	ST-MEMD Brute Force	65.9	76.1
9	MEMD Knowledge-based	40.4	32.6
	ST-MEMD Knowledge-based	53.2	32.6
	MEMD Brute Force	66.0	74.4
	ST-MEMD Brute Force	76.6	69.8
10	MEMD Knowledge-based	77.1	64.3
	ST-MEMD Knowledge-based	79.2	61.9
	MEMD Brute Force	83.3	76.2
	ST-MEMD Brute Force	83.3	71.4
11	MEMD Knowledge-based	40.0	53.3

	ST-MEMD Knowledge-based	60.0	48.9
	MEMD Brute Force	62.2	77.8
	ST-MEMD Brute Force	71.1	64.4
12	MEMD Knowledge-based	64.4	71.1
	ST-MEMD Knowledge-based	57.8	53.3
	MEMD Brute Force	86.7	80.0
	ST-MEMD Brute Force	88.9	80.0
13	MEMD Knowledge-based	44.7	55.8
	ST-MEMD Knowledge-based	53.2	69.8
	MEMD Brute Force	80.9	76.7
	ST-MEMD Brute Force	74.5	81.4
14	MEMD Knowledge-based	45.5	52.2
	ST-MEMD Knowledge-based	54.5	54.3
	MEMD Brute Force	72.7	67.4
	ST-MEMD Brute Force	77.3	77.3
15	MEMD Knowledge-based	40.0	57.8
	ST-MEMD Knowledge-based	71.1	73.3
	MEMD Brute Force	86.7	80.0
	ST-MEMD Brute Force	88.9	77.8
16	MEMD Knowledge-based	46.7	44.4
	ST-MEMD Knowledge-based	55.6	44.4
	MEMD Brute Force	80.0	68.9
	ST-MEMD Brute Force	71.1	64.4
17	MEMD Knowledge-based	34.8	29.5
	ST-MEMD Knowledge-based	52.2	45.5
	MEMD Brute Force	73.9	72.7
	ST-MEMD Brute Force	73.9	54.5
18	MEMD Knowledge-based	47.7	63.0
	ST-MEMD Knowledge-based	25.0	50.0
	MEMD Brute Force	65.9	69.6
	ST-MEMD Brute Force	61.4	69.6
Mean	MEMD Knowledge-based	48.9	52.4
	ST-MEMD Knowledge-based	53.5	50.9
	MEMD Brute Force	76.0	74.7
	ST-MEMD Brute Force	75.7	71.5
Standard Deviation	MEMD Knowledge-based	12.5	12.7
	ST-MEMD Knowledge-based	15.9	14.2
	MEMD Brute Force	8.5	4.5

	ST-MEMD Brute Force	8.7	8.1

As with T-MEMD, the brute force method consistently outperformed the knowledge-based one significantly, with the knowledge-based selection criteria returning the same performance as random chance would. Like before, the difference in performance between the MEMD and ST-MEMD methods was negligible, again indicating that the added temporal dynamics did not contribute anything to the classifier. MEMD and ST-MEMD did outperform EMD and T-MEMD with an approximate 5% increase in sensitivity and specificity, showing that the extra spatial information did enhance the classifier slightly. Figure 4.8 shows a spectrogram of the average signals for each processing and classification method.

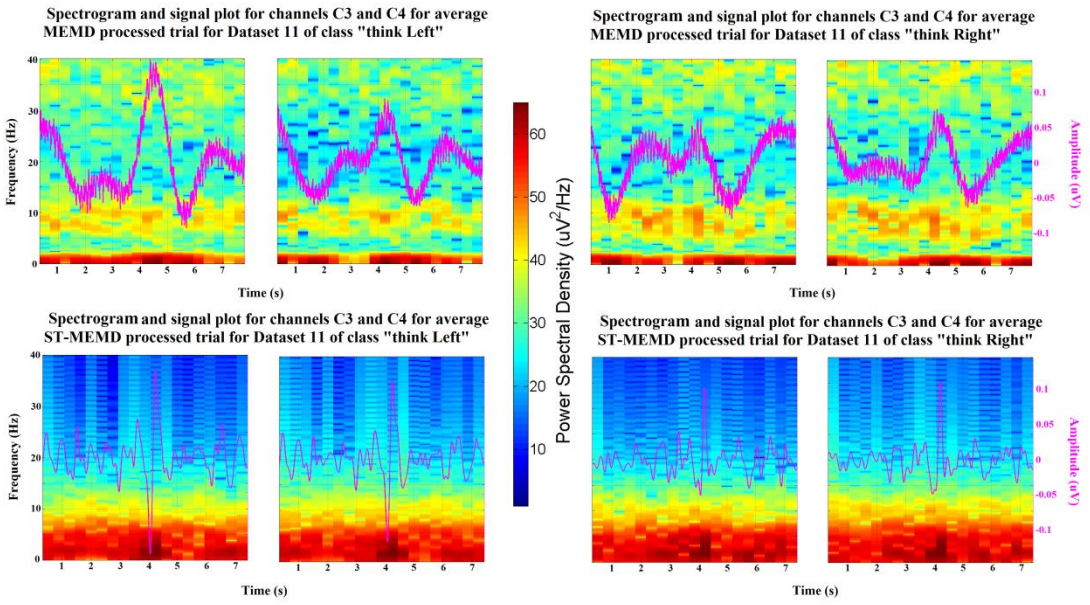

Fig. 4.9: This figure shows the spectrograms for the average processed signal obtained with the brute force method with the waveform itself superimposed in purple. The plots are for electrodes C3 and C4, for the classes "think Left" and "think Right" respectively for the EEG data of User 11. The first row is the original MEMD method and the bottom row is the enhanced ST-MEMD method with the direction stimulus occurring exactly half way across the x-axis. In this case, ST-MEMD has created much more visibly clearer ERD/ERS peaks at the 4 second mark when motor imagery is initiated, with all the power concentrated in the lower frequencies.

The fact that ST-MEMD maintained performance parity with MEMD shows that the extra spatial information was preserved, and reinforces the idea that temporal dynamics contribute nothing to classifying MI as the differences between the two classes are inherently spatial and housed in the lateralised changes in power. This means that ST-MEMD and T-MEMD could still produce an increase in performance if applied to a signal dataset that relied heavily on temporal dynamics to distinguish between the possible classes.

Table 4.3 in section 4.3.4 reports on the results obtained by Park *et al.* 2013 [11] for a range of different signal processing methods for several participants from the same dataset T-MEMD and ST-MEMD have been applied to in this study. This study used data from three of the same participants that Park *et al.* 2013 [11] used, allowing for a direct comparison in performance, as reported in Table 4.7.

TABLE 4.7. COMPARISON OF PERFORMANCE BETWEEN DIFFERENT METHODS IN THE LITERATURE AND THE PERFORMANCE IN THIS STUDY FOR PHYSIONET DATASET

Participant	Processing Method	Trials correctly classified (%)
12	None	62.7
	CWT	62.9
	SWT	54.6
	MEMD (Park *et al.* 2013 [11])	64.0
	EMD (Brute Force)	66.7
	T-MEMD (Brute Force)	72.2
	MEMD (Brute Force)	83.3
	ST-MEMD (Brute Force)	84.4
13	None	65.6
	CWT	64.3
	SWT	59.1
	MEMD (Park *et al.* 2013 [11])	65.5
	EMD (Brute Force)	66.6
	T-MEMD (Brute Force)	75.6
	MEMD (Brute Force)	78.8
	ST-MEMD (Brute Force)	77.9
15	None	69.5
	CWT	70.9

	SWT	64.2
	MEMD (Park *et al.* 2013 [11])	71.2
	EMD (Brute Force)	76.7
	T-MEMD (Brute Force)	83.3
	MEMD (Brute Force)	83.3
	ST-MEMD (Brute Force)	83.3
Mean	None	65.9
	CWT	66.0
	SWT	59.3
	MEMD (Park *et al.* 2013 [11])	66.9
	EMD (Brute Force)	70.0
	T-MEMD (Brute Force)	77.0
	MEMD (Brute Force)	81.8
	ST-MEMD (Brute Force)	81.9

As mentioned in sections 4.3.2 and 4.3.4, Park *et al.* 2013's [11] MEMD method outperformed the other methods applied to the same dataset: EMD, CWT and SWT. As can be seen in Table 4.7, the results obtained in this study outperformed Park *et al.* 2013's [11] in terms of classification accuracy, sometimes by up to 15%. However, as the highest performing methods are those that use the same spatial MEMD method as a basis that Park *et al.* 2013 [11] created, it can be concluded that the differences in performance are due to the IMF selection methods. Should the same selection methods and classifier have been used so that the MEMD performance in this study was on a par with Park *et al.* 2013's [11], then EMD and T-MEMD would have performed worse than SWT and CWT if they had maintained the same proportional difference in performance compared to MEMD. It should also be noted that whilst in Table 4.7 T-MEMD consistently outperforms EMD, when using the much larger dataset in Table 4.4 its performance is shown to be on a par with EMD. In fact with all three of the participants used by both Park *et al.* 2013 [11] and this study, by chance they are all participants that achieved above average performance in the results reported in sections 4.6.2 and 4.8.2, highlighting the importance of using a large dataset when evaluating new signal processing methods.

For further comparison, Sleight *et al.* 2009 [108] applied ICA to the same PhysioNet MI database. However, it cannot be a direct comparison as they evaluated 103 participants from the database compared to the 11 in this study, and used data from only channels C3, Cz and C4. Using ICA combined with an SVM classifier they achieved 64% classification accuracy with a 5% standard deviation. Whilst this performed approximately 10% worse compared to this study's MEMD and ST-MEMD methods, to achieve a lower standard deviation for their method despite the much larger dataset means that their classifier was very consistent in the features it extracted from the data.

Sita and Nair 2013 [109] also applied ICA with an SVM classifier to all 64 channels of 30 unlabelled participants, achieving a classification accuracy of 67.8%, lower than that of MEMD and ST-MEMD, but a few percentage points higher than that of EMD and T-MEMD.

This study was published in the paper "Using Empirical Mode Decomposition with Spatio-Temporal Dynamics to Classify Single-Trial Motor Imagery in BCI" as part of the conference proceedings for the 2014 Annual International of the IEEE Engineering in Medicine and Biology Society [110].

4.8 Summary

EMD's adaptive, data-driven nature has been shown to make a good application for decomposing EEG signals into components by frequency. Initial studies showed that the original EMD method could achieve good performance when used to extract features from an MI BCI paradigm. The MEMD method obtained from the literature built on EMD by applying it to all the signals simultaneously in order to use their spatial information to inform each channel's decomposition. This was shown to produce a significant increase in performance, and on that basis it was developed further by using it as the basis for the novel methods of T-MEMD and ST-MEMD. It was hypothesised that MEMD applied to multi-temporal channels would produce a similar boost in performance that its application

to multi-variate channels did, and that MEMD applied to both multi-temporal and multi-variate channels would result in their combined performance increases.

To that end a large dataset of 990 trials from 11 different participants was obtained from an MI BCI system from the literature, and all four methods of EMD, T-MEMD, MEMD and ST-MEMD were applied under the same circumstances in order to produce directly comparable results. The results showed that the added temporal dynamics did not produce an increase in performance, though the extra spatial dynamics produced by MEMD and ST-MEMD did. This reinforces the idea that the key attributes of MI are spatial. Compared to other methods in the literature applied to the same dataset the spatial variants of EMD outperformed them all. The brute force method applied in this study led to an increase in performance over Park *et al.* 2013's [11] application of MEMD to this dataset. This method of evaluating every single possible combination of signal component derived using an EMD-based signal processing technique is only possible with techniques that decompose a signal into non-abstracted domains, the same domain as the original signal in EMD's case, something that many methods such as CWT cannot do.

CHAPTER 5

A Novel form of stimulation in BCI

This chapter will cover the subject of tactile stimulation in greater detail and the hypothesis of exploiting a person's absolute threshold of vibrotactile stimulation to generate evoked potentials in EEG. To evaluate this hypothesis a study was carried out to gather preliminary data. An experimental protocol was devised and a stimulus system constructed to help characterise the required forms of vibrotactile stimulation. Once this was finalised and ethical approval was granted and subsequently recruitment of participants began, a series of experiments were carried out and the data analysed. The results appear to disprove the hypothesis, though the presence of large persistent rhythmic artefacts from the equipment may have compromised and invalidated the data.

5.1 Tactile stimulation

The brain can be stimulated through three primary channels: visual, auditory and tactile [111]. BCIs that make use of visual and auditory stimuli tend to be the focus of the majority of BCI research as it is easier to make those forms of stimuli applied consistently and the equipment to produce the stimuli is readily available with any personal computer. However sight and sound are the primary channels through which people receive information about the world around them, and it would be preferable to leave them clear for day-to-day actions instead of occupying them entirely with a stimulus for a BCI. Also, people suffering from conditions such as ALS can eventually lose motor control over their eyes and eyelids, making a stimulus dependent on voluntary eye-gazing such as SSVEPs difficult to control.

Any BCI paradigm can function no matter the form the stimulus takes. For example, a P300 BCI that relies on a rare but expected stimulus occurring amongst a repetition of another stimulus could use a picture of a person for the rare stimulus and a solid red screen for the common one for visual stimuli, a high-pitched note for the rare stimulus and a low-pitched for the common one for auditory stimuli, and a vibratory pulse on the participant's left hand for the rare stimulus versus one applied to their right hand for the common one for tactile stimuli [111]. Studies from the literature give mixed results on how effective one type of stimulus is compared to another. Brouwer *et al.* 2010 [112] compared the offline classification accuracies for tactile and visual P300 BCIs for 8 participants, and on average the resulting classification accuracies were almost identical with a +/- 1% difference in each of the 10 variations of classifier applied. Thurlings *et al.* 2012 [113] carried out the same experiment for 10 participants, and found on average that classification accuracy for the tactile P300 BCI was consistently 20% worse than the visual P300 BCIs' for each type of classifier. Whilst Kaufmann *et al.* 2013 [114] tested visual, auditory and tactile P300s on a single locked-in patient and found the offline classification accuracy for the tactile P300 BCI to be anywhere from 20-50% better than the visual P300 BCIs', and 40-70% better than the auditory P300 BCIs', depending on the classifier used. Chang *et al.* 2013 [115] compared the performance of visual and auditory P300 BCIs for 16 participants and found on average that the visual P300 BCI performed 43% better than the auditory one. Comparatively Severens *et al.* 2014 [116] found on average that the performance of tactile and visual P300 BCIs for 11 participants were similar, with the tactile BCI performing 3% worse. Whilst it is not conclusive which form of stimulus performs best, there is overwhelming evidence that visual, auditory and tactile BCIs each perform well enough to function practically.

The fingers, being very sensitive due to large clusters of nerve cells as shown in Figure 5.1, are an ideal site for stimulation. Johansson and Flanagan 2009 [117] analysed the different nerve endings in the human hand and catalogued their properties:

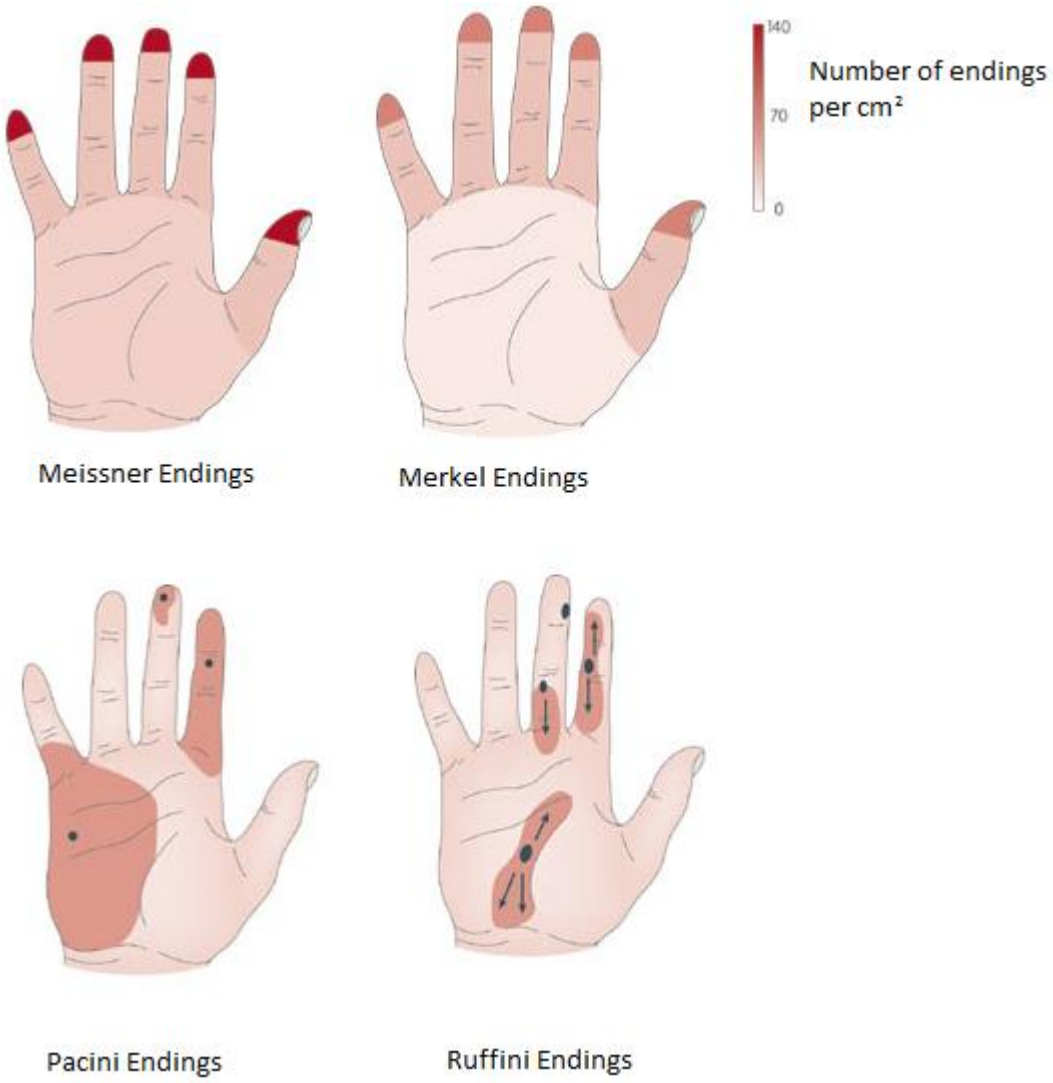

Fig. 5.1: The relative densities and locations of the different types of nerve endings. Meissner endings are the most numerous and uniformly present on the fingertips [117].

- Meissner endings are the most numerous and are present throughout the whole hand, but most dense on the fingertips. They are sensitive to dynamic skin deformation from stimuli between 5 – 50 Hz.
- Merkel endings are the second most prevalent. They are also mostly located on the fingertips with mild density around the inner-facing skin of the fingers. They are sensitive to dynamic skin deformations at frequencies that are less than 5 Hz.

- Pacini endings have a more dense distribution than Merkel endings but are only present on the index finger, the fingertip of the middle finger, and the inner palm. They are sensitive to high-frequency vibrations between 40 – 400 Hz.
- Ruffini endings are the least prevalent and are located around tension points on the inner hand, such as where the palm or knuckles fold. They are sensitive to tension placed on the skin from stretching.

As Meissner endings are uniformly present on all fingers and their stimulus range of 5 – 50 Hz overlaps the most with the frequencies of brain activity (0.5 – 40 Hz), meaning the frequencies they detect will result in SSSEPs occurring in the same spectrum as most EEG activity, they make the most likely target for receiving external stimuli. Johansson and Flanagan 2009 [117] also note that they are very sensitive, second only to the sensitivity of Pacini endings.

5.2 Steady-State Somatosensory Evoked Potentials

SSEPs are one of the easiest brain responses to stimuli to measure so it made sense for tactile research to start with this BCI paradigm. Snyder 1992 [118] investigated the changes in Steady-State Somatosensory Evoked Potential (SSSEP) response in order to identify the stimulus frequency that resulted in the SSSEP with the highest SNR. 17 volunteers aged between 18 – 28 had electrodes placed on 10-20 positions Fp1, Fp2, F3, F4, C3, C4, P3, P4, O1, 02, F7, F8, T3, T4, T5 and T6. Participants placed one hand on a vibrating plastic hemisphere 8 cm in diameter to receive vibrotactile stimuli. The frequencies of 2, 3, 5, 7, 11, 17, 26 and 40 Hz were selected for testing. The vibrationary device could not oscillate at frequencies that low so a modulated carrier wave was used, as shown in Figure 5.2. This is where a higher-frequency carrier wave is turned on and off at consistent intervals to generate a modulated low-frequency wave. For the experiment participants closed their eyes whilst their hand rested on the stimulus device. Eight blocks of stimulation lasting six

seconds each with the frequency changing between each block were applied. Snyder concluded that the FFTs showed that 26 Hz consistently gave the largest increase in PSD in comparison to the brain's background activity, with the SSSEP being centred on the motor cortex. Overall there was a latency of 0.058 seconds between onset of stimulus and detecting the presence of an SSSEP.

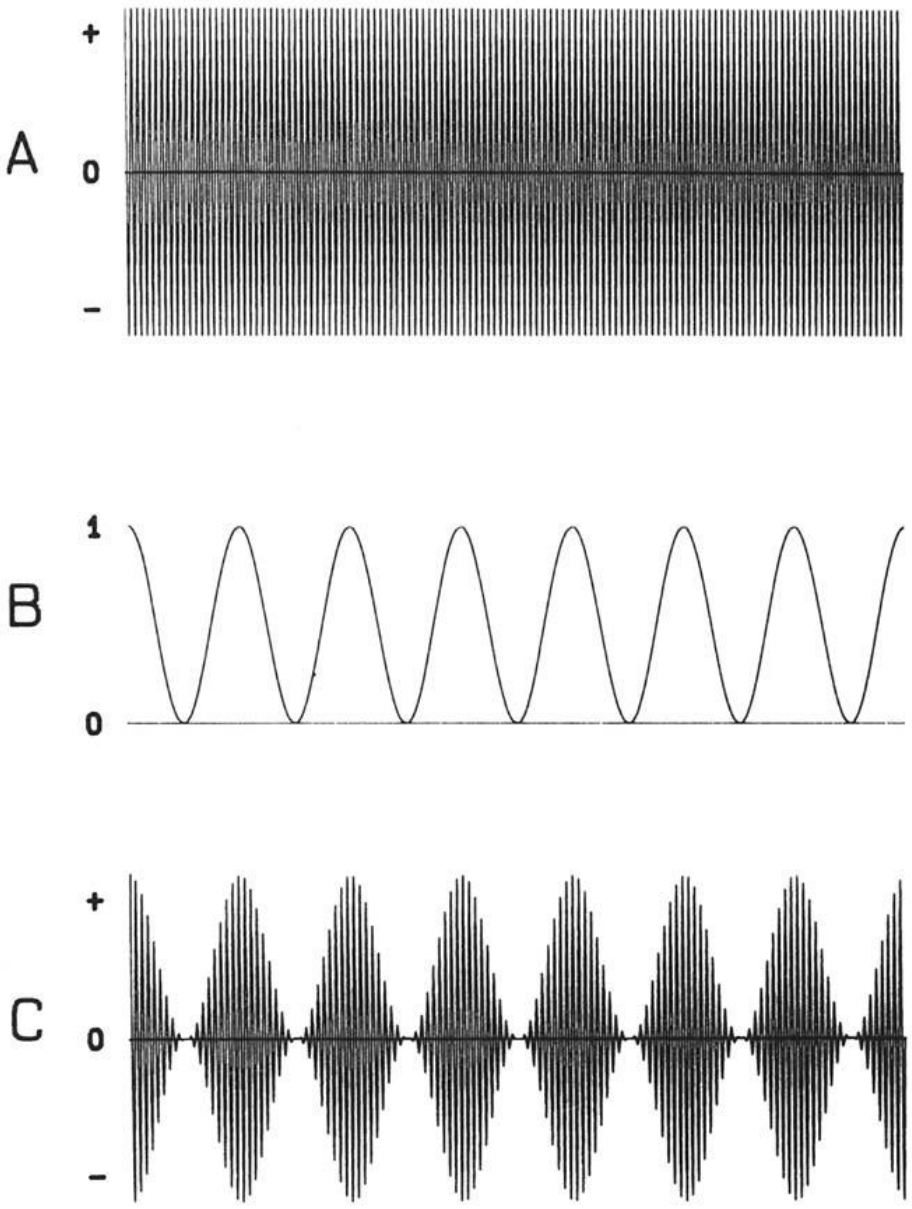

Fig. 5.2: Waveform A represents the high frequency carrier wave, B is the modulation frequency and C is the final stimulus signal. This combination of carrier and modulation frequencies allows high-frequency source to produce low-frequency waveforms [118].

5.2.1 SSSEP Performance

Giabbiconi *et al.* 2004 [119] carried out a study to see if attentional modulation could impact the amplitude of SSSEPs. If confirmed, it would provide a new approach to investigate the neural mechanisms of spatial attention. 11 healthy adults were recruited. Participants were seated in a chair with their hands resting on small tables either side of them. A 6 mm rod connected to a shielded solenoid transducer protruding through each table stimulated the left and right index fingers of the participants at a force of 4.9 N. The left finger was stimulated at 20 Hz and the right at 26 Hz. 0.05 seconds into the trial one finger would be briefly stimulated by the transducer, indicating to the participant to focus on that hand for the duration of the trial. After a variable 0.2 – 0.3 second pause both fingers would be stimulated for 3 seconds. EEG was recorded using 30 electrodes at a sampling frequency of 250 Hz. Analysis of the data found that on average the amplitude of the SSSEP being focused on increased by 29.2%, showing that attentional modulation does affect the amplitude of SSSEPs. Furthermore they found that the amplitude was greatest in the channels contralateral to the finger being focused on, which conforms to the known physiology of the somatosensory cortex. They also found no decrease in the SSSEP amplitude over time, indicating that habituation was not a factor.

Muller-Putz *et al.* 2006 [42] detail the creation and testing of an attentional modulation SSSEP-based BCI in order to show that SSSEPs can be a suitable basis for a BCI, as it would dispense with the need for voluntary gaze control compared to SSVEP-based BCIs, something that ALS patients have difficulty with as their condition progresses. Five volunteers had electrodes applied to channels C3 and C4 with a sampling frequency of 200 Hz. Figure 5.3 shows the timings of the experiment. Each trial began with two seconds of no stimuli. After the two seconds two frequencies of equal amplitude were applied to each hand of the participants, producing two SSSEPs in the EEG recordings. After one more

second a visual cue indicating left or right was displayed. If the cue was left the participant focused on the sensation in their left hand and if it was right they focused on their right hand. This lasted for three more seconds. At the 5.7 second mark an "amplitudinal twitch", a sudden but brief decrease in the stimulus amplitude, was sent through the transducers. This twitch is what the participants were instructed to be aware of, causing them to focus attention on the relevant hand. The paradigm is the same as that in the study by Giabbiconi *et al.* 2004 [119], the SSSEP produced by the frequency applied to the hand that was being focused on would increase in amplitude whilst the SSSEP produced by the other hand would decrease, thus giving us a two-class selection where participants could choose between left or right.

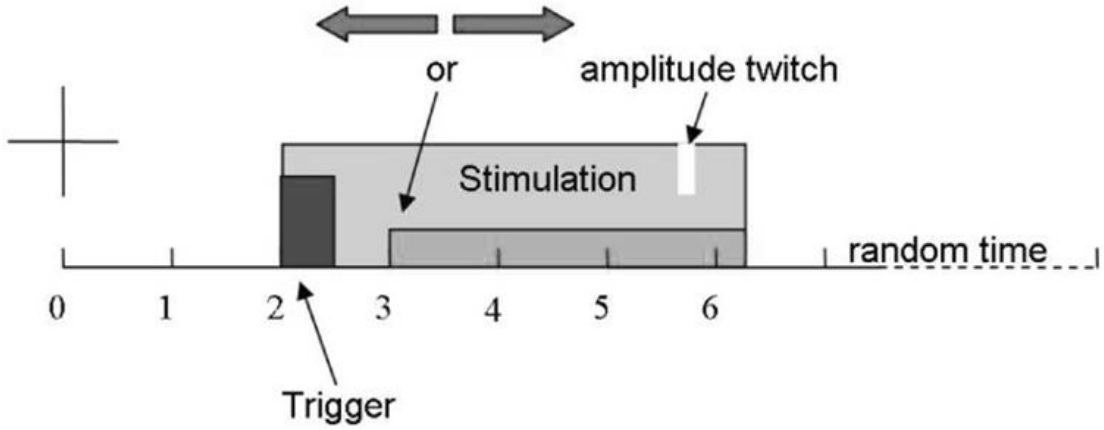

Fig. 5.3: Timing of Muller-Putz et al. 2006's BCI paradigm. After a 2 second pause the stimulus is activated. After another second a directional cue is displayed to the participant. The participant focuses on the indicated hand for the next 3 seconds. At the 5.7 second mark the amplitudinal twitch will occur for 0.125 seconds [42].

160 trials per subject were carried out per day, with 80 trials per class. Participants returned for a further 160 trials per day for up three times over a period of five days. The 180 trials from the first day were used to create an LDA classifier to provide online feedback to the participants in the subsequent trials. However, when calculating the accuracy of the results the offline classifier was used. The time point of the sample that produced the optimum classifier was also recorded. This study's offline classifier consisted

of a Lock-in Analyser System (LAS) to extract a set of features and then classified them using LDA. An LAS can be defined as

$$f_{out}(t) = \frac{1}{T}\int_{s-T}^{T} \sin\left(2\pi f_{ref} s + \varphi\right) f_{in}(t)\mathrm{d}s \tag{5.1}$$

where T is the integration period, t is the current time sample, φ is the phase, f_{ref} is the reference signal, and f_{in} is the input signal. An LAS is similar to a very narrow bandpass filter, except that it also provides information on the signal's phase and amplitude. It can extract a low-amplitude sinusoidal signal from a mixture of signals so long as it has a reference signal of the same frequency, which is the case in an SSSEP BCI. The LAS multiplies the EEG signal with the reference signal and then integrates it over the specified time, T. This results in a signal where frequencies dissimilar to that of the reference signal are attenuated to zero. If the signal is out of phase it will also be attenuated. The LAS's phase must be specified beforehand.

Whilst the results shown in Table 5.1 indicate that some intent could be discerned, they rarely exceeded the minimum accuracy of 70%, which is considered the minimum limit for an assistive communications device [120]. Muller-Putz *et al.* 2006 [42] surmise this is down to possible concentration issues. An SSVEP allows you to eliminate the other class's stimulation by turning your head until it is out of view. However with an SSSEP the other class's stimulation is still felt and relies on the participant's mental focus to block it out. The optimum time point where the classes were at their most distinct from each other was consistently towards the end of the trial. Whilst Muller-Putz *et al.* 2006 [42] do not discuss why, it could be speculated that the participant would be most consciously focusing on the stimulus near the time point of the amplitudinal twitch in anticipation of it, which is in the final second of the trial.

TABLE 5.1. OFFLINE CLASSIFICATION RATES OF SSSEPS AND THE CLASSIFIER'S OPTIMUM TIME POINT FOR MULLER-PUTZ *ET AL.'S* 2006 STUDY [42]

Subject	Accuracy (%)	Optimum time point (s)
s1	83.9	6.0
s2	68.1	6.0
s3	66.9	6.1
s4	68.8	5.4
s5	64.4	5.5

Zhang *et al.* 2007 [121] evaluated a bimodal BCI that used SSSEPs and SSVEPs. Their initial investigation of the SSSEP component replicates the BCI paradigm put forward by Muller-Putz *et al.* 2006 [42] 8 subjects were recruited. As before, each hand was stimulated by a transducer at a different frequency, with the frequencies decided for each participant individually in pre-trial testing. Subjects were made to naively attend a hand by being asked to anticipate an "amplitudinal twitch" for 40 trials, with each trial lasting approximately 5 seconds. A 32 channel EEG was used to record the data.

Signal processing consisted of subtracting an average of all the channels from each channel for all trials. This helps emphasise the signal components that are present in all channels and helps negate artefacts present in single channels. Next FFTs were calculated for each channel and averaged together. The PSD values for each stimulus frequency were identified and the coefficient of determination between values for each trial calculated. The coefficient of determination, r^2, is a measure of the relationship between two values [122]. An r^2 value of 1 means the systems that inform the magnitudes of the two values are highly interlinked, whilst a value of 0 means there is no link between them. The coefficient of determination can be calculated the following way,

$$r^2 = 1 - \frac{\sum_i (y_i - f_i)^2}{\sum_i (y_i - \bar{y})^2}, \tag{5.2}$$

where y_i is the i^{th} sample of the set of variables y and f_i is the i^{th} sample of the related set of variables f. Two channels with the highest r^2 values, indicating that they were the channels whose features change most between tasks, were selected and their individual

PSD values used as inputs for an SVM. These channels tended to be located on the left and right sides of the C-band of the 10-20 system, above the somatosensory area.

Zhang *et al.* 2007 [121] concluded briefly that their results, viewable in Table 5.2, are in line with Muller-Putz *et al.* 2006's [42].

TABLE 5.2. OFFLINE CLASSIFICATION RATES OF SSSEPS AND THE CLASSIFIER'S OPTIMUM TIME POINT FOR ZHANG *ET AL.*'S 2007 STUDY [121]

Subject	Accuracy (%)
CL	55.8
IN	63.8
NI	63.1
ZH	69.4
WA	78.5
CO	48.8
AL	64.3
TI	60.4

This SSSEP BCI paradigm detailed in these papers appears to be the simplest platform to build a tactile-based BCI on.

5.3 Novel SSSEP Stimulus

As Muller-Putz *et al.* 2006 note in [42], the stimuli for both classes are always present and differentiation between the two resulting evoked potentials relies on a slight change in amplitude due to the conscious focus of the user, which can be difficult to maintain due to inexperience or fatigue. This thesis proposed the study of a novel SSSEP stimulus designed to generate a response similar to that of a negative response. In essence, instead of distinguishing between two very similar positive responses the classifier is trying to distinguish between a positive response and a false negative. But, the false negative will need to be distinguishable from a true negative. To that end the variables in the creation of SSSEPs were investigated to see which effects could be exploited.

5.3.1 Effects of Variable Change on Stimulus Response

Verrillo 1963 [123] carried out a comprehensive analysis of the effects of vibrotactile stimulus perception in response to changes to the area of the transducer, stimulus frequency, skin deformation, displacement gradient, and amplitude. Three subjects had transducers of varying shape and size applied at frequencies of 25, 40, 80, 160, 250, 320, and 640 Hz. For each frequency, a change was made in either the transducer shape or its area and the amplitude of the vibration was reduced until it was below the user's Absolute Tactile Threshold (ATT). The ATT is the lowest level a tactile stimulus can be before it is no longer consciously felt.

To vary the skin deformation and subsequently the gradient and curvature of the displacement, three different caps were placed on the transducer the subjects rested their hand on: a concave contactor, a convex contactor, and a flat contactor. It was found that the convex and concave caps resulted in equal performance, whilst the flat cap resulted in raising the user's ATT and decreasing sensitivity. The resulting plots of the contactor's respective ATTs vs frequency showed that the displacement gradient only had an effect on the ATT at frequencies higher than 100 Hz. ATTs decreased as frequency increased irrespective of contactor shape up until 250 Hz when they began increasing again, as shown in Figure 5.4.

To vary the area, flat contactors of areas 0.005, 0.02, 0.08, 0.32, 1.3, 2.9, and 5.1 cm^2 were tested. The resulting plots of their respective ATTs vs frequency showed that the users' ATTs decreased by approximately 3 dB every time the contactor areas doubled. This matches the effects on the Absolute Auditory Threshold in response to increasing the area of stimulation on the basilar membrane [124]. As before, ATTs decreased as frequency increased up until 250 Hz when they began increasing again. This led Verillo to conclude that as the number of sensory cells being stimulated is increased, the ATT decreases, with

changing the area of displacement being the most effective way to stimulate a larger number of cells.

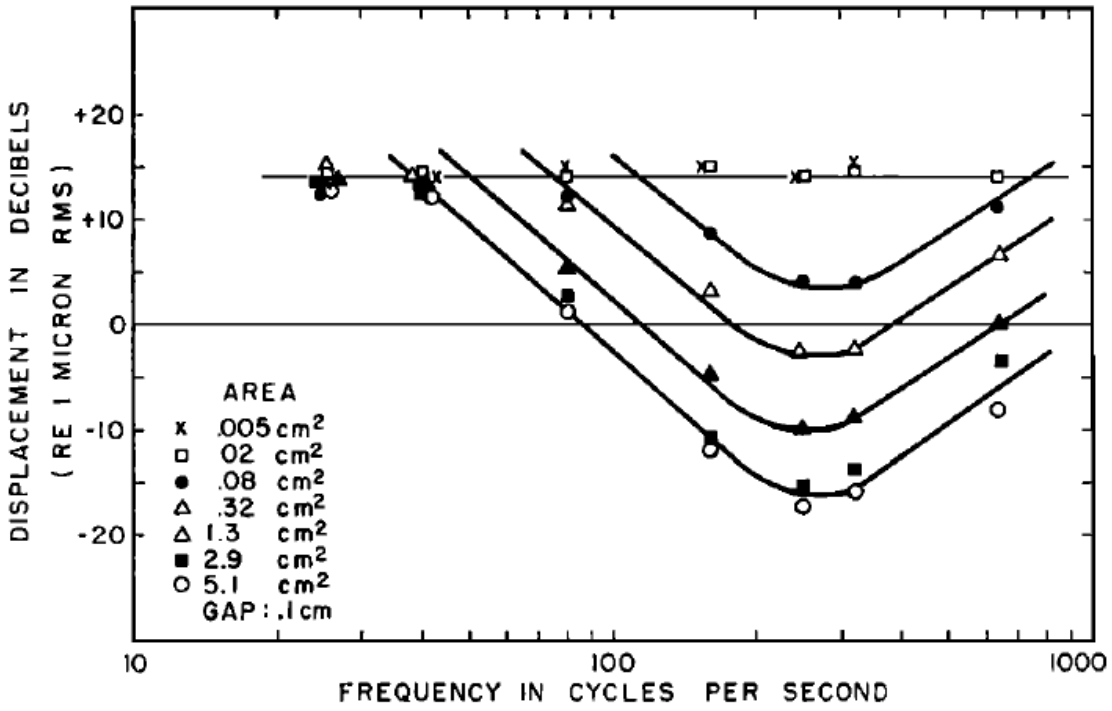

Fig. 5.4: A plot of how frequency and surface area of the stimulus affected the ATT. An increase in surface area results in a decrease in the ATT, unless the frequency of the stimulus is too low. An increase in frequency results in a decrease in the ATT up until 250 Hz where the ATT begins increasing again [123].

5.3.2 Proposed Novel Stimulus

Verillo's 1963 paper [123] shows that a person's ATT is most affected by the area of the transducer. The ATT is the lowest level a tactile stimulus can be before it is no longer consciously felt, therefore it can be expected that distinguishing between a stimulus above and a stimulus below a person's ATT will be as effective as distinguishing between an SSSEP occurring and neutral activity. It is anticipated that the false negative of the stimulus below the ATT is distinguishable from a true negative. One potential area of difference would be the α band of brain activity (8 – 13 Hz). As described in Chapter 2, the α activity is viewed as the brain's "idle" signal, and has been shown to decrease in amplitude as a response to

attentiveness, mental tasks or stimuli [125]. It is expected that the conscious effort to detect tactile stimulation would increase a person's focus. Therefore if the participant is receiving no stimulus at all, we would see no change in α activity. But if they know they are receiving a stimulus but struggle to sense it, they would have the increase in focus and subsequent decrease in α waves but no detectable SSSEP.

5.4 Experimental Protocol

The experiment described in this thesis is closely based on Muller-Putz *et al.*2006's design [42], with a longer stimulus duration and the removal of the "amplitudinal twitch" concept in addition to the different types of stimuli. Each hand has a different tactile stimulus applied to it with the participant receiving cues to focus on one hand over the other using the timing sequence in Figure 5.5. After two seconds rest a directional cue appears on screen and the stimulus to both hands commences. Participants focus on the hand in question for five seconds. A random inter-stimulus interval of up to +/- 0.5 seconds is inserted between each trial to help prevent habituation.

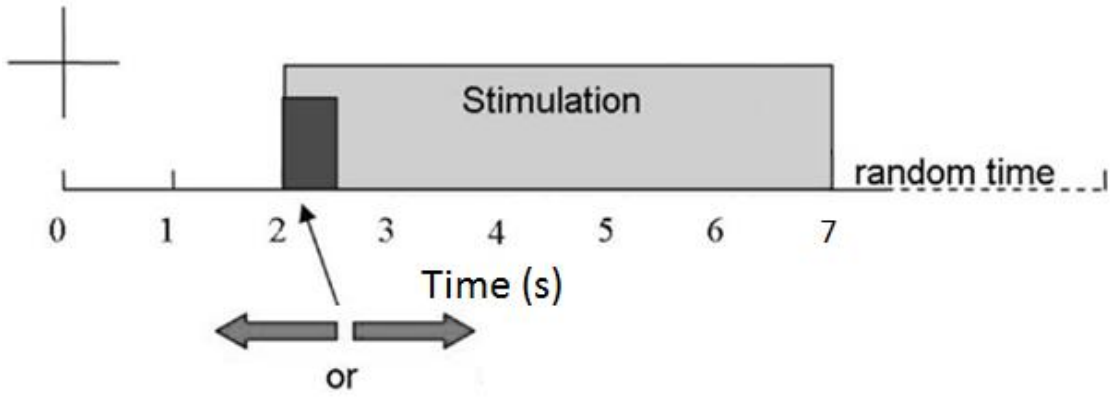

Fig. 5.5: Timing of experimental BCI paradigm. The directional cue and stimulation occur at 2 seconds in and last for 5 seconds. A random time gap is inserted in between trials to help prevent habituation (figure modified from [42]).

The various stimuli that required testing were as follows:

- Standard stimulus – As in Muller-Putz *et al.* 2006 [42] vibrating stimuli of equal amplitude and contactor area, but of unique frequency, is applied to each hand. This provides a point-of-reference for comparing the accuracy of the novel stimulus to. The frequencies 16 Hz and 25 Hz were chosen as they generated strong SSSEPs according to Verillo 1963 [123] and will not combine constructively to form rhythmic pulses as they are not multiples of each other.
- Novel stimulus – The novel stimulus requires the vibrations to be of equal frequency, but of lower contact area and amplitude on one hand so that they are below the participant's ATT, and on the other hand greater contact area and amplitude. Prior to the main experiment, participants have a single transducer secured firmly to their hand, with the vibrationary amplitude gradually lowered until they confirmed that they could no longer feel the stimulus. The other hand has a greater number of motors secured to it and with the vibrational stimulus applied at a greater amplitude, ensuring that it was above the participant's ATT and detectable. The frequency selected was 25 Hz as that was within the frequency range of SSSEP responses that had the highest increase in PSD and highest SNR according to Snyder.
- Neutral stimulus – As the novel stimulus was deliberately mimicking that of a negative on one hand, or "no stimulus applied" response, a null test is needed to make sure the resulting response is not an exact duplication of a state where no stimulus was applied. This neutral stimulus would have a vibrational frequency of 25 Hz applied to one hand, and no stimulus at all applied to the other.

100 trials were carried out for each form of stimulus, resulting in 300 trials in total. After 50 trials the motors and their respective stimuli swapped hands to ensure that the

participant's dominant hand was not causing the stimulus applied to it to be easier to detect. Participants were offered a break in between each set of 50 trials. To prevent fatigue, inexperience, or habituation skewing the results the order that each stimulus block of 100 trials were applied to participants was randomised. The vibrations of the motors can cause sound of the same frequency as the carrier wave to be emitted. To prevent any possible audio stimulus white noise was played at 50 dB, the same decibel level as a loud conversation. This noise was delivered through speakers as headphones would get in the way of the EEG cap. Ethical approval was submitted and approved by the University of Warwick's Biomedical and Scientific Research Ethics Sub-Committee (BSREC), application reference REGO-2014-880, *"Exploiting the absolute threshold of vibrotactile stimulation to generate evoked potentials in EEG"*, and 16 participants were recruited from the student population and their consent recorded. Confirmation of ethical approval is attached in Appendix A, with the ethics application, participant information leaflet, and consent form attached in appendices B, C, and D respectively.

5.4.1 Characterisation of Stimulus

Custom hardware had to be designed and constructed to generate the vibrotactile stimuli and apply them to the participant's fingertips.

For the transducers themselves four Pico Vibe brand 10mm Vibrating Motor Model No. 310-004 were purchased [126]. They were specified as being capable of 145 – 170 Hz vibrations so obviously a modulated carrier wave like Snyder 1992 [118] used would be required to deliver the desired lower stimulus frequencies. These motors were then secured to the participant's fingers using hook and loop cable ties, as shown in Figure 5.6. To prevent additional pressure being applied to the motors, and thereby affecting the level of stimulation, participants sat in a chair with their arms supported by armrests, but with their hands hanging in the air.

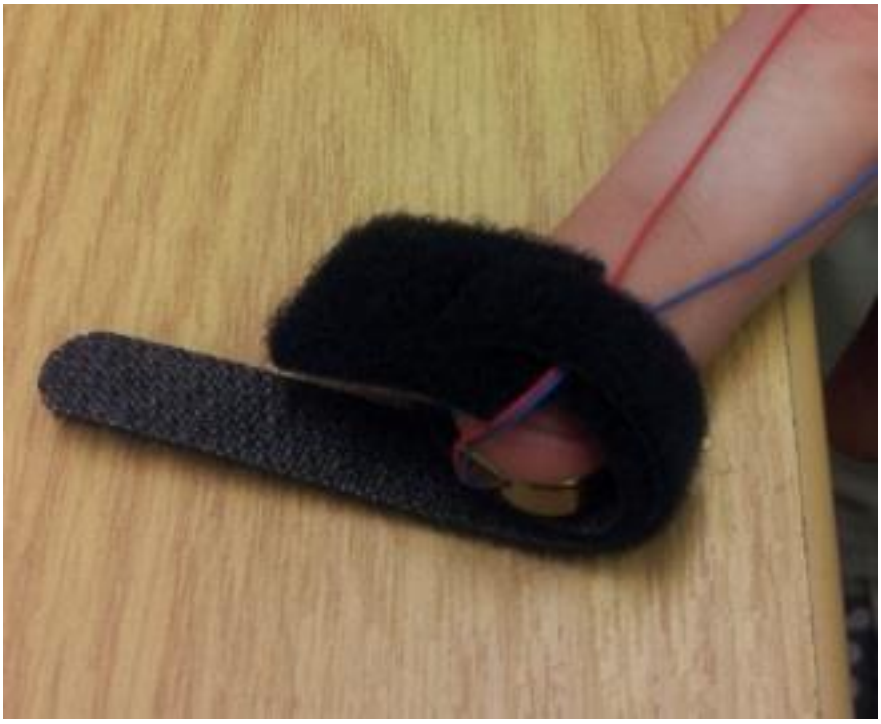

Fig. 5.6: A 10mm motor secured to a person's fingertip using a hook-and-loop cable tie.

For control of the motors, an Arduino Pro ATmega328 circuit board was used [127]. Arduinos are simple open-source circuit boards that can have a multitude of input and output components connected to them. These components and the circuit they are placed in are shown in Figure 5.7. They can also send and receive instructions from PCs using a USB connection.

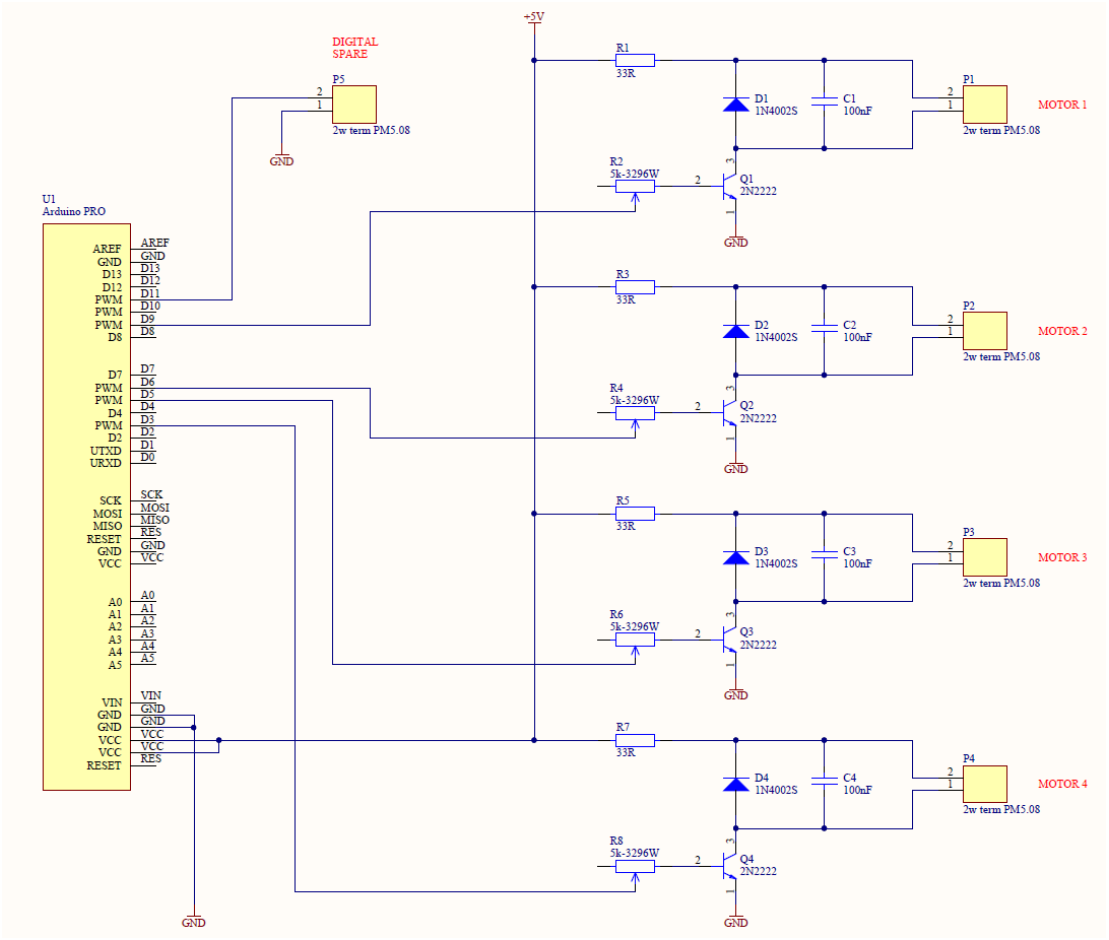

Fig. 5.7: The circuit diagram of the Arduino board responsible for controlling the motors' frequency and amplitude.

5.4.2 Validating the Stimulus Generator

To test that the circuit functioned as designed, the board was examined using an oscilloscope to confirm that the square wave the circuit was applying to the motors for modulation was consistent, as can be seen in Figure 5.8.

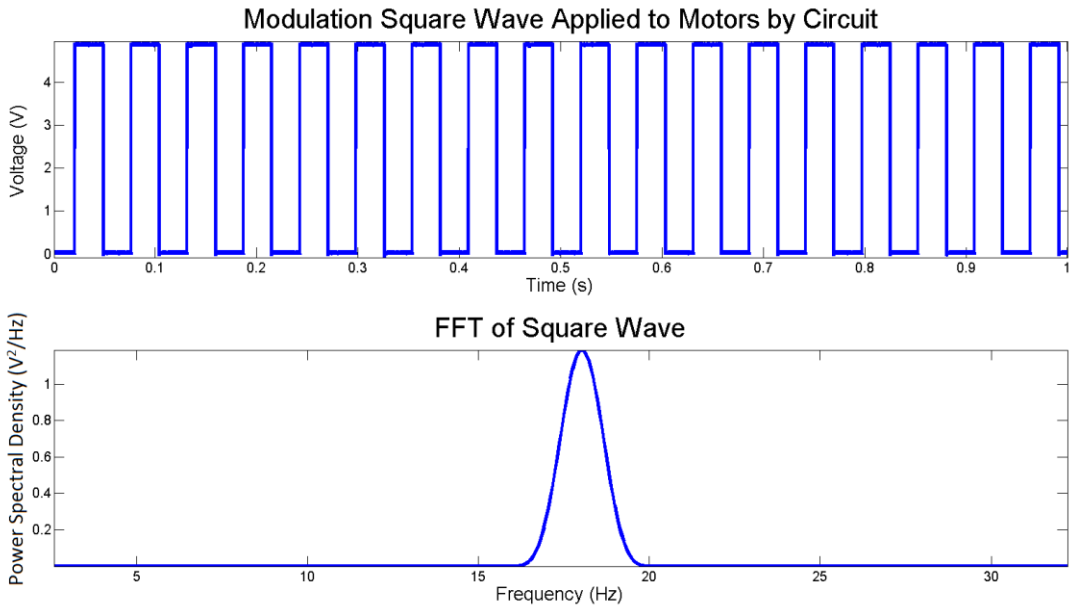

Fig. 5.8: The modulation wave recorded by the oscilloscope from the Arduino circuit. The voltage oscillates between 0 and just under 5 V at precisely the pre-selected test frequency of 18 Hz.

In order to record the motors' frequency ranges and corresponding Arduino current values they were connected to the accelerometer shown in Figure 5.9 and their oscillations at different settings were recorded.

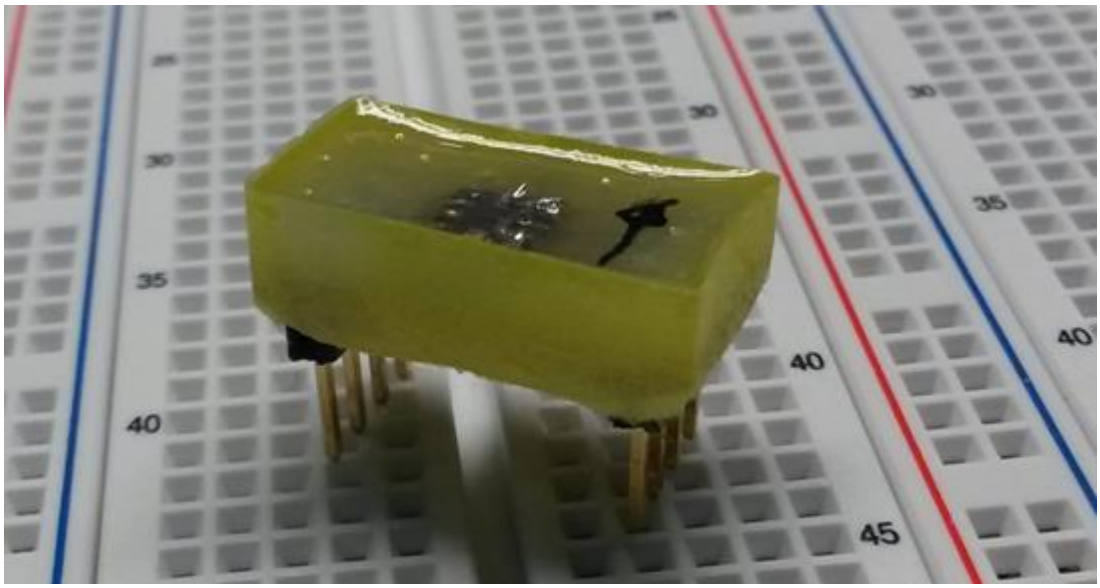

Fig. 5.9: The accelerometer encased in a block of resin. Each motor was attached to the resin and a range of current values were applied. The resulting signal recorded by the accelerometer was analysed to determine the motor's speed and power.

The current values assigned to the motors in the Arduino program, from 0 – 255, were decreased by intervals of 50 and their subsequent vibrations recorded. FFTs were then calculated to find the frequency and PSD of the vibrations in question. An example of this can be seen with Motor 2 in Figures 5.10, 5.11 and 5.12.

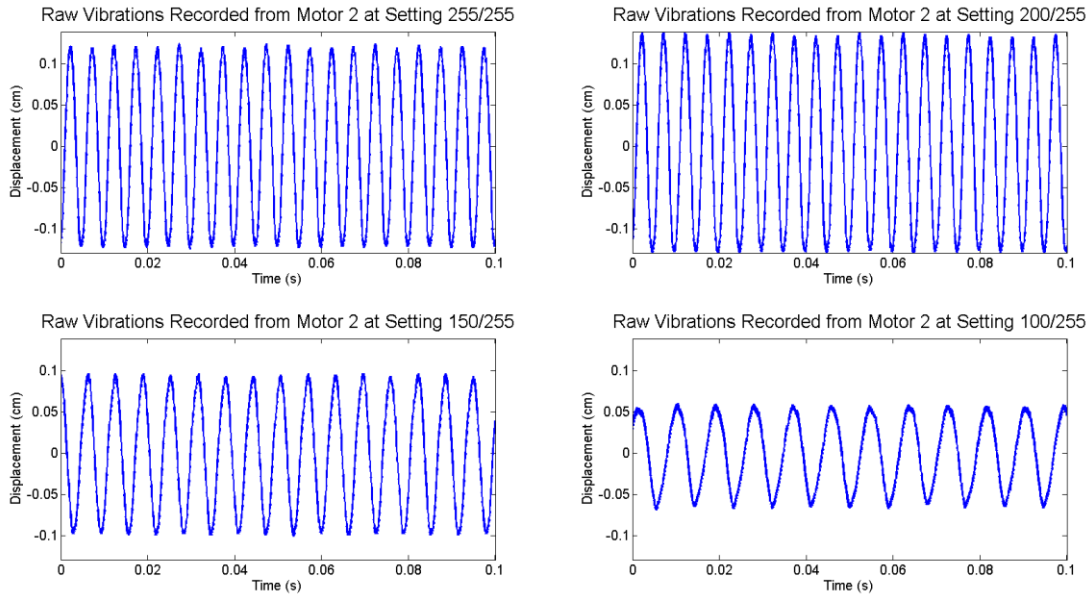

Fig. 5.10: The recorded vibrations of the second motor at settings 255/255, 200/255, 150/255 and 100/255 with the oscillations visibly slowing between steps.

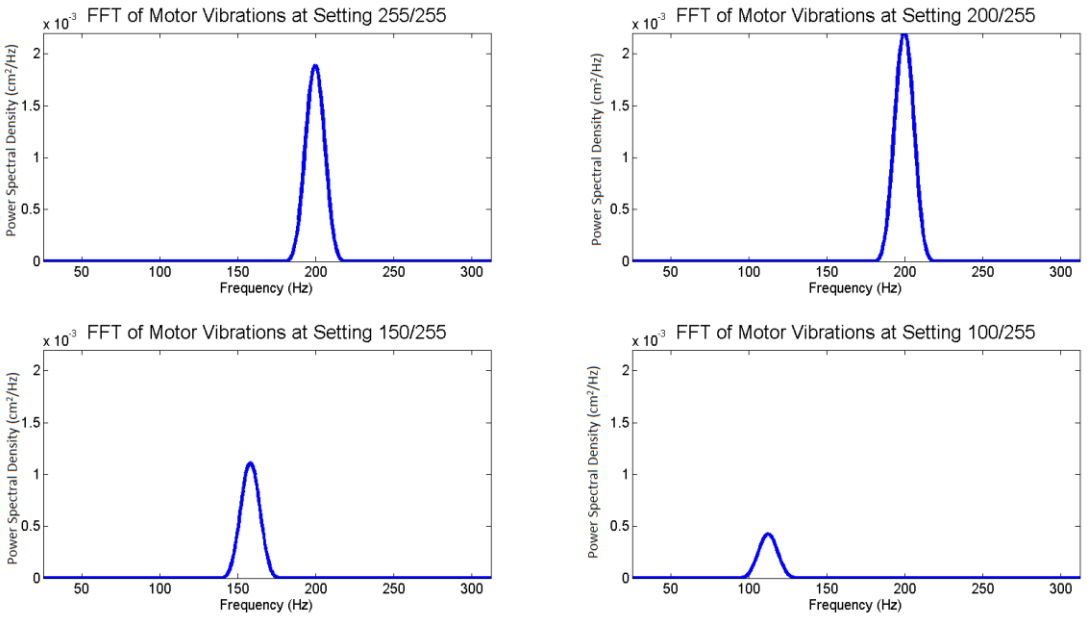

Fig. 5.11: The FFTs calculated from the signal plots in Figure 5.10, showing the decrease in the PSD as the setting is lowered.

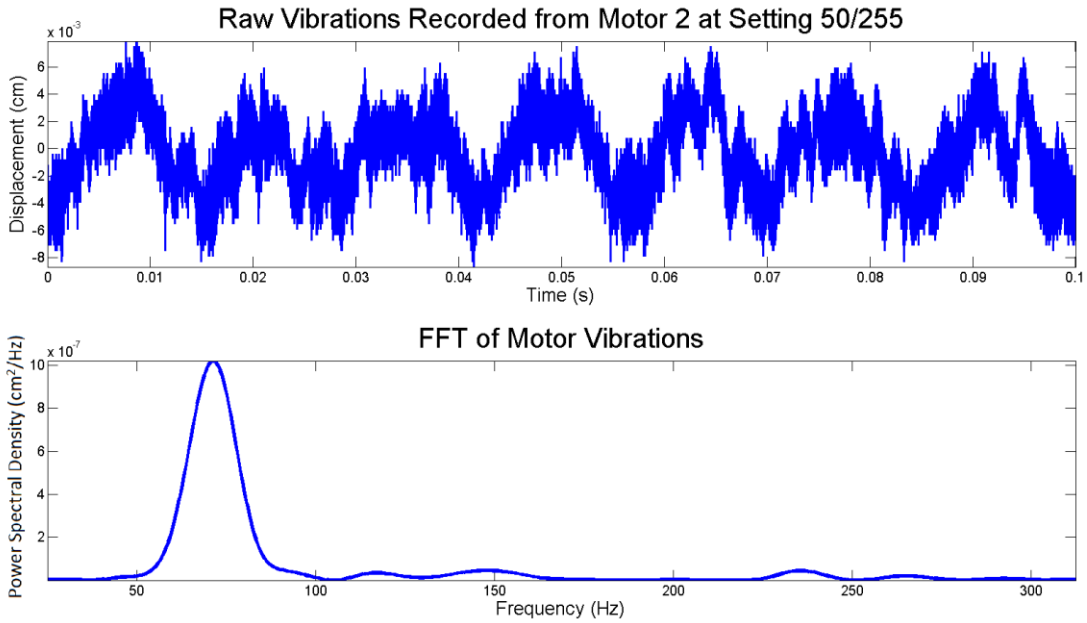

Fig. 5.12: The recorded vibrations of the second motor at setting 50/255 and the FFT showing its frequency and PSD.

The results of all four motors showed that the frequency and oscillatory amplitudes in response to changing current levels differed between individual motors, as shown in Table 5.3. The different responses between the same models of motor were speculated to be caused by minor variations in the manufacturing process. This model of motor was not designed to be run at highly specific frequencies and if repeated, different motors would be used in the design of the stimulus generator.

TABLE 5.3. SOFTWARE SETTINGS' CORRESPONDING VIBRATIONAL FREQUENCY AND ITS PSD FOR EACH MOTOR

Motor	Code Value	Frequency of Vibration (Hz)	PSD of Vibration (cm^2/Hz)
1	255	200	0.0020
	200	200	0.0022
	150	158	0.0011
	100	112	0.0004
	50	71	0.0001
2	255	212	0.0027
	200	175	0.0012
	150	153	0.0013
	100	120	0.0006
	50	63	0.0001
3	255	248	0.0023

	200	224	0.0017
	150	196	0.0012
	100	139	0.0006
	50	78	0.0001
4	255	222	0.0034
	200	188	0.0025
	150	154	0.0009
	100	116	0.0003
	50	63	0.0001

These data points were then plotted and used to extrapolate a graph predicting the frequency and amplitude of all the current values for each of the four motors. An example of this with Motor 1 can be seen in Figures 5.13 and 5.14.

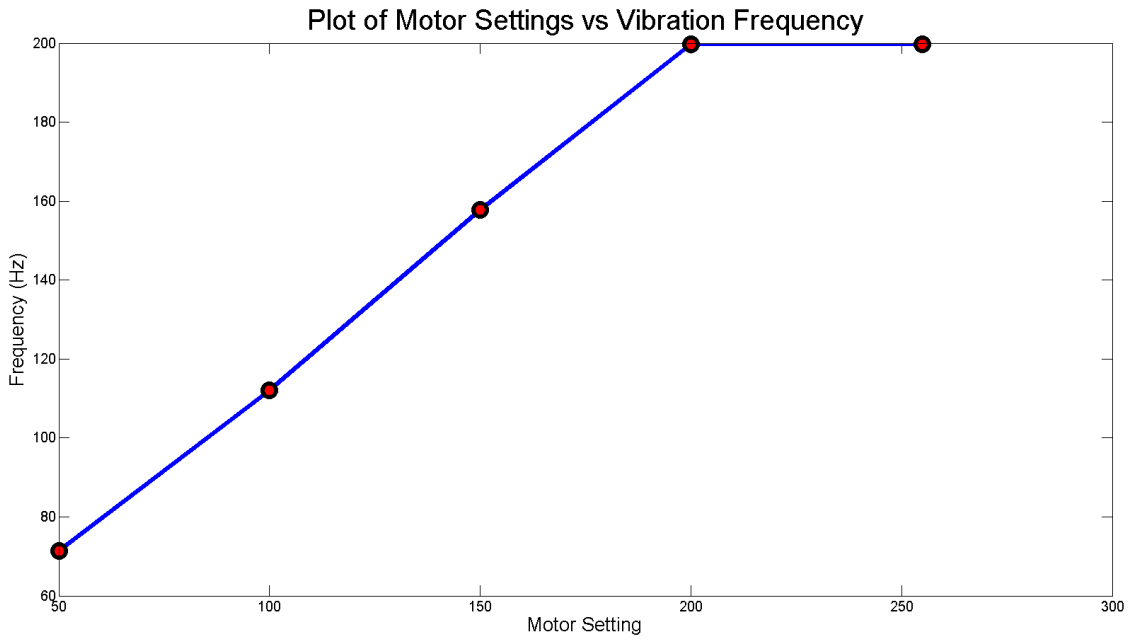

Fig. 5.13: The resulting frequencies of the motor's vibrations from a range of different current values. In this case the relationship extrapolated from the datapoints indicates a positive linear relationship that plateaus once the current value reaches a certain level.

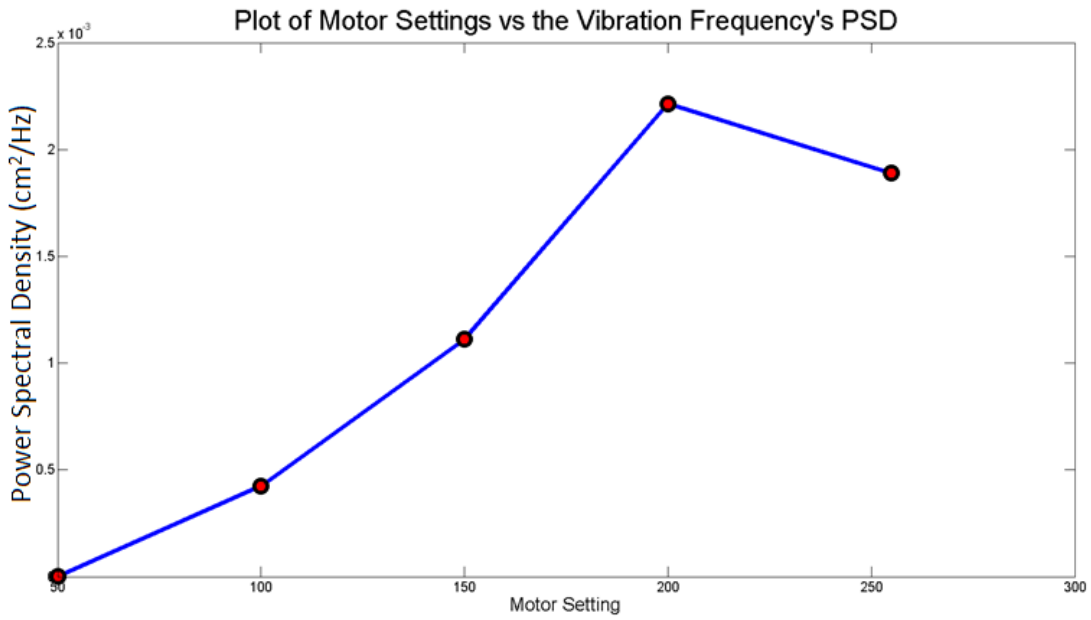

Fig. 5.14: The resulting PSD of the motor's vibrations from a range of different current values. The relationship extrapolated from the datapoints is similar to that of the frequencies but not as strong or well-defined. It was speculated that the decrease in the PSD at setting 255 might be due to heat causing the casing to swell slightly and increase friction between it and the motor.

This allowed the selection of software settings during calibration of the system that caused all four motors to vibrate at the same frequency and amplitude. As the frequency/amplitude vs current relationship differed for each motor, having the motors vibrate at the same amplitude was prioritised over having the same carrier frequency. This was because one motor being of greater amplitude than another could unbalance the stimuli in the "standard" experimental protocol. The carrier frequency was considered too high to impact the EEG readings and the modulation frequency would be unchanged.

Verillo's study in [123] of vibrotactile perception, mentioned previously, found that users were most sensitive to frequencies between 150 – 200 Hz. The motors' values are all well within that range meaning that a carrier frequency that Verillo found the nerve endings in the fingers to be highly sensitive to can be used, combined with a modulation frequency that was found by Snyder 1992 [118] to produce the largest SSSEPs.

When it came to implementing the stimulus using the motors the equipment set-up was as follows:

- Standard stimulus – Two motors were placed on each hand on the index and middle fingertips. Motors 1 and 2 on one hand used a 25 Hz modulation frequency, and motors 3 and 4 on the other hand used a 16 Hz modulation frequency.
- Novel stimulus – Motor 1 was placed on one hand's index finger at the value deemed to be below the participant's ATT by the pre-test. Motors 2, 3 and 4 were placed on the index, middle and ring fingers of the other hand. Both had a modulation frequency of 25 Hz.
- Neutral stimulus – Motors 1 and 2 were secured to one hand but were not activated. Motors 3 and 4 were placed on the other hand's index and middle fingers with a modulation frequency of 25 Hz.

The details of the 16 participants recruited are listed below:

TABLE 5.4. PERTINENT DETAILS OF THE PARTICIPANTS FOR NOVEL SSSEP STUDY

Participant	Age	Sex	Dominant Hand	BCI Aware
P1	20	Male	Right	No
P2	34	Male	Right	Yes
P3	27	Female	Right	No
P4	28	Female	Right	Yes
P5	22	Male	Right	No
P6	25	Female	Right	No
P7	19	Male	Right	No
P8	25	Male	Right	No
P9	63	Male	Right	Yes
P10	34	Male	Right	No
P11	25	Female	Right	Yes
P12	33	Female	Right	Yes
P13	23	Male	Right	No
P14	27	Male	Right	Yes
P15	25	Female	Right	No
P16	37	Male	Right	No

No participant suffered from any pre-existing neurological condition and all were ably-sighted.

5.4.3 Equipment

Aside from the custom stimulus delivery system, a 64 channel gtec brand g.GAMMAcap with active g.LADYbird electrodes connected to a g.HIamp EEG amplifier with a sampling frequency of 512 Hz was used to record brain activity. The electrodes were positioned according to the 10-20 coordinates pictured in Figure 5.15. A water-soluble, non-irritant, non-corrosive conductive gel was injected into each of the electrodes. The EEG amplifier's in-house recording software, g.Recorder, was used. The visual cues were displayed on a 21 inch monitor approximately four feet from the participant. Processing IDE, a desktop counterpart to the Arduino programming environment [128], was used to trigger the program uploaded to the Arduino. It in turn received data from the Arduino's serial port about the cue displayed and current trial number. It also directed a command towards the g.Recorder application to mark the current data point denoting it as either the beginning of a new trial or the onset of the stimulus. The programs written for each stimulus protocol are reproduced in Appendix E. The full experimental set-up used by participants can be seen in Figure 5.16.

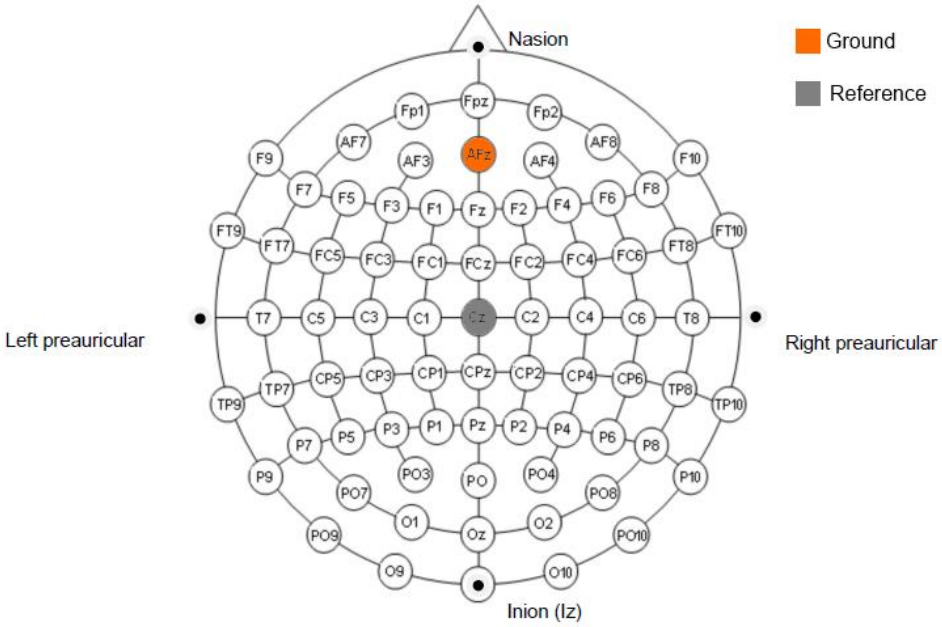

Fig. 5.15: The electrode layout of the EEG cap according to the 10-10 system with channel AFz acting as the ground and channel Cz as the reference (figure modified from [129]).

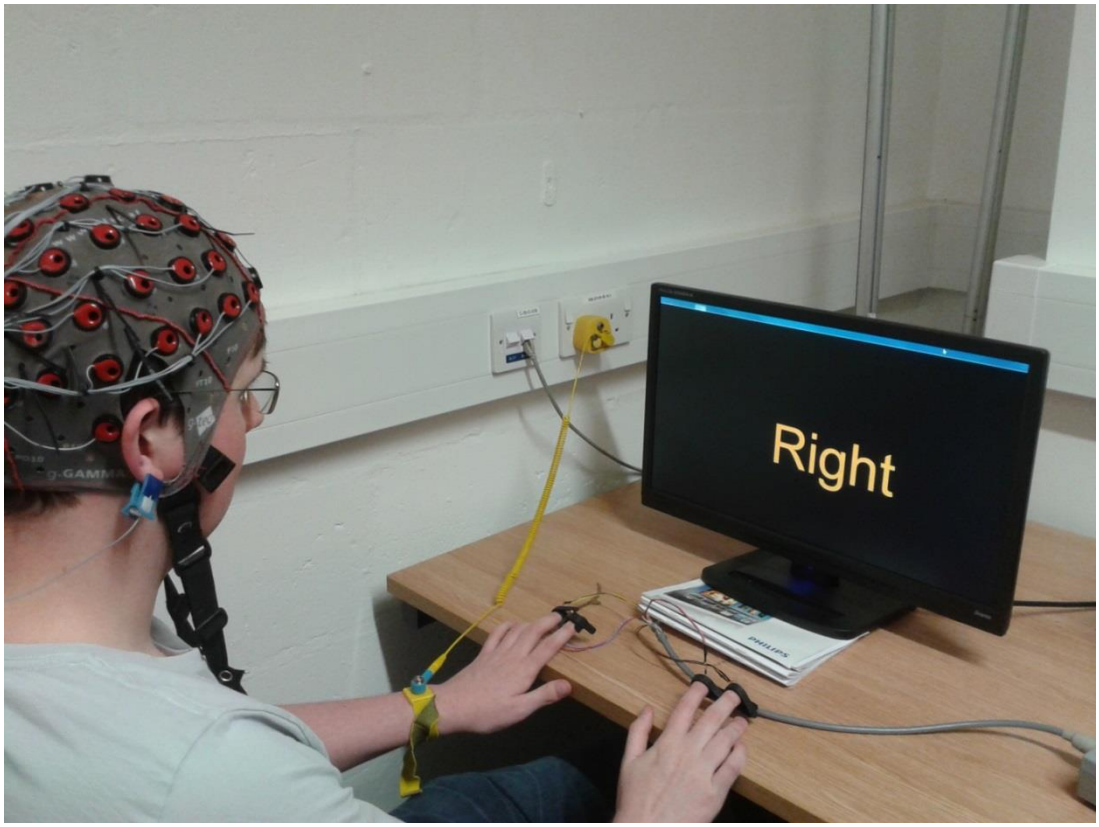

Fig. 5.16: Photograph of a participant performing the experiment. In this case a grounding strap was worn to try and suppress EMI artefacts.

5.5 Analysis

The standard SSSEP paradigm achieved a classification accuracy of 63.3% ± 6.6%, on a par with other studies in the literature that used the same paradigm. The novel and neutral SSSEP paradigms achieved a classification accuracy of 61.8% ± 6.5% and 60.5% ± 6.6% respectively, well-within each other's standard deviations. Several changes to the equipment were made in an attempt to reduce the large presence of external noise, but no variations in their resulting performance were recorded.

These results show that there was no difference between the performances of the stimuli. However the large presence of signal contamination in the trials may have impacted upon them.

5.5.1 Signal Contamination

Figures 5.17 and 5.18 show that the EEG recordings contained large contamination of rhythmic 16 Hz, 25 Hz and 75 Hz signals in the trials using the standard stimuli, and 25 and 75 Hz in the other trial sets. The frequencies of the signals meant that they were obviously related to the stimulus, with the 75 Hz signal being resonant to the 25 Hz one. The large amplitude and instantaneous nature of their appearance led to the conclusion that it was an artefact and unrelated to neural response to the stimuli. This was further confirmed when noise suppression methods, described later in this section, reduced the presence of the contamination. This interferes greatly with classification as the contamination shares the same frequency domains as the features of the evoked potentials we are looking for. Further testing showed that the contamination only occurred when the motors were active and when the participants' fingers were either touching or within a few centimetres of the motors, and was therefore most likely down to Electro-magnetic Interference (EMI). It was thought that the motors would not be able to generate any significant interference and

that their encapsulation cases and the Arduino sharing the desktop PC's grounding point would prevent any contamination. As this was not the case participants were then asked to wear a grounding cable attached to their wrist and connected to a grounding point of the Arduino board, ensuring that all the equipment shared the same grounding point. This reduced but did not eliminate the contamination entirely, as shown in Figures 5.19 and 5.20. However its reduction in magnitude does confirm that it is an external source causing the increase in amplitude and not a neural response from the participants.

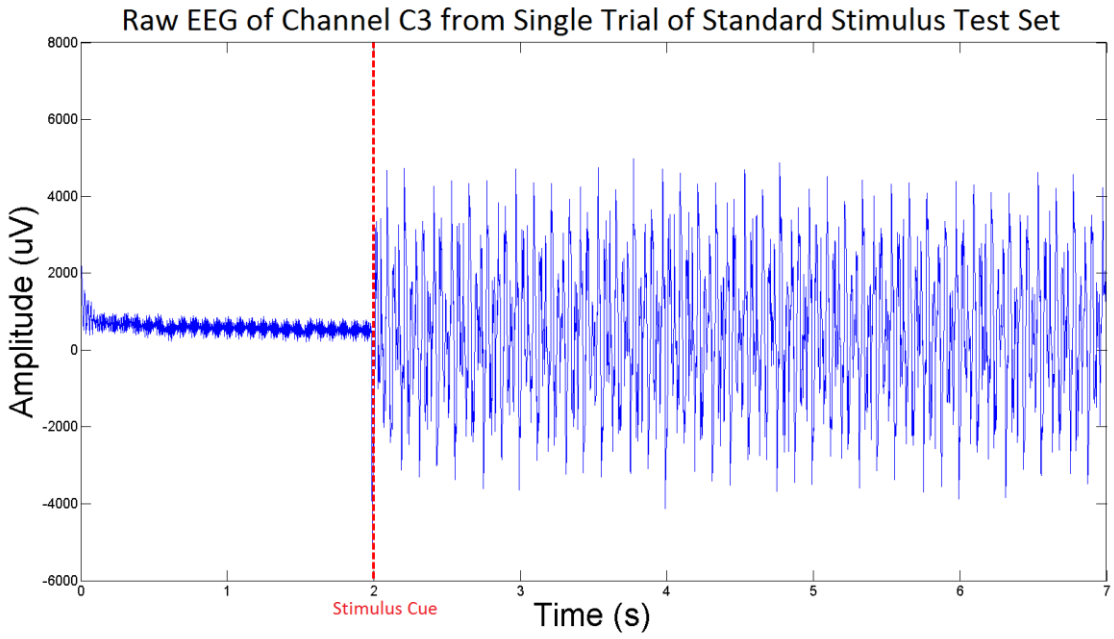

Fig. 5.17: A graph showing the raw EEG of a random trial from the first experiments using a vibrationary stimulus of 25 Hz and 16 Hz. There is a huge surge in amplitude at the onset of transducer activation. This is down to the EMI from the motors that is occurring in time with their oscillations.

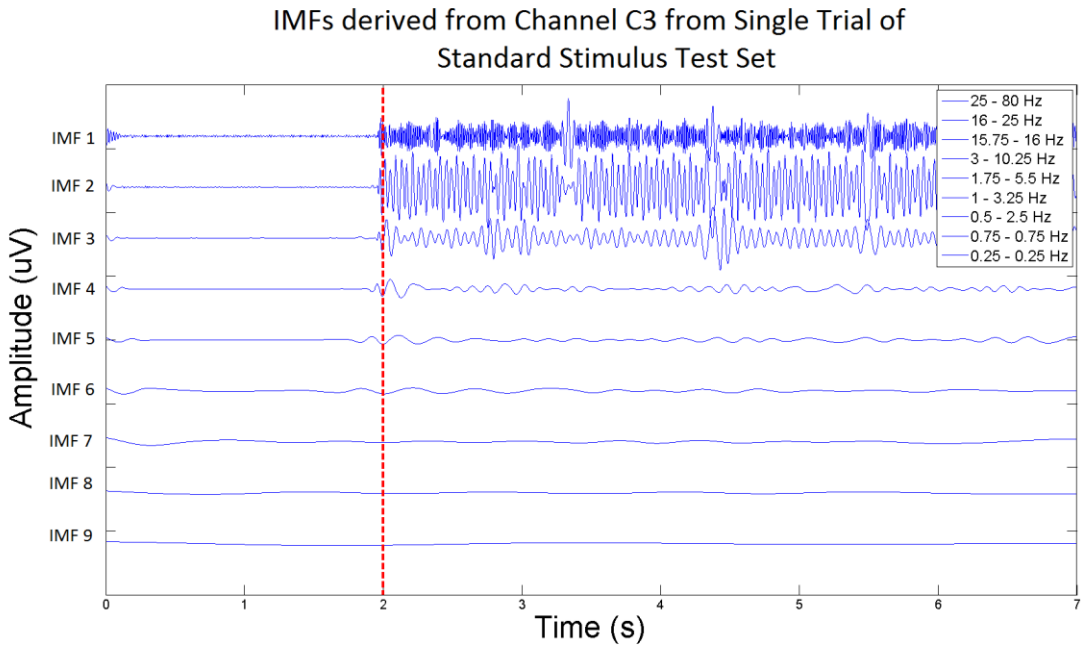

Fig. 5.18: A graph showing the resulting IMFs after MEMD has been applied to C3 and its adjacent electrodes from the trial in Figure. 5.17. The rhythmic EMI interference is more visible and is confined to the frequency domains of the motor stimuli and their resonance frequencies.

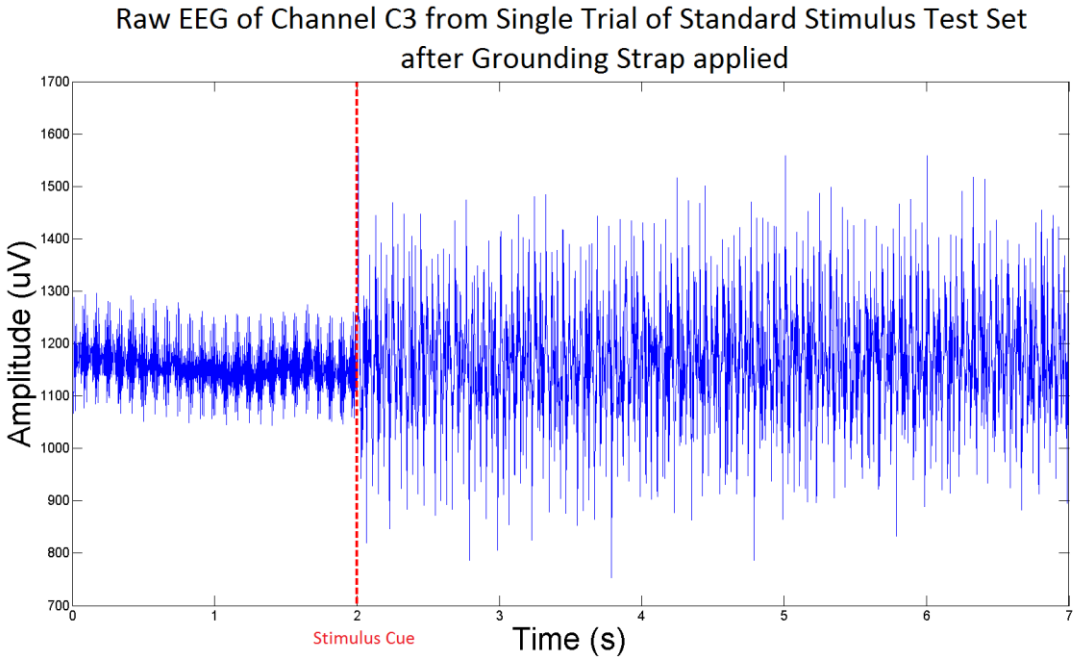

Fig. 5.19: A graph showing the raw EEG of a random trial from a participant using a vibrationary stimulus of 25 Hz and 16 Hz after the grounding strap was introduced in an effort to eliminate EMI. The amplitude of the contamination is reduced but a rhythmic artefact that occurs instantaneously after the activation of the motors is still present in the signal.

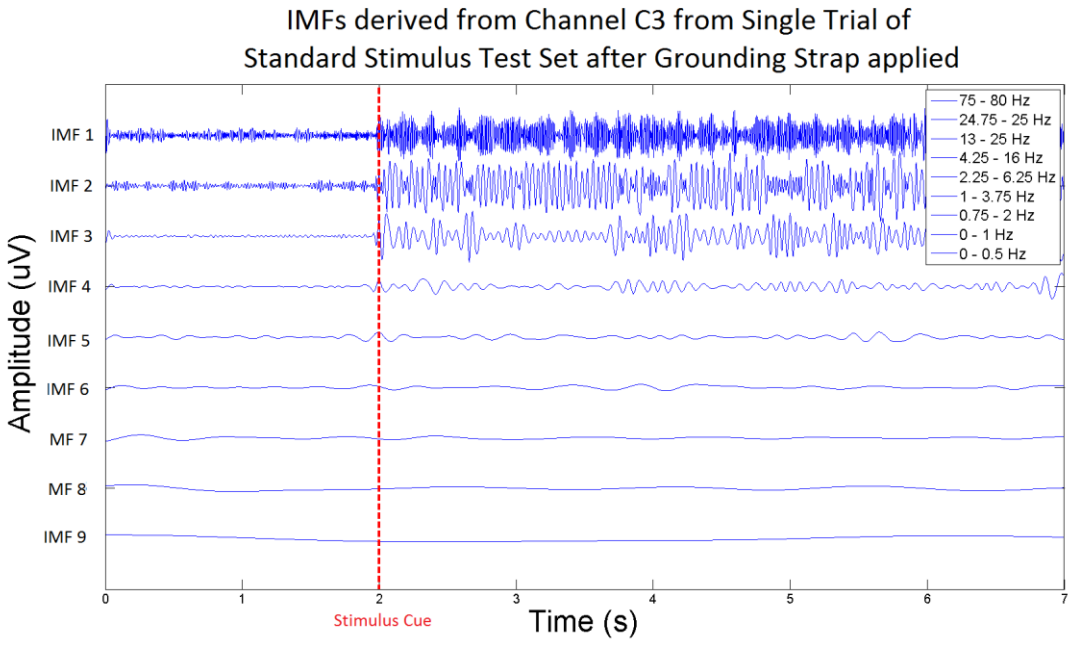

Fig. 5.20: A graph showing the resulting IMFs after MEMD has been applied to C3 and its adjacent electrodes from the trial in Figure 5.19. Again, the rhythmic EMI interference is now more visible and is confined to the frequency domains of the motor stimuli and their resonance frequencies.

As it was still unclear if the contamination was masking the EEG signal, a new device was constructed that could conduct the motors' vibrations and apply them to the participant's hands from a safe distance. After measuring the distance from the motor that the interference seemed to stop occurring in the EEG, plastic hemispheres of a greater radius were obtained to act as transducer casings. Flaps the size and shape of the index and middle fingers were cut into the casings so that they were free to vibrate from the rest of the casing. Solid rods were glued to the motors at one end and pushed against each finger flap at the other. The same structure that held the rods in place held the plastic casing in place to ensure they did not move apart from each other. Each casing held two motors, with a diagram shown in Figure 5.21. For the Standard and Neutral stimuli only one motor for each hand needed to vibrate. For the Novel stimuli one hand had two motors vibrating to double the contactor area compared to the other hand. These new casings initially

greatly reduced the EMI, and when combined with a grounding strap seemed to eliminate it almost completely, as can be seen in Figures 5.22 and 5.23.

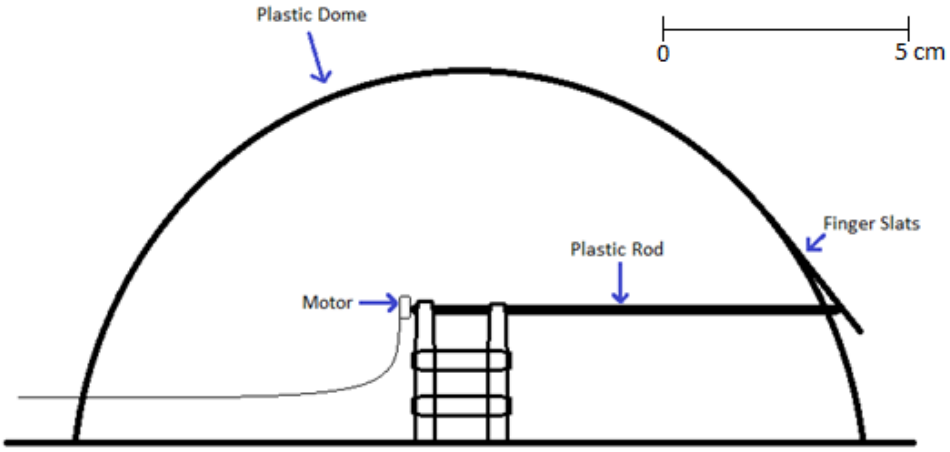

Fig. 5.21: Diagram of the new transducers. The participant rests their hand on top of the dome with their fingers on the bendable slats. A solid rod connected to a motor pushes against the slat. When the motor vibrates, so does the rod, pushing against the slat and stimulating the participant's finger whilst maintaining a distance of several centimetres between them and the EMI-producing motors.

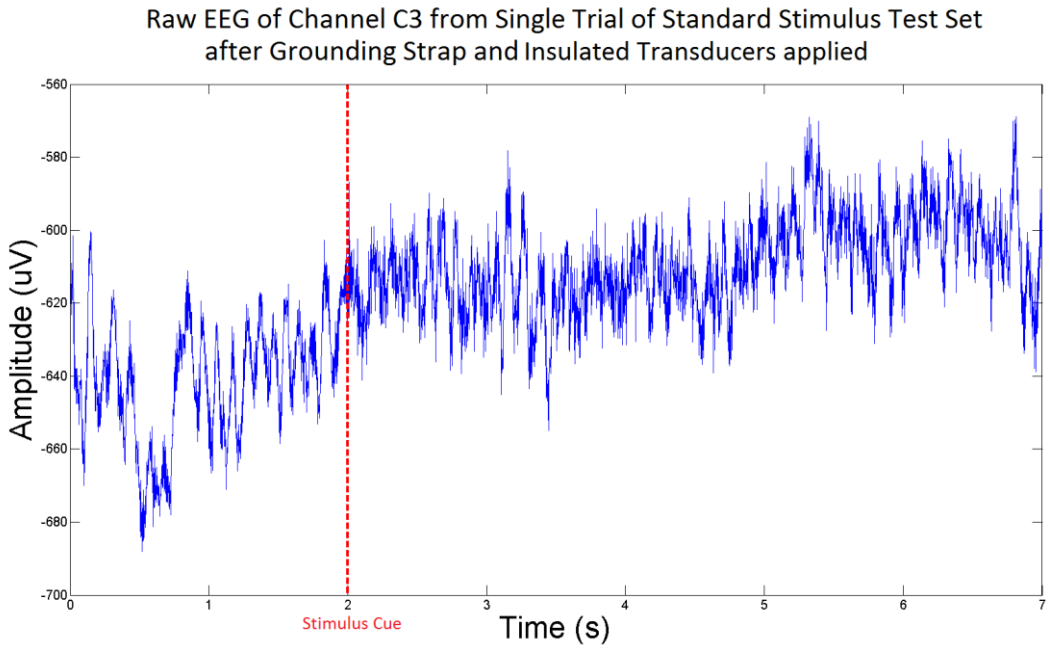

Fig. 5.22: A graph showing the raw EEG of a random trial from a participant using a vibrationary stimulus of 25 Hz and 16 Hz after the insulated transducers were introduced in an effort to eliminate EMI. The amplitude of the contamination is reduced

to the extent that it is equal to that of the neutral, EMI-free pre-stimulus EEG activity. However, this proved to only be temporary.

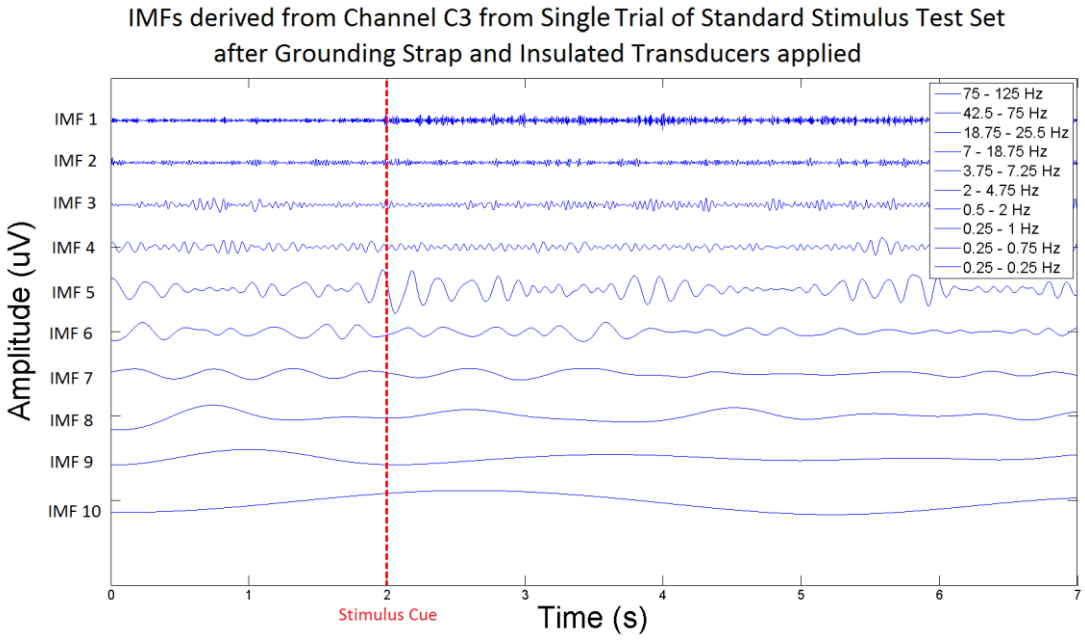

Fig. 5.23: A graph showing the resulting IMFs after MEMD has been applied to C3 and its adjacent electrodes from the trial in Figure 5.22. IMFs 3 and 4, which occupy the frequency domain of the tactile stimuli, do not appear to have any high amplitude EMI artefacts.

These new, upgraded transducers were applied to two further participants. However, these subsequent trials saw the noise return. It was further surmised that the small lengths of wire connecting the motors to the sheathed cable were acting as aerials and conducting the EMI. This hypothesis was reinforced by the negative effect of twisting the wires for each motor on the EMI. Twisted pair cabling is when wires for the same component of a circuit are twisted together to cancel out each other's EMI [130]. As the wires are carrying equal but opposite charges they emit opposing EMI that combines with a destructive interference. Unfortunately this tended to have the consequence of snapping the thin wires connecting the motors to the Arduino due to the extra tension placed on them.

0.1 µF capacitors were added between the motors and the wiring to help suppress the noise. As EMI is high-frequency in nature and a capacitor's impedance reduces the higher

the signal's frequency, a suppression capacitor will pass the noise to the circuit's grounding point [131]. However this also had little effect as a small length of wire still connected the motors to the capacitors and this was still enough to emit EMI, as shown in Figures 5.24 and 5.25.

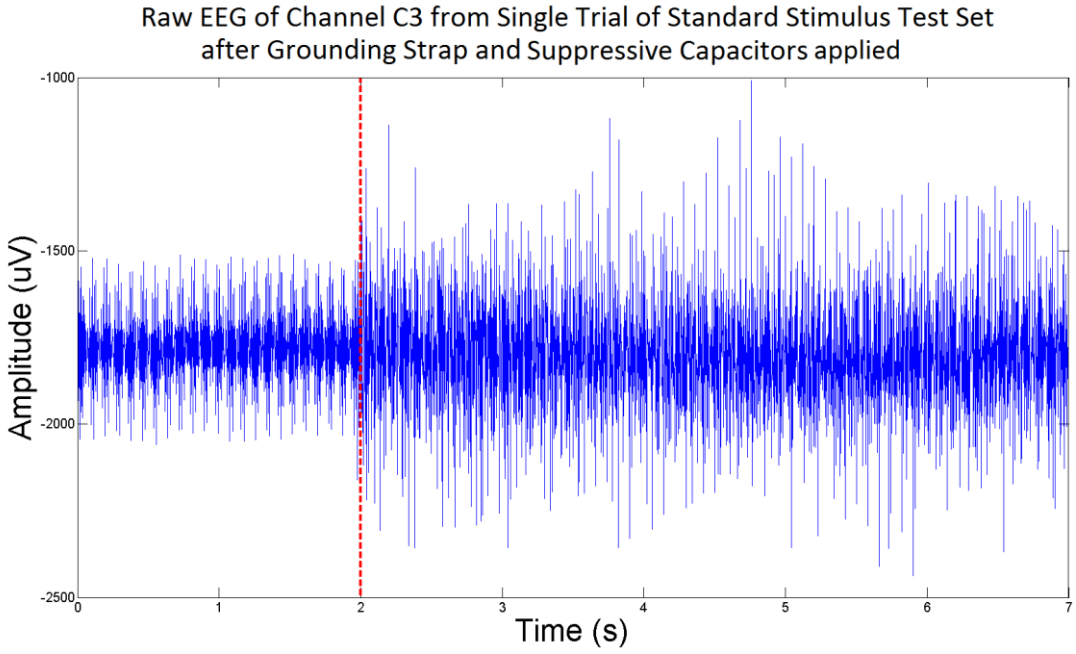

Fig. 5.24: A graph showing the raw EEG of a random trial from a participant using a vibrationary stimulus of 25 Hz and 16 Hz with the suppressive capacitors added. The amplitude of the contamination is lower than that of the trials with just the grounding strap applied but it is still present.

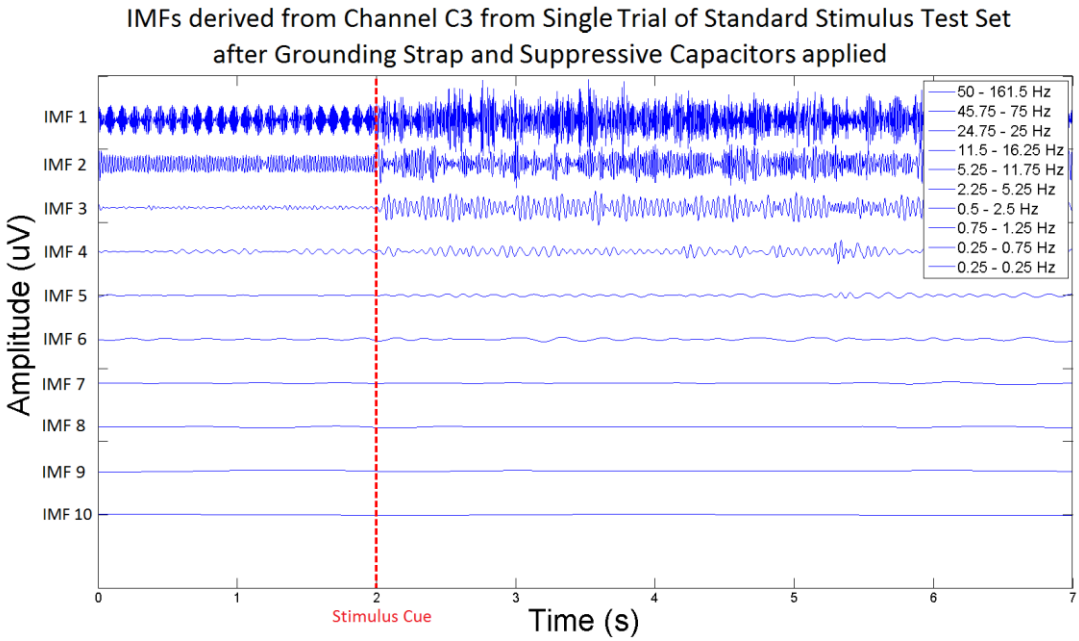

Fig. 5.25: A graph showing the resulting IMFs after MEMD has been applied to C3 and its adjacent electrodes from the trial in Figure 5.24. Like before the EMI contamination is limited to the frequency domains of the transducers and their resonant frequencies. In this case an artefact from the participant's pulse can be seen in the pre-stimulus section. Post-stimulus it is masked by the EMI.

Finally, a software-based solution was attempted with a noise-adaptive suppression filter using the Normalised Least Mean Squares (NLMS) algorithm implemented to try and remove the noise. An adaptive noise filter is a closed loop system that adjusts the filter coefficients as it receives the signal input according to a cost function [132]. In this case the cost function is minimising the NLMS of the error signal, which is the difference between the desired and actual signal. The filter must have two inputs, the primary input that contains the noise-corrupted signal and a reference input that contains only the correlated noise. After each input sample, the NLMS filter adjusts its coefficients as follows,

$$\omega_{l,k+1} = \omega_{l,k} + \left(\frac{2\mu_\sigma}{\sigma^2}\right)\epsilon_k x_{k-l} \tag{5.3}$$

where ω is the set of coefficients, l is the current coefficient, k is the current sample, x is the reference signal, ϵ is the primary input signal minus the current output of the filter, μ is the convergence factor, and σ^2 is the sum total power of the input signal. The coefficients

are initially small and changes are made based on the gradient of the normalised mean square error. A positive gradient means that the error rate is increasing and the magnitude of the coefficient needs to be reduced. A negative gradient means that the error rate is decreasing and the magnitude of the coefficient needs to be increased. As there is a direct reading of the digital 16 and 25 Hz signals produced by the circuit this can be used as a reference. Cross correlation was used to sync the noise with the EEG signal. Unfortunately the performance was worse with the filter applied for all subjects; nearing the same values that random classification would produce. The noise negation methods applied to each subject and their experimental results are listed in Table 5.5, followed by a bar chart of the classification accuracies for each subject and stimulus type in Figure 5.26.

5.5.2 Results

TABLE 5.5. RESULTS OF NOVEL SSSEP STUDY

Subject	Stimulus Method	Sensitivity (%)	Specificity (%)	Supplementary Noise Negation Methods
P1	Standard	58	46	None
	Novel	78	74	
	Neutral	86	62	
P2	Standard	66	52	None
	Novel	28	90	
	Neutral	10	78	
P3	Standard	94	58	None
	Novel	56	56	
	Neutral	36	92	
P4	Standard	52	68	None
	Novel	32	80	
	Neutral	80	58	
P5	Standard	44	100	None
	Novel	54	60	
	Neutral	68	60	
P6	Standard	80	54	None
	Novel	72	62	
	Neutral	70	52	
P7	Standard	54	52	None
	Novel	64	80	
	Neutral	66	50	
P8	Standard	92	46	None
	Novel	46	64	
	Neutral	50	60	
P9	Standard	58	80	Grounding Strap
	Novel	56	62	
	Neutral	58	58	
P10	Standard	76	56	Grounding Strap
	Novel	60	70	
	Neutral	64	64	
P11	Standard	64	58	Grounding Strap

	Novel	62	58	
	Neutral	64	60	
P12	Standard	68	58	Grounding Strap
	Novel	82	42	
	Neutral	56	60	
P13	Standard	56	56	Grounding Strap Insulated Transducers
	Novel	62	62	
	Neutral	48	72	
P14	Standard	70	56	Grounding Strap Insulated Transducers
	Novel	60	70	
	Neutral	54	56	
P15	Standard	70	56	Grounding Strap Suppressive Capacitors
	Novel	64	68	
	Neutral	54	72	
P16	Standard	56	72	Grounding Strap Suppressive Capacitors Insulated Transducers
	Novel	44	58	
	Neutral	56	62	
Average	Standard	66.1	60.5	N/A
	Novel	57.5	66.0	
	Neutral	57.5	63.5	

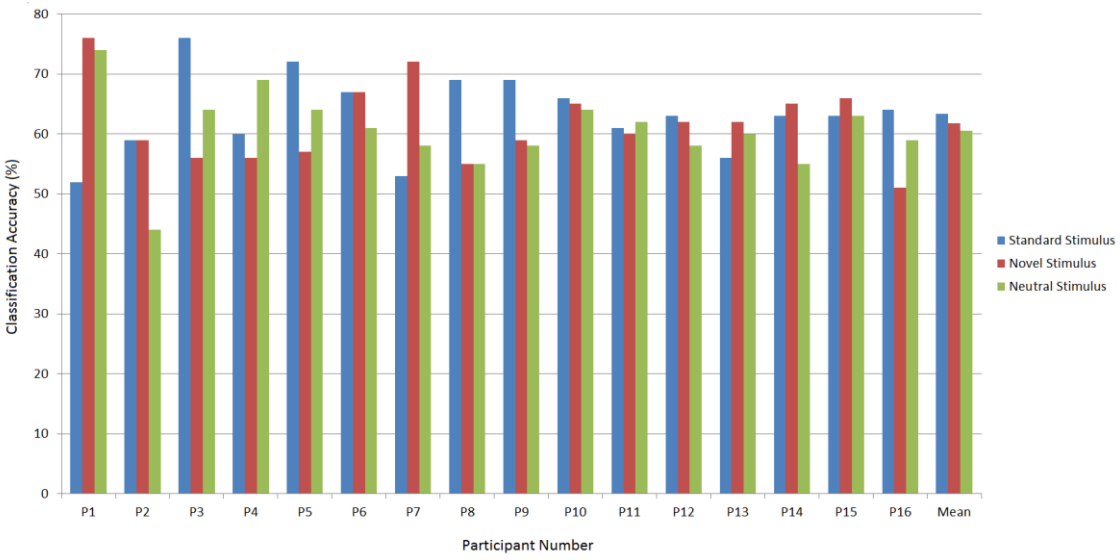

Fig. 5.26: A bar chart showing the classification accuracies of each stimulus method for each participant. No method appears to clearly outperform or underperform compared to the others.

The results are similar to those obtained by Zhang *et al.* 2007 [121], with only minor differences between the performances of the three types of stimuli. However, it is not known how much of an impact the EMI is having on the results.

Table 5.6 averages the results by their EMI suppression methods. However, again there is no discernable difference between each group. This implies that either the EMI is off-setting all channels by an equal amount and is therefore not masking the SSSEPs, or that

even a small amount of EMI is enough to mask the SSSEPs and therefore all trials are equally compromised. As the average results for each EMI suppression method are all above that of random chance, it suggests that the former is more likely.

TABLE 5.6. RESULTS OF SSSEP STUDY AVERAGED BY NOISE NEGATION METHOD

Subjects	Stimulus Method	Average Sensitivity (%)	Average Specificity (%)	Supplementary Noise Negation Methods
P1 – P8	Standard	67.5	59.5	None
	Novel	53.8	70.8	
	Neutral	58.3	64.0	
P9 – P12	Standard	66.5	63.0	Grounding Strap
	Novel	65.0	68.0	
	Neutral	60.5	60.5	
P13 – P14	Standard	63.0	56.0	Grounding Strap Insulated Transducers
	Novel	61.0	66.0	
	Neutral	51.0	64.0	
P15	Standard	70.0	56.0	Grounding Strap Suppressive Capacitors
	Novel	64.0	68.0	
	Neutral	54.0	72.0	
P16	Standard	56.0	72.0	Grounding Strap Suppressive Capacitors Insulated Transducers
	Novel	44.0	58.0	
	Neutral	56.0	62.0	
P1 – P16	Standard	66.1	60.5	Any
	Novel	57.5	66.0	
	Neutral	57.5	63.5	

Table 5.7 provides a comparison of the average classification accuracy of several studies that used the same experimental set-up. The results of this thesis' study are lower than the other studies, but their standard deviations put them within range of each other.

TABLE 5.7. AVERAGE RESULTS OF SSSEP STUDY IN COMPARISON WITH RESULTS OF SIMILAR STUDIES FROM THE LITERATURE

Source	Number of Subjects	Stimulus Method	Average Classification Accuracy (%)	Standard Deviation
Davies	16	Standard	63.3	6.6
		Novel	61.8	6.5
		Neutral	60.5	6.6
Muller-Putz *et al.* 2006 [42]	5	Standard	70.4	7.7
Zhang *et al.*2007 [121]	8	Standard	63.0	8.8

In order to make sure the order that the participant received each different stimulus was not a factor, either in terms of fatigue leading to a decrease in performance over time or in terms of experience leading to an increase, the order for each participant was randomised. Figure 5.27 shows a plot of the participants' results versus chronological time and no

relationship is present, confirming that the results for each stimulus were not skewed by the order in which they were administered.

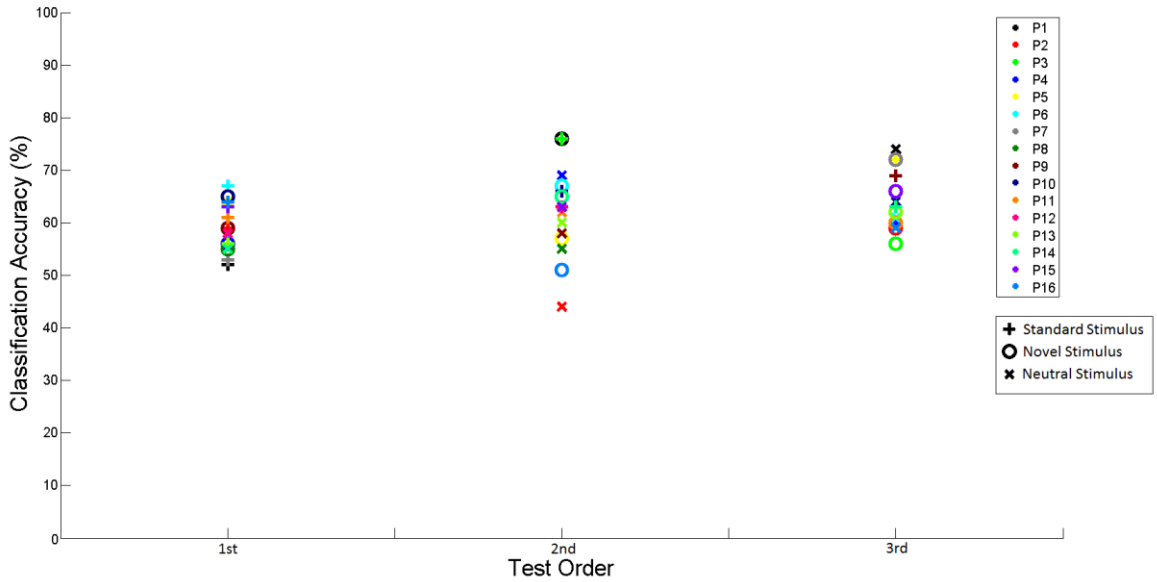

Fig. 5.27: A scatter plot of each participants classification accuracies plotted in the order the tests were administered. No relationship is visible.

As the vast majority of people have a dominant hand instead of being ambidextrous they may be more sensitive to stimulation in the dominant hand compared to their non-dominant one. This could skew the results by causing the SSSEP produced from the stimulus to their dominant hand being consistently more prevalent in the EEG even if the amplitudes of the vibrations to both hands are equal. To prevent this, the stimuli for each hand were swapped round every 50 trials, and during processing the signals were normalised by the maximum absolute value in their respective groups of 50.

Figure 5.28 shows a plot of the un-normalised PSD values of a random dataset. The average PSD when the participant's dominant hand was being stimulated is considerably higher, regardless of the stimulus they were attending to. This was found to be the case for all participants, regardless of the stimulus paradigm. This confirms that not accounting for the increased sensitivity in the participant's dominant hand could skew the results in one class's favour.

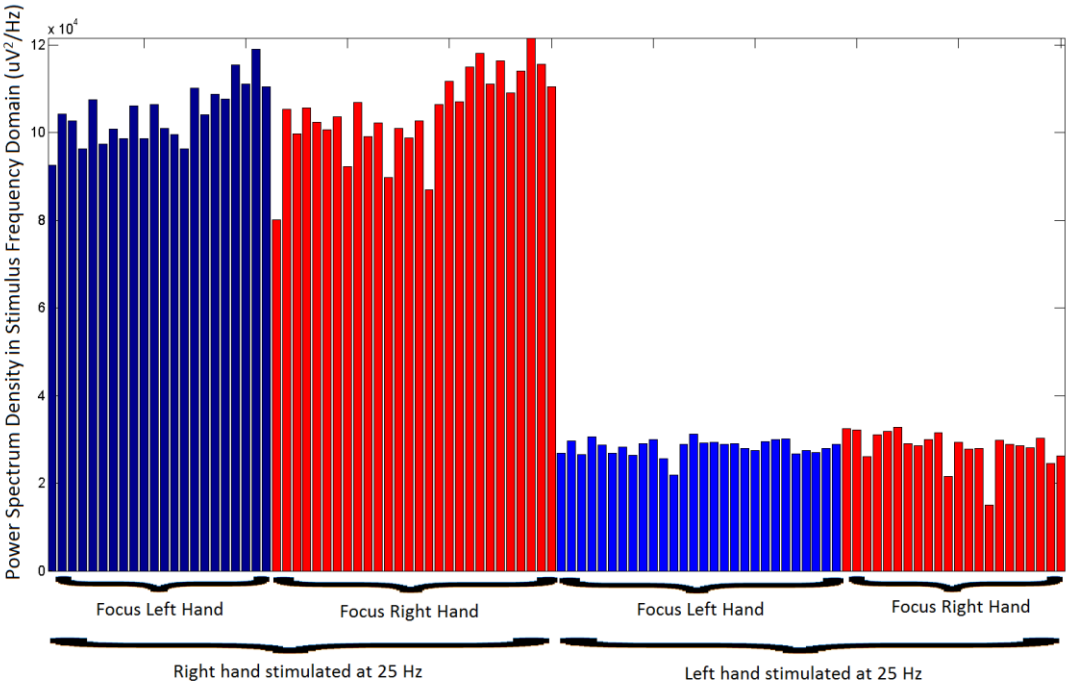

Fig. 5.28: A bar chart showing the variation in the PSD of the SSSEP over all trials from a randomly-selected dataset for the neutral stimulus. There is a significant drop in the PSD regardless for what stimulus is being attended to by the participant when the left hand is being stimulated versus the right. The participant in this case was right-handed.

5.6 Summary

Overall, little to no difference was found between the performances of the different types of stimuli. A possible reason is that the key to SSSEP performance might lie with the user's ability to focus effectively, and not with the differences in the underlying neurological responses to different types of tactile stimuli. If that is the case then changes in stimuli will only have an effect if they make it easier for the user to focus on one stimulus over another. Muller-Putz *et al.* 2006 [42] noted the difficulty of trying to block out one tactile stimulus over another compared to a visual one as the former is always present. The novel and neutral stimulus paradigms in this thesis' study do make the stimuli on one hand easier to block out due to its weakness or absence, but this will make the stimuli on the other hand comparatively more difficult to block out as it will be the dominating sensation, although there were no large differences between the sensitivities and specificities of these

stimuli to indicate this. A possible solution could be to have the stimuli on both hands set at just above a person's ATT, meaning they are barely felt and would be easy to mentally block either of them out.

The question of contamination cannot be ignored either. Though attempts to suppress the noise met with limited success, because it occupies the same frequency domain as the evoked potential being generated the SSSEP may be being masked by the EMI, potentially compromising the readings and affecting performance. The EMI was only apparent due to its magnitude. Vibrotactile transducers used in other studies may also be generating EMI that is going unnoticed because its amplitude is comparable to that of an SSSEP. It may be of value to construct and test a stimulus device with a focus on preventing EMI being emitted entirely to see if it impacts the performance of a standard SSSEP BCI.

CHAPTER 6

Conclusions and Future Work

Patients suffering from severe paralysis can be unable to use conventional assistive communication technologies, severely impacting their quality of life [133]. The use of EEG to help bridge the gap between mental command and execution of action has led to the creation of BCIs. BCIs can come in many different forms as they are made up of several components, depicted in Figure 6.1.

Fig 6.1: The fundamental components of a BCI.

EEG amplifiers can make use of several types of electrodes, their differences tending to be determined by a focus on signal quality over convenience and vice versa. The closer the EEG electrodes are to the source of the signal, the less noise and interference present in the recording. Electrographic electrodes are placed beneath the brain's surface, requiring surgery and carrying all the risks of infection and complications it entails [15]. At the opposite end of the spectrum are passive surface electrodes placed on the scalp. The dense materials, such as the bone that the signals pass through add significant distortions and noise [134]. However, only the scrubbing of the skin and the addition of some conductive gel to reduce impedance is needed to place these types of electrodes.

Next there is the choice of BCI paradigm – the method of generating an evoked potential through a conscious decision on the part of the user. Evoked potentials fall into two categories: self-generated and reflexive. A self-generated, self-paced, asynchronous evoked

potential relies on the user instigating the change in brain activity that results in an evoked potential being produced without any underlying neurological component being triggered by an external stimulus. Self-generated evoked potentials are easier to interpret as they appear at the user's command, but they can require a lot of training to generate them consistently and some people never master the concept. It can also be very fatiguing for the user to concentrate repeatedly on producing the same changes in brain activity, something not desirable if the user already suffers from a physical trauma that inhibits parts of their body.

Reflexive evoked potentials pair their evoked potential generation to the regular application of a unique stimulus. The evoked potentials produced from the reception of these stimuli are automatic and the user is not even aware their brain is reacting to the stimulus. Consequently little training is needed and there is also less latency in their production. A more complex BCI paradigm is typically needed to ascribe intent to the detection of these evoked potentials in EEG recordings, such as the P300 Speller.

Due to the very low SNR of surface EEG, the raw recordings are too noisy to easily distinguish between the different evoked potentials present in them. Signal processing methods must be applied to extract a set of features that best represent the differences between the possible types of evoked potential the user is generating. Surface EEG presents its own unique problems as a multitude of different signal sources will be contributing to the data recorded in each channel, meaning the signal will have a very low spatial resolution. The differences between the evoked potentials can sometimes be too subtle to quantify, or there is insufficient knowledge of the neurological processes that underpin them. This leads to the application of Blind Source Separation (BSS) techniques – algorithms that focus on identifying consistent statistical differences between EEG recordings. The right technique must be chosen for the right set of features that are to be

extracted from the EEG recording. Practical considerations outside of the lab setting such as time, computational requirements and the number of channels needed must also be taken into account.

The current state of the field is such that a classification accuracy of 70% can be seen as sufficient [120] and that information transfer rates (ITR) rarely exceed 10 bits per minute. Whilst for a patient deprived of all methods of communication this could be enough to improve their quality of life, there is definitely room for improvement in the efficiency of BCIs.

6.1 Objectives

The objectives of this thesis were to enhance existing BCI systems via the design and evaluation of novel techniques that underpin the components of BCIs – namely the generation of evoked potentials through paradigms and the signal processing and feature extraction techniques used to process them.

These objectives were met in part. The novel signal processing techniques T-MEMD and ST-MEMD did not result in a change in performance compared to EMD and MEMD respectively, but may do so if applied to a signal more temporally dependent. New evidence that the differences between different types of MI are inherently spatial was found during the techniques' evaluations.

The evaluation of the novel SSSEP BCI paradigm was inconclusive, possibly due to the presence of an extra-physiological artefact. However solutions to the problem were identified and implemented with partial success.

The results are discussed in further detail in the proceeding subsections.

6.1.1 Novel Signal Processing Technique

The approach for creating a novel signal processing technique used the existing technique of Empirical Mode Decomposition (EMD), a data-driven method that splits a signal by frequency in to a group of component signals called Intrinsic Mode Functions (IMFs), as a basis. EMD was chosen because of its ability to objectively decompose a signal into a group of components, with no pre-selected variables needed.

A proof-of-concept study was first carried out by applying EMD to two different pre-recorded dataset to ascertain if it could be used successfully in conjunction with EEG. This was confirmed as possible with accuracy rates of 88.5% and 64.4% respectively, with both results performing well in comparison to other studies in the literature that had used different methods on the same datasets.

Next, two variants of EMD were developed, based on the enhanced Multi-variate EMD (MEMD) method. MEMD decomposes all spatial signal channels simultaneously, so that their data can be used to inform their neighbours' decompositions, resulting in superior performance thanks to the new spatial information incorporated into the IMFs. The idea was to then use Takens' theorem, an algorithm that dynamically embeds a signal so that it is represented by a set of signals that represent the original as it changes over time. This set of temporal channels could then be decomposed using MEMD so that the neighbouring temporal channels could inform a channel's decomposition and incorporate temporal information into the IMFs. This resulted in two methods: Temporal MEMD (T-MEMD) which decomposed the temporal channels of spatial channels individually, and Spatio-temporal MEMD (ST-MEMD) which decomposed the temporal channels of all spatial channels at the same time in order to incorporate both the spatial and temporal dynamics into the resulting IMFs.

These techniques were applied to a large dataset of 990 trials, along with EMD and MEMD for comparison. The results showed that T-MEMD performed on a par with EMD, and ST-EMD performed on a par with MEMD with both spatial methods giving the best performance. This lead to the conclusion that the added temporal information was not contributing to the classifier at all, but that the spatial information was. This was hypothesised to be the case because the differences between the classes of the dataset the methods were applied to, the EEG recordings from a Motor Imagery BCI, are inherently spatial and not temporal. This helps reinforce studies in the literature that show that the neurological systems that underpin the control of different limbs are divided spatially.

6.1.2 Novel Stimulus Paradigm

The approach for creating a novel stimulus paradigm used tactile stimuli as its basis. This is because BCIs that use visual stimuli still require the user to have voluntary gaze control, something that the patients most likely to need a BCI often do not have. It also leaves the visual and auditory inputs of the human body free for social interaction. Steady-State Somatosensory Evoked Potentials (SSSEPs) were selected as this combines tactile stimuli with the reflexive evoked potential of SSEPs, which are simpler to detect with their well-defined frequency and temporal domains. These properties mean they also pose an optimal application for EMD-based techniques when it comes to processing the EEG recordings.

To try and enhance the performance of the BCI a novel form of SSSEP stimulus was designed and evaluated. Due to the difficulty of differentiating between the changes in amplitude of two different SSSEPs in the standard SSSEP BCI paradigm, it was hypothesised that being able to differentiate between the onset of an SSSEP and the absence of an SSSEP would result in better performance. To that end an SSSEP stimulus was developed that would be similar to the absence of an SSSEP but still distinguishable from neutral EEG

activity. Studies in the literature showed that the surface area the stimulus was being applied to and its amplitude had the greatest impact on the conscious detection of vibrotactile stimuli. If a stimulus was applied to a low surface area on the user's hand, its amplitude could be reduced until it was just below the user's threshold for conscious detection, or Absolute Tactile Threshold (ATT). It was hypothesised that a stimulus just below the ATT would generate a very small SSSEP yet still suppress the α activity associated with EEG activity when no stimuli is being experienced.

16 participants were recruited and extensive work put in over several months to design a stimulus generator that could produce vibrotactile stimuli at the desired frequencies and amplitudes. Each participant performed 100 trials of an SSSEP BCI that used two stimuli of equal amplitude but differing frequencies, 100 trials of an SSSEP BCI that used two stimuli of equal frequency but differing amplitudes and surface areas so that one stimulus was above the participant's ATT and the other below it, and 100 trials of an SSSEP BCI were only one hand was stimulated. These represented the "Standard", "Novel", and "Neutral" stimuli paradigms.

The resulting performance showed little to no difference between stimulus paradigms. However, this may be because of the presence of a large amount of Electro-magnetic Interference (EMI) artefact. These artefacts were being generated by the stimulus equipment by the current used to power the transducers. This meant the EMI occupied the same frequency and temporal domains as the SSSEPs being produced, potentially masking them. Various solutions were implemented to reduce the magnitude of the EMI but the artefact was still present to some degree in all trials, and thus it became unclear whether the hypothesis could be proved or disproved conclusively.

6.2 Future Work

Possible directions to take the work contained in this thesis is finding an appropriate application for the T-MEMD signal processing technique and its spatio-temporal variation ST-MEMD in order to confirm if the temporal dynamics it incorporates into the IMFs it produces contain any information of significance that would enhance the features extracted from the signal. Such an application does not have to be limited to EEG or even BCI. Temporal dynamics play a large part in functional Magnetic Resonance Imaging (fMRI) signals [135]. When part of the brain activates to perform a task the blood flow increases after a short delay and is maintained for a short while after the task has been performed in order to supply that part of the brain with oxygen. fMRI can detect this using Blood-oxygen-level Dependent (BOLD) contrast imaging, where the magnetic signal varies due to the amount of oxygenated or de-oxygenated haemoglobin present in the blood [136]. Like EEG, fMRI devices use multiple channels all over the user's scalp to record their inputs so minimal adaptation to implement the T-MEMD and ST-MEMD algorithms for fMRI data would be needed.

Another avenue of research would be the design and testing of a noise-free vibrotactile stimulator. This could be done by taking the idea behind the upgraded transducers used in Chapter 5 to try and mitigate the EMI, and extending it even further – namely the distancing of all electronic components from the participant and conducting the vibrationary stimulus through solid plastic rods to such a degree that the participant is out of range from all EMI sources.

An alternative SSSEP-based BCI paradigm to evaluate could be one where the different stimuli are equally easy for the user to block out. Muller-Putz *et al.* 2006 [42] noted the difficulty in concentrating on the desired SSSEP stimulus versus switching attention between different SSVEP stimuli as the tactile sensation is always present. If the

"standard" SSSEP BCI of having each hand stimulated by a vibration of equal amplitude but different frequency were to be used, the amplitudes of both stimuli could be reduced so that they were both just above the user's Absolute Tactile Threshold (ATT). This would make it easier for the user to block out the unwanted stimulus in favour of the desired one, resulting in greater differences between the two classes of trial.

References

[1] D. Johnston, and S.M. Wu, *"Foundations of Cellular Neurophysiology,"* 4th Edition, Massachusetts: The MIT Press, pp. 39-51, November 1994.

[2] T.F. Collura, "*History and Evolution of Electroencephalographic Instruments and Techniques*," Journal of Clinical Neurophysiology, vol. 10, pp. 476-504, October 1993.

[3] P.N. Leigh, and K Ray-Chaudhuri, "*Motor Neuron Disease*," Journal of Neurology, Neurosurgery and Psychiatry, vol. 57, pp. 886-896, August 1994.

[4] J.R. Wolpaw, N. Birbaumer, D.J. McFarland, G. Pfurtscheller, and T.M. Vaughan, "*Brain-computer interfaces for communication and control*," Clinical Neurophysiology, vol. 113, pp. 767-791, March 2002.

[5] T. Ball, M. Kern, I. Mutschler, A. Aertsen, and A. Schulze-Bonhage, "*Signal quality of simultaneously recorded invasive and non-invasive EEG*," NeuroImage, vol. 46, pp. 708-716, July 2009.

[6] C. Ramon, P. Schimpf, J. Haueisen, M. Holmes, and A. Ishimaru, "*Role of Soft Bone, CSF and Gray Matter in EEG Simulations,*" Brain Topography, vol. 16, pp. 245-248, June 2004.

[7] K.H. Chiappa, and A.H. Ropper, "*Evoked Potentials in Clinical Medicine*," The New England Journal of Medicine, pp. 1140-1150, May 1982.

[8] F. Nijboer, E.W. Sellers, J. Mellinger, M.A. Jordan, T. Matuz, A. Furdea, S. Halder, U. Mochty, D.J. Krusienski, T.M. Vaughan, J.R. Wolpaw, N. Birbaumer, and A. Kübler, "*A P300-based brain–computer interface for people with amyotrophic lateral sclerosis,*" Clinical Neurophysiology, vol. 119, pp. 1909-1916, August 2008.

[9] P. Celka, "*Neuronal coordination in the brain: A signal processing perspective,*" Signal Processing, vol. 85, pp. 2063-2064, November 2005.

[10] J.R. Wolpaw, D.J. McFarland, G.W. Neat, and C.A. Forneris, "*An EEG-based brain-computer interface for cursor control*," Electroencephalography and Clinical Neurophysiology, vol. 78, pp. 252-259, March 1991.

[11] C. Park, D. Looney, N. Rehman, A. Ahrabian, and D.P. Mandic, "*Classification of Motor Imagery BCI using Multivariate Empirical Mode Decomposition*," IEEE Transactions On Neural Systems And Rehabilitation Engineering, vol. 21, pp. 10-22, January 2013.

[12] T.F. Pettijohn, "*Lobes of the cerebral cortex*", Diagram, 1998, Psychology: A ConnecText, http://www.mhhe.com/cls/psy/ch02/brain.mhtml (accessed April 28th, 2015).

[13] C.A. Chin, A. Barreto, J.G. Cremades, and M. Adjouadi, "*Integrated electromyogram and eye-gaze tracking cursor control system for computer users with motor disabilities*," Journal of Rehabilitation Research and Development, vol. 45, pp. 161-174, June 2008.

[14] E.C. Leuthardt, K.J. Miller, G. Schalk, R.P.N. Rao, and J.G. Ojemann, "*Electrocorticography-based brain computer interface – the Seattle experience*," IEEE Transactions on Neural Systems and Rehabilitation Engineering, vol. 14, pp. 194-198, June 2006.

[15] R.L. Swank, and S.J. Brendler, "*The cerebellar electrogram: Effects of anesthesia, analeptics, and local novocaine*," Electroencephalography and Clinical Neurophysiology, vol. 3, pp. 207-212, May 1951.

[16] A.C. MettingVanRijn, A.P. Kuiper, T.E. Dankers, and C.A. Grimbergen, "*Low-cost Active Electrode Improves the Resolution in Biopotential Recordings*," Engineering in Medicine and Biology Society, vol. 1, pp. 101-102, November 1996.

[17] H.J. Landau, and N. J. Murray Hill, "*Sampling, data transmission, and the Nyquist rate*," Proceedings of the IEEE, vol. 55, pp. 1701-1706, October 1967.

[18] A. Schnürer, "*gtec_gGAMMAsys_girl*", Photograph, 2012, The Neuro Network, http://theneuronetwork.com/photo/gtec-ggammasys-girl (accessed April 28th, 2015).

[19] A. Schnürer , "g.HIAmp Multichannel Amplifier", Photograph, 2012, g.tec Medical Engineering, http://www.gtec.at/Products/Hardware-and-Accessories/g.HIamp-Specs-Features (accessed April 28th, 2015).

[20] H. Jasper, "*The ten-twenty electrode system of the International Federation*," Electroencephalography and Clinical Neurophysiology, vol. 10, pp. 370-375, 1958.

[21] G.E. Chatriana, E. Letticha, and P.L. Nelsona, "*Ten Percent Electrode System for Topographic Studies of Spontaneous and Evoked EEG Activities*," American Journal of EEG Technology, vol. 25, pp. 83-92, May 1985.

[22] G. Schalk, D.J. McFarland, T. Hinterberger, N. Birbaumer, J.R. Wolpaw, "*BCI2000: A General-Purpose Brain-Computer Interface (BCI) System*," IEEE Transactions on Biomedical Engineering, vol. 51, pp. 1034-1043, June 2004.

[23] J.J. Vidal, "*Toward Direct Brain-Computer Communication*," Annual Review of Biophysics and Bioengineering, vol. 2, pp. 157-180, June 1973.

[24] A.M. Halliday, W.I. McDonald, and J. Mushin, "*Visual Evoked Response in Diagnosis of Multiple Sclerosis*," British Medical Journal, vol. 4, pp. 661-664, December 1973.

[25] G. Pfurtscheller, and C. Neuper, "*Motor imagery and direct brain-computer communication*," Proceedings of the IEEE, vol. 89, pp. 1123-1134, July 2001.

[26] G. Pfurtscheller, C. Brunner, A. Schlogl, and F.H. Lopes da Silva, "*Mu rhythm (de)synchronization and EEG single-trial classification of different motor imagery tasks*," NeuroImage, vol. 31, pp. 153-159, May 2006.

[27] G. Pfurtscheller, and F.H. Lopes da Silva, "*Event-related EEG/MEG synchronization and desynchronization: basic principles*," Clinical Neurophysiology, vol. 110, pp. 1842-1857, November 1999.

[28] S. Lemm, K.-R. Müller, and G. Curio, "*A Generalized Framework for Quantifying the Dynamics of EEG Event-Related Desynchronization*," PLOS Computational Biology, vol. 5, August 2009.

[29] J.R. Wolpaw, D.J. McFarland, G.W. Neat, and C.A. Forneris, "*An EEG-based brain-computer interface for cursor control*," Electroencephalography and Clinical Neurophysiology, vol. 78, pp. 252-259, March 1991.

[30] J. Kalcher, D. Flotzinger, C. Neuper, S. Gölly, and G. Pfurtscheller, "*Graz brain-computer interface II: towards communication between humans and computers based on online classification of three different EEG patterns*," Medical and Biological Computing and Engineering, vol. 34, pp. 382-388, September 1996.

[31] N. Birbaumer, A. Kübler, N. Ghanayim, T. Hinterberger, J. Perelmouter, J. Kaiser, I. Iversen, B. Kotchoubey, N. Neumann, and H. Flor, "*The Thought Translation Device (TTD) for Completely Paralyzed Patients*," IEEE Transactions on Rehabilitation Engineering, vol. 8, pp. 190-193, June 2000.

[32] The-Crankshaft Publishing, "*Negativity and positivity from SCP EEGs*", Figure, 2008, Current Practices in Electroencephalogram-Based Brain-Computer Interfaces, http://what-when-how.com/information-science-and-technology/current-practices-in-electroencephalogram-based-brain-computer-interfaces-information-science/ (accessed August 10th, 2015).

[33] N. Birbaumer, A. Kübler, N. Ghanayim, T. Hinterberger, J. Perelmouter, J. Kaiser, I. Iversen, B. Kotchoubey, N. Neumann, and H. Flor, "*The Thought Translation Device (TTD) for Completely Paralyzed Patients*," IEEE Transactions on Rehabilitation Engineering, vol. 8, pp. 190-193, June 2000.

[34] L.A. Farwell, and E. Donchin, "*Talking off the top of your head: toward a mental prosthesis utilizing event-related brain potentials*," Electroencephalography and Clinical Neurophysiology, vol. 70, pp. 510-523, December 1988.

[35] E.W. Sellers, A. Kubler, and E. Donchin, "*Brain-computer interface research at the university of south Florida cognitive psychophysiology laboratory: the P300 speller*," IEEE Transactions on Neural Systems and Rehabilitation Engineering, vol. 14, pp. 221-224, June 2006.

[36] G. Townsend, B.K. LaPallo, C.B. Boulay, D.J. Krusienski, G.E. Frye, C.K. Hauser, N.E. Schwartz, T.M. Vaughan, J.R. Wolpaw, and E.W. Sellers, "*A novel P300-based brain-computer interface stimulus presentation a paradigm: moving beyond rows and columns*," Clinical Neurophysiology, vol. 121, pp. 1109-1120, July 2010.

[37] B.Z. Allison, D.J. McFarland, G. Schalk, S.D. Zheng, M.M. Jackson, and J.R. Wolpaw, "*Towards an independent brain-computer interface using steady state visual evoked potentials*," Clinical Neurophysiology, vol. 119, pp. 399-408, February 2008.

[38] J.H. Lim, H.J. Hwang, C.H. Han, K.Y. Jung, and C.H. Im, "*Classification of binary intentions for individuals with impaired oculomotor function: 'eyes-closed' SSVEP-based brain-computer interface (BCI)*," Journal of Neural Engineering, vol. 10, pp. 79-80, April 2013.

[39] K. Hecox, and R. Galambos, "*Brain Stem Auditory Evoked Responses in Human Infants and Adults*," Archives of Otolaryngology, vol. 99, pp. 30-33, January 1974.

[40] G.R. McMillan, G.L. Calhoun, M.S. Middendorf, J.H. Schnurer, D.F. Ingle and V.T. Nasman, "*Direct brain interface utilizing self regulation of Steady-State Visual Evoked Response (SSVER)*," 18th Rehabilitation Engineering and Assistive Technology Society of North America Conference, pp.693-695, 1995.

[41] M. Middendorf, G. McMillan, G. Calhoun, and K.S. Jones, "*Brain–Computer Interfaces Based on the Steady-State Visual-Evoked Response*," IEEE Transactions on Rehabilitation Engineering, vol. 8, pp. 211-214, June 2000.

[42] G.R. Muller-Putz, R. Scherer, C. Neuper, and G. Pfurtscheller, "*Steady-state somatosensory evoked potentials: suitable brain signals for brain-computer interfaces?*" IEEE Transactions on Neural Systems and Rehabilitation Engineering, vol. 14, pp. 30-37, March 2006.

[43] B.A. Eriksen, and C.W. Eriksen, "*Effects of noise letters upon the identification of a target letter in a nonsearch task*," Attention, Perception, and Psychophysics, vol. 16, pp. 143-149, January 1974.

[44] C. Roussel, G. Hughes, and F. Waszak, "*Action prediction modulates both neurophysiological and psychophysical indices of sensory attenuation*," Frontiers in Human Neuroscience, vol. 8, February 2014.

[45] S.A. Hillyard, and M. Kutas, "*Reading senseless sentences: brain potentials reflect semantic incongruity*," Science, vol. 207, pp. 203-205, January 1980.

[46] H.M. Müller, S. Weiss, and G. Rickheit, "*Experimentelle Neurolinguistik: Der Zusammenhang von Sprache und Gehirn*," Linguistics: the Bielefeld View, pp. 125-128, 1997.

[47] S. Marella, "*EEG Artifacts*," 2012, Slideshare.net, http://www.slideshare.net/SudhakarMarella/eeg-artifacts-15175461 (accessed April 28th, 2015).

[48] E.C. Cherry, "*Some experiments on the recognition of speech, with one and with two ears*," Journal of the Acoustical Society of America, vol. 25, pp. 975-979, 1953.

[49] A.V. Oppenheim, R. W. Schafer, and J.R. Buck, "*Discrete-time Signal Processing*," 2nd Edition, New Jersey: Prentice-Hall, Inc., January 1999.

[50] M.T. Heideman, D.H. Johnson, and C.S. Burrus, "*Gauss and the history of the fast Fourier transform*," Archive for History of Exact Sciences, vol. 34, pp. 265-277, 1985.

[51] M.T. Heideman, D.H. Johnson, and C.S. Burrus, "*Gauss and the history of the fast Fourier transform*," Archive for History of Exact Sciences, vol. 34, pp. 265-277, 1985.

[52] J.B. Allen, "*Short term spectral analysis, synthesis, and modification by discrete Fourier transform*," IEEE Transactions on Acoustics, Speech and Signal Processing, vol. 25, pp. 235-238, June 1977.

[53] A. Grossmann, and J. Morlet, "*Decomposition of Hardy Functions into Square Integrable Wavelets of Constant Shape*," Society for Industrial and Applied Mathematics Journal on Mathematics, vol. 15, pp. 723-736, September 1982.

[54] N. Ahuja, S. Lertrattanapanich, and N.K. Bose, "*Properties determining choice of mother wavelet*," Vision, Image and Signal Processing, vol. 152, pp. 659-664, October 2005.

[55] I. Daubechies, "*The wavelet transform, time-frequency localization and signal analysis*," IEEE Transactions on Information Theory, vol. 36, pp. 961-1005, September 1990.

[56] M. Guo, G. Xu, L. Wang, and J. Wang, "*Research on auditory BCI based on wavelet transform*," 2012 IEEE International Conference on Virtual Environments Human-Computer Interfaces and Measurement Systems, pp. 171-175, July 2012.

[57] W. Ting, Y. Guo-zheng, Y. Bang-hua, and S. Hong, "*EEG feature extraction based on wavelet packet decomposition for brain computer interface*," Measurement, vol. 41, pp. 618-625, July 2008.

[58] M.B. Khalid, N.I. Rao, I. Rizwan-i-Haque, S. Munir, and F. Tahir, "*Towards a Brain Computer Interface using wavelet transform with averaged and time segmented*

adapted wavelets," 2nd International Conference on Computer, Control and Communication, pp. 1-4, February 2009.

[59] I. Daubechies, J. Lu, and H.-T. Wu, "*Synchrosqueezed wavelet transforms: An empirical mode decomposition-like tool*," Applied and Computational Harmonic Analysis, vol. 30, pp. 243-261, March 2011.

[60] T.M. Rutkowski, and H. Mori, "*Tactile and bone-conduction auditory brain computer interface for vision and hearing impaired users*," Journal of Neuroscience Methods, vol. 244, pp. 45-51, April 2015.

[61] D.E. Newland, "*Harmonic Wavelet Analysis*," Proceedings of the Royal Society of London A, vol. 443, pp. 203-225, October 1993.

[62] H. Adeli, Z. Zhou, and N. Dadmehr, "*Analysis of EEG records in an epileptic patient using wavelet transform*," Journal of Neuroscience Methods, vol. 123, pp. 69-87, February 2003.

[63] A. Cichocki, and R. Unbehauen, "*Robust learning algorithm for blind separation of signals*," Electronics Letters, vol. 30, pp. 1386-1387, August 1994.

[64] K. Pearson, "*On Lines and Planes of Closest Fit to Systems of Points in Space*," Philosophical Magazine, vol. 2, pp. 559-572, 1901.

[65] Steven Holland, "*Principal Components Analysis*," Diagram, 2013, Data Analysis in the Geosciences, http://strata.uga.edu/6370/lecturenotes/principalComponents.html (accessed April 28th, 2015).

[66] R. Kottaimalai, I. Srivilliputtur, M.P. Rajasekaran, V. Selvam, and B. Kannapiran, "*EEG signal classification using Principal Component Analysis with Neural Network in Brain Computer Interface applications*," 2013 International Conference on Emerging Trends in Computing, Communication and Nanotechnology, pp. 227-231, March 2013.

[67] C. Guan, M. Thulasidas, and J. Wu, "*High performance P300 speller for brain-computer interface*," 2004 IEEE International Workshop on Biomedical Circuits and Systems, December 2004.

[68] P. Comon, "*Independent Component Analysis*," Higher-Order Statistics, pp. 29-38, 1992.

[69] C.I. Hung, P.L. Lee, Y.T. Wu, L.F. Chen, T.C. Yeh, and J.C. Hsieh, "*Recognition of motor imagery electroencephalography using independent component analysis and machine classifiers*," Annals of Biomedical Engineering, vol. 33, pp. 1053-1070, August 2005.

[70] M. Naeem, C. Brunner, R. Leeb, B. Graimann, and G. Pfurtscheller, "*Seperability of four-class motor imagery data using independent components analysis*," Journal of Neural Engineering, vol. 3, pp. 208-216, September 2006.

[71] F. Piccione, F. Giorgi, P. Tonin, K. Priftis, S. Giove, S. Silvoni, G. Palmas, and F. Beverina, "*P300-based brain computer interface: reliability and performance in healthy and paralysed participants*," Clinical Neurophysiology, vol. 117, pp. 531-537, March 2006.

[72] B. Kamousi, Z. Liu, and B. He, "*Classification of motor imagery tasks for brain-computer interface applications by means of two equivalent dipoles analysis*," vol. 13, pp. 166-171, June 2005.

[73] Z.J. Koles, M.S. Lazar, and S.Z. Zhou, "*Spatial patterns underlying population differences in the background EEG*," Brain Topography, vol. 2, pp. 275-284, July 1990.

[74] W. Samek, C. Vidaurre, K.-R Müller, and M. Kawanabe, "*Stationary common spatial patterns for brain–computer interfacing*," Journal of Neural Engineering, vol. 9, August 2011.

[75] Y. Wang, S. Gao, and X. Gao, "*Common Spatial Pattern Method for Channel Selelction in Motor Imagery Based Brain-computer Interface*," 27th Annual International Conference of the Engineering in Medicine and Biology Society, pp. 5392-5395, January 2006.

[76] C. Cortes, and V. Vapnik, "*Support-vector networks*," Machine Learning, vol. 20, pp. 273-297, September 1995.

[77] N.E. Huang, Z. Shen, S.R. Long, M.C. Wu, H.H. Shih, Q. Zheng, N.-C. Yen, C.C. Tung, and H.H. Liu, "*The empirical mode decomposition and the Hilbert spectrum for nonlinear and non-stationary time series analysis*," Proceedings of the Royal Society of London A, vol. 454, pp. 903-995, November 1998.

[78] N.E. Huang, M.-L. Wu, W. Qu, S.R. Long, and S.S.P. Shen, "*Applications of Hilbert–Huang transform to non-stationary financial time series analysis*," Applied Stochastic Models in Business and Industry, vol. 19, pp. 245-268, September 2003.

[79] T. Schlurmann, "*Spectral Analysis of Nonlinear Water Waves Based on the Hilbert-Huang Transformation*," Journal of Offshore Mechanics and Arctic Engineering, vol. 124, pp. 22-27, August 2001.

[80] P.F. Diez, V. Mut, E. Laciar, A. Torres, and E. Avila, "*Application of the empirical mode decomposition to the extraction of features from EEG signals for mental task classification*," International Conference of the IEEE Engineering in Medicine and Biology Society, pp. 2579-2582, September 2009.

[81] P. Wei, Q. Li, and G. Li, "*Classifying motor imagery EEG by Empirical Mode Decomposition based on spatial-time-frequency joint analysis approach*," International Conference on Future BioMedical Information Engineering, pp. 489-492, December 2009.

[82] N. Williams, I. Daly, S.J. Nasuto, D. Saddy, and K. Warwick, "*ERP Classification using Empirical Mode Decomposition*," 5th IEEE EMBS UK and RI Postgraduate Conference in Biomedical Engineering and Medical Physics, July 2009.

[83] W. He, P. Wei, L. Wang, and Y. Zou, "*A novel EMD-based Common Spatial Pattern for motor imagery brain-computer interface*," International Conference on Biomedical and Health Informatics, pp. 216-219, January 2012.

[84] C.H. Wu, H.C. Chang, P.L. Lee, K.S. Li, J.J. Sie, C.W. Sun, C.Y. Yang, P.H. Li, H.T. Deng, and K.K. Shyu, "*Frequency recognition in an SSVEP-based brain computer interface using empirical mode decomposition and refined generalized zero-crossing*," Journal of Neuroscience Methods, vol. 196, pp. 170-181, March 2011.

[85] A.E. Zadeh, A. Khazaee, and V. Ranaee, "*Classification of the electrocardiogram signals using supervised classifiers and efficient features*," Computer Methods and Programs in Biomedicine, vol. 99, pp. 179-194, August 2010.

[86] A. Buttfield, P.W. Ferrez, and J.R. Millán, "*Towards a robust BCI: error potentials and online learning*," IEEE Transactions on Neural Systems & Rehabilitation Engineering, vol. 14, pp. 164-168, June 2006.

[87] R.A. Fischer, "*The Use of Multiple Measurements in Taxonomic Problems*," Annals of Eugenics, vol. 7, pp. 179-188, September 1936.

[88] W.S. McCulloch, and W. Pitts, "*A logical calculus of the ideas immanent in nervous activity*," Bulletin of Mathematical Biophysics, vol. 5, pp. 115-113, December 1943.

[89] C. Sergiu, "*Artifical neural network*", Diagram, 2011, Financial Predictor via Neural Network, http://www.codeproject.com/Articles/175777/Financial-predictor-via-neural-network (accessed April 28th, 2015).

[90] D. Garrett, D.A. Peterson, C.W. Anderson, M.H. Thaut, "*Comparison of linear, nonlinear, and feature selection methods for EEG signal classification*," IEEE

Transactions on Neural Systems and Rehabilitation Engineering, vol. 11, pp. 141-144, June 2003.

[91] S.M. Zhou, J.Q. Gan, and F. Sepulveda, "*Classifying mental tasks based on features of higher-order statistics from EEG signals in brain–computer interface*," Information Sciences, vol. 178, pp. 1629-1640, March 2008.

[92] D.G. Altman, and J.M. Bland, "*Diagnostic tests. 1: Sensitivity and specificity*," British Medical Journal, vol. 308, pp. 1552, June 1994.

[93] J.R. Pearce, "*An introduction to information theory: symbols, signals and noise*," 2nd Edition, New York: Dover Publications, January 1980.

[94] M. Cheng, X. Gao, S. Gao, and D. Xu, "Design and implementation of a brain-computer interface with high transfer rates," IEEE Transactions on Biomedical Engineering, vol. 49, pp. 1181-1186, November 2002.

[95] B. Blankertz, K.-R. Muller, G. Curio, T.M. Vaughan, G. Schalk, J.R. Wolpaw, A. Schlogl, C. Neuper, G. Pfurtscheller, T. Hinterberger, M. Schroder, and N. Birbaumer, "*The BCI competition 2003: progress and perspectives in detection and discrimination of EEG single trials*," IEEE Transactions on Biomedical Engineering, vol. 51, pp. 1044-1051, June 2004.

[96] L.L. McQuitty, "*Hierarchical Linkage Analysis for the Isolation of Types*," Educational and Psychological Measurement, vol. 20, pp. 55-67, April 1960.

[97] B.-G. Xu, and A.-G. Song, "*Pattern recognition of motor imagery EEG using wavelet transform*," Journal of Biomedical Science and Engineering, vol. 1, pp. 64-67, June 2008.

[98] S.R.H. Davies, and C.J. James, "*Multi-Channel Empirical Mode Decomposition in Brain-Computer Interfaces*", 7th IEEE EMBS UK and RI Postgraduate Conference in Biomedical Engineering and Medical Physics, pp. 21, July 2013.

[99] W. Jia, X. Zhao, H. Liu, X. Gao, S. Gao, and F. Yang, "*Classification of Single Trial EEG during Motor Imagery based on ERD*," 26th Annual International Conference of the IEEE Engineering in Medicine and Biology Society, pp. 5-8, September 2004.

[100] B. Blankertz, K.-R. Muller, D. Krusienski, G. Schalk, J.R. Wolpaw, A. Schlogl, G. Pfurtscheller, J.R. Millan, M. Schroder, and N. Birbaumer, "*The BCI competition III: validating alternative approaches to actual BCI problems*," IEEE Transactions On Neural Systems And Rehabilitation Engineering, vol. 31, pp. 153-159, June 2006.

[101] S.R.H. Davies, and C.J. James, "*Novel use of empirical mode decomposition in single-trial classification of motor imagery for use in Brain-Computer Interfaces*", 35th Annual International Conference of the IEEE EMBS, pp. 5610-5613, July 2013.

[102] P. Peart, "*The dispersion of the Hammersley Sequence in the unit square*", Monatshefte für Mathematik, vol. 94, pp. 249-261, 1982.

[103] B. Blankertz, G. Dornhege, M. Krauledat, K.-R. Müller, and G. Curio, "*The non-invasive Berlin Brain-Computer Interface: Fast acquisition of effective performance in untrained subjects*," NeuroImage, vol. 37, pp. 539-550, January 2007.

[104] C.J. James, and D. Lowe, "*Extracting multisource brain activity from a single electromagnetic channel*," Artificial Intelligence in Medicine, vol. 28, pp. 89-104, May 2003.

[105] F. Takens, "*Detecting strange attractors in turbulence*," in Lecture Notes in Mathematics, D.A. Rand and L.-S. Young, Berlin: Springer, pp. 366-381, 1981.

[106] S.R.H. Davies, and C.J. James, "*Including Temporal Dynamics in Single Trial Motor Imagery Classification using Empirical Mode Decomposition",* 6th International Brain-Computer Interface Conference, pp. 52-55, September 2014.

[107] P.A. Lachenbrucha, and M.R. Mickey, "*Estimation of Error Rates in Discriminant Analysis*," Technometrics, vol. 10, pp. 1-11, 1968.

[108] J. Sleight, P. Pillai, and S. Mohan, "*Classification of Executed and Imagined Motor Movement EEG Signals*," Ann Arbor: University of Michigan, pp. 1-10, December 2009.

[109] J. Sita, and G.J. Nair, "*Feature Extraction and Classification of EEG Signals for Mapping Motor Area of the Brain*," 2013 International Conference on Control Communication and Computing, pp. 463-468, December 2013.

[110] S.R.H. Davies, and C.J. James, "*Using Empirical Mode Decomposition with Spatio-Temporal Dynamics to Classify Single-Trial Motor Imagery in BCI",* 36th Annual International Conference of the IEEE EMBS, pp. 4631-4634, September 2014.

[111] T. Kaufmann, E.M. Holz, and A. Kübler, "*Comparison of tactile, auditory, and visual modality for brain-computer interface use: a case study with a patient in the locked-in state,*" Frontiers in Neuroscience, vol. 7, July 2013.

[112] A.-M. Brouwer, J.B.F. van Erp, F. Aloise, and F. Cincotti, "*Tactile, Visual, and Bimodal P300s: Could Bimodal P300s Boost BCI Performance?*" SRX Neuroscience, vol. 2010, May 2010.

[113] M.E. Thurlings, A.M. Brouwer, J.B.F. Van Erp, B. Blankertz, and P.J. Werkhoven, "*Does bimodal stimulus presentation increase ERP components usable in BCIs?*" Journal of Neural Engineering, vol. 9, July 2012.

[114] T. Kaufmann, E.M. Holz, A. Kübler, "*Comparison of tactile, auditory, and visual modality for brain-computer interface use: a case study with a patient in the locked-in state*," Frontiers in Neuroscience, vol. 7, pp. 1-12, July 2013.

[115] M. Chang, N. Nishikawa, Z.R. Struzik, K. Mori, S. Makino, D. Mandic, and T.M. Rutkowski, "*Comparison of P300 Responses in Auditory, Visual and Audiovisual Spatial Speller BCI Paradigms*," Proceedings of the Fifth International Brain-Computer Interface Meeting, May 2013.

[116] M. Severens, M. Van der Waal, J. Farquhar, and P. Desain, "*Comparing tactile and visual gaze-independent brain-computer interfaces in patients with amyotrophic lateral sclerosis and healthy users*," Clinical Neurophysiology, vol. 125, pp. 2297-2304, November 2014.

[117] R.S. Johansson, and J.R. Flanagan, "*Coding and use of tactile signals from the fingertips in object manipulation tasks*," Nature Reviews Neuroscience, vol. 10, pp. 345-359, May 2009.

[118] A.Z. Snyder, "*Steady-state vibration evoked potentials: description of technique and characterization of responses*," Electroencephalography and Clinical Neurophysiology/Evoked Potentials Section, vol. 84, pp. 257-268, May 1992.

[119] C.M. Giabbiconi, C. Dancerb, R. Zopfa, T. Grubera, and M.M. Müller, "*Selective spatial attention to left or right hand flutter sensation modulates the steady-state somatosensory evoked potential*," Cognitive Brain Research, vol. 20, pp.58-66, June 2004.

[120] A. Kübler, A. Furdea, S. Halder, E.M. Hammer, F. Nijboer, and B. Kotchoubey, "*A brain-computer interface controlled auditory event-related potential (p300) spelling system for locked-in patients*," Annals of the New York Academy of Sciences, vol. 1157, pp. 90-100, March 2009.

[121] D. Zhang, Y. Wang, A. Maye, A.K. Engel, X. Gao, B. Hong, and S. Gao, "*A Brain-Computer Interface Based on Multi-Modal Attention*," 3rd International IEEE/EMBS Conference on Neural Engineering, pp. 414-417, May 2007.

[122] R.G. Carpenter, "*Principles and procedures of statistics, with special reference to the biological sciences*," The Eugenics Review, vol. 52, pp. 172-173, October 1960.

[123] R.T. Verrillo, "*Effect of Contactor Area on the Vibrotactile Threshold*," Journal of the Acoustical Society of America, vol. 35, September 1963.

[124] E. Zwicker, G. Flottorp, and S.S. Stevens, "*Critical Band Width in Loudness Summation*," Journal of the Acoustical Society of America, vol. 29, February 1957.

[125] N. Wang, T. Qian, Q. Zhuo, and X. Gao, "*Discrimination between idle and work states in BCI based on SSVEP*," 2nd International Conference on Advanced Computer Control, vol. 4, pp. 355-358, March 2010.

[126] *"Pico Vibe 10mm Vibrating Motor – 3mm Type Data Sheet*," 2015, Precision Microdrives, https://catalog.precisionmicrodrives.com/order-parts/datasheet/310-004-10mm-vibration-motor-3mm-type (accessed April 28th, 2015).

[127] "*Arduino Pro Overview*," 2015, Arduino, http://www.arduino.cc/en/Main/ArduinoBoardPro (accessed April 28th, 2015).

[128] "*Processing Environment IDE Overview*", 2001, Processing, https://processing.org/reference/environment/ (accessed April 28th, 2015).

[129] "*EEG 10-20 System*", Diagram, 2012, g.tec Mounting g.EEGCap, http://www.gtec.at/Support-Offer/FAQ/Tips/(show)/1560/#p1560 (accessed April 28th, 2015).

[130] C. Buccella, M. Feliziani, G. Manzi, and F. Maradei, "*Prediction of voltage and current propagation in twisted wire pairs (TWPs) by a circuit model*," 2005 International Symposium on Electromagnetic Compatibility, pp. 51-55, August 2005.

[131] S. Wang, F.C. Lee, and J.D. van Wyk, "*Design of Inductor Winding Capacitance Cancellation for EMI Suppression*," IEEE Transactions on Power Electronics, vol. 21, pp. 1825-1832, November 2006.

[132] J.R. Treichler, C.R. Johnson, and M.G. Larimore, "*Theory and Design of Adaptive Filters*," New Jersey: Prentice Hall, pp.82-83, March 2001.

[133] A. Gauthier, A. Vignola, A. Calvo, E. Cavallo, C. Moglia, L. Sellitti, R. Mutani, and A. Chio, "*A longitudinal study on quality of life and depression in ALS patient–caregiver couples*," Neurology, vol. 68, pp. 923-926, March 2007.

[134] S.K. Law, "*Thickness and resistivity variations over the upper surface of the human skull*," Brain Topography, vol. 6, pp. 99-109, December 1993.

[135] R.M. Birn, M.A. Smith, T.B. Jones, and P.A. Bandettini, "*The Respiration Response Function: The temporal dynamics of fMRI signal fluctuations related to changes in respiration*," NeuroImage, vol. 40, pp. 644-654, April 2009.

[136] S. Ogawa, T.M. Lee, A.R. Kay, and D.W. Tank, "*Brain magnetic resonance imaging with contrast dependent on blood oxygenation*," Proceedings of the National Academy of Sciences, vol. 87, pp. 9868-9872, December 1990.

[137] S.R.H. Davies, and C.J. James, "*Exploiting the Absolute Threshold of Vibrotactile Stimulation to Generate Evoked Potentials in EEG*", 8th IEEE EMBS UK and RI Postgraduate Conference in Biomedical Engineering and Medical Physics, pp. 15-16, July 2014.

APPENDIX A

Ethical Approval for SSSEP BCI Paradigm Study

28th July 2014

Warwick Medical School

PRIVATE
Simon Davies
Room A408C
School of Engineering
University of Warwick
Coventry
CV4 7AL

Dear Simon,

Study Title and BSREC Reference: *Exploiting the absolute threshold of vibrotactile stimulation to generate evoked potentials in EEG* REGO-2014-880

Thank you for submitting your revisions to the above-named project to the University of Warwick's Biomedical and Scientific Research Ethics Sub-Committee for approval.

I am pleased to confirm that approval is granted and your study may commence.

Please keep a copy of the signed version of this letter with your study documentation.

Yours sincerely

P.P. Graham Hewitt

David Davies
Chair
Biomedical and Scientific
Research Ethics Sub-Committee

Biomedical and Scientific Research Ethics Sub-Committee
A010 Medical School Building
Warwick Medical School,
Coventry, CV4 7AL.
Tel: 02476-151875
Email: BSREC@Warwick.ac.uk

Medical School Building
The University of Warwick
Coventry CV4 7AL United Kingdom
Tel: +44 (0)24 7657 4880
Fax: +44 (0)24 7652 8375

THE UNIVERSITY OF WARWICK

APPENDIX B

Application to BSREC for Ethical Approval for SSSEP BCI Paradigm Study

THE UNIVERSITY OF WARWICK

BIOMEDICAL & SCIENTIFIC RESEARCH ETHICS COMMITTEE (BSREC)
PROTOCOL GUIDANCE

Title:	**Exploiting the absolute threshold of vibrotactile stimulation to generate evoked potentials in EEG**
Abstract:	This study aims to evaluate the change in brain activity in response to tactile stimuli oscillating at the same frequency but different amplitudes that straddle a person's absolute tactile threshold (ATT). Typically this paradigm, used in Brain-Computer Interfaces in order to facilitate communication for patients with little to no muscle control, consists of a tactile stimulus of a certain frequency applied to one hand and a stimulus of a different frequency applied to the other. The user attends one hand over the other and the resonance of the attended stimulus frequency is detected by an electroencephalogram (EEG). The novel changes to this test mean that both hands are stimulated with the same frequency, but the amplitude of one of them is below the user's ATT. The ATT is the minimum level a tactile stimulus must be for the user to consciously detect it. Past literature has shown that it is very easy to detect when a resonance signal is occurring but more difficult to identify the specific frequency due to signal noise. The expectation of this study is that the stimulus below the ATT will register as a false negative, and therefore be easier to differentiate from the other stimulus, but in a way that is distinguishable from a true negative.
Contact details	
Chief Investigator: *NB: If this study is below PhD level, the CI will be your Academic Supervisor*	Prof Christopher James
Principal Investigator(s):	Simon Davies
Background – why are you researching this area? What does the previous evidence say? What are the gaps in knowledge?	
A Brain-Computer Interface (BCI) is a device that uses the brain-activity of a person as an input to select desired outputs on a computer [1]. One method of obtaining a person's brain activity as a	

digital input is by using surface electrodes and an electroencephalogram (EEG) amplifier. However as the electrodes are placed on the scalp the data suffers from a very low signal-to-noise ratio due to it having to travel through bone, tissue, etc before reaching the electrodes. A common way to overcome this problem is to use a stimulus that triggers a significant change in the amplitude or frequency of a user's brain activity. These are called evoked potentials [2]. An evoked potential can be triggered by any sensory data received by the brain, such as visual, auditory and tactile. In this case it was decided to use tactile as there is less research in this area, patients with severe paralysis often have trouble focusing and moving their eyes, and it leaves the visual and auditory channels clear for other tasks.

A very common BCI paradigm is Steady State Evoked Potentials (SSEPs) [3]. SSEPs are resonance signals generated by the user attending to a repeated stimulus of fixed frequency, in this case tactile. These resonance signals can then be extracted from the EEG data and we can identify the specific tactile stimulus the user was attending. This deciphering of intent allows us to associate certain actions with a stimulus so that the BCI user can select them. Previous work has shown this paradigm to be successful due to the distinctiveness and consistency of the evoked potential and its reflexive nature, i.e. it does not have to be consciously modulated by the user's thinking [3].

However, there is room for improvement in the process, as although it is quite easy to distinguish when an SSEP is occurring compared to normal brain activity, it is considerably more difficult to identify the specific resonance frequency. A possible solution to this lies within the exploitation of the user's absolute tactile threshold (ATT).

The ATT is the lowest level a tactile stimulus can be before it is no longer consciously felt. Therefore it can be expected that distinguishing between two stimuli above and below a person's ATT will be as effective as distinguishing between an SSEP occurring and neutral activity. It is anticipated that the false negative of the stimulus below the ATT is distinguishable from a true negative.

Aims/Objectives and Purpose of the study

This project aims to see whether a tactile stimulus for generating SSEPs gives better performance when using stimuli of the same frequency but straddling a user's ATT instead of using stimuli of two different frequencies.

Objectives

1. Collect primary data for SSEPs generated by a stimulus above the ATT, SSEPs generated by a stimulus below the ATT and brain activity under no stimulus. Identify distinguishing characteristics and classify.

2. Collect primary data for a standard tactile BCI in the literature from the same users and compare classification performance to data in objective 1.

Design/Methodology – please include information about whether your study is qualitative/quantitative, retrospective/prospective; what interventions you will use (e.g. describe all surveys, tests, observations); what sample size you will use; how you reached that sample size and how you will analyse the data; how you will recruit/select your participants/subjects; what allowances will you put in place so that participants/subjects can withdraw from the study at any time; and, what your process is for gathering informed consent:

This is a quantitative study generating primary data.

Equipment

Any EEG experiment will involve applying electrodes to a person's scalp. In this case an EEG sensory

cap will be applied to a person's head and tied with a cord to a chest belt to ensure the cap is seated firmly on the person's scalp.

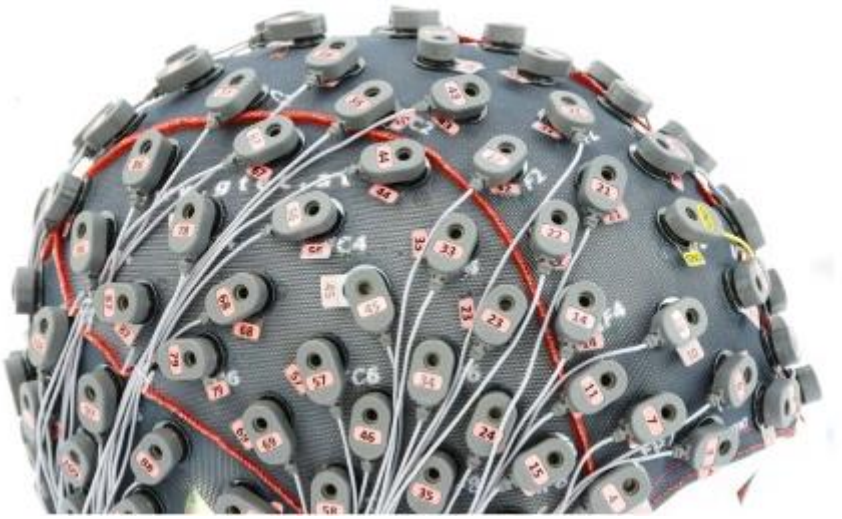

Fig. 1. gtec g.GAMMAcap for fitting electrodes on a person's scalp

For conductivity, gel is inserted into the holes in the cap and onto the person's scalp using a needless syringe. The gel in question is g.GAMMAgel: a water-soluble, non-irritant, non-corrosive conductive gel with a CE Class 1 stamp sold by a biomedical company.

Fig. 2. gtec g.HIamp brand EEG amplifier

Active chlorided silver electrodes are inserted into the holes in the cap and plugged in at the other end to an EEG amplifier. The amplifier, a g.tec g.HIamp, is connected to a PC desktop via USB. The amplifier and its electrodes have a CE class 2 certification.

Tactile stimulation is delivered through several 10mm x 3.4mm encapsulated vibrating motors identical to those used in mobile phones. They are secured to the user's fingertips using hook and loop ties and are controlled by an Arduino circuit board connected to a PC via USB which is grounded.

After the experiment the electrodes and the cap will be soaked in warm water for 10 minutes. Then a cotton bud will be used to remove any remaining gel and the cap and electrodes will be left hung up until dry.

Fig. 3. A small encapsulated motor secured to a person's finger.

Experimental Protocol

The design of the test will be taking its lead from the protocol outlined in Muller-Putz et al [4], as this is the standard tactile BCI that this novel tactile BCI is based on. For the standard, or "control", tactile BCI experiment a motor is secured to each index finger. Both motors oscillate at specific frequencies. Snyder's [5] analysis of tactile stimulus frequencies concluded that 26 Hz produced the strongest evoked potential on average. Like in Snyder's study, the motors used cannot oscillate that slowly so a carrier wave will be used to deliver the pulses. 156 Hz is a multiple of the stimulus frequency that falls within the frequency specs of the motors and is above the 40 Hz limit a stimulus has to be under in order to trigger a SSEP, so it will not contaminate the EEG readings.

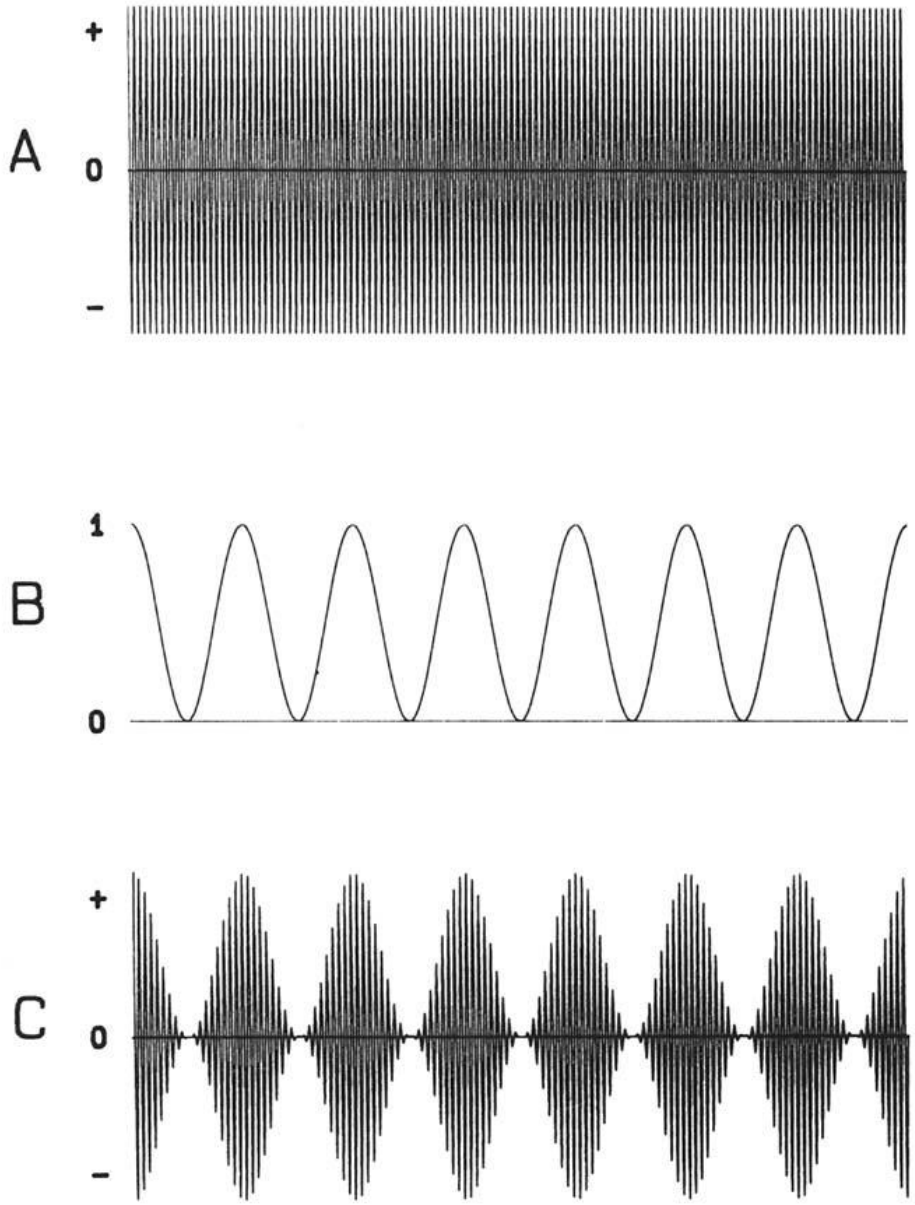

Fig. 4.Waveform A represents the high frequency carrier wave, B is the modulation frequency and C is the final stimulus signal.

The user's index finger receives this tactile stimulus frequency. Like in Muller-Putz et al [4], the other hand's index finger receives a tactile stimulus whose frequency is also a multiple of the carrier frequency (156 Hz) but not a multiple of the first modulation frequency (26 Hz) in order to avoid resonance occurring in the same frequencies. In this case the other frequency will be 12 Hz. It is quite possible that the frequency of the sound the motors produce will also trigger an SSEP through auditory stimulus. Whilst this would only serve to increase the power of the evoked potential the study is investigating the performance of tactile stimulation only, as a lack of background noise cannot be guaranteed in the field. Therefore white noise will be played to users during the experiment at a volume of 50dB, the same volume as a normal conversation. For each trial one of three possible visual cues will be presented: a left arrow that indicates to focus on the left hand, a right arrow that indicates to focus on the right hand or a fixation cross that indicates no stimulus will be provided. The 3rd option provides a neutral baseline to compare against the other two classes. For the latter half of the trials the stimuli will be swapped round to make sure the user's left-handed or right-handedness has no effect on the sensitivity to one of the stimuli. The timing of the experiment is shown below:

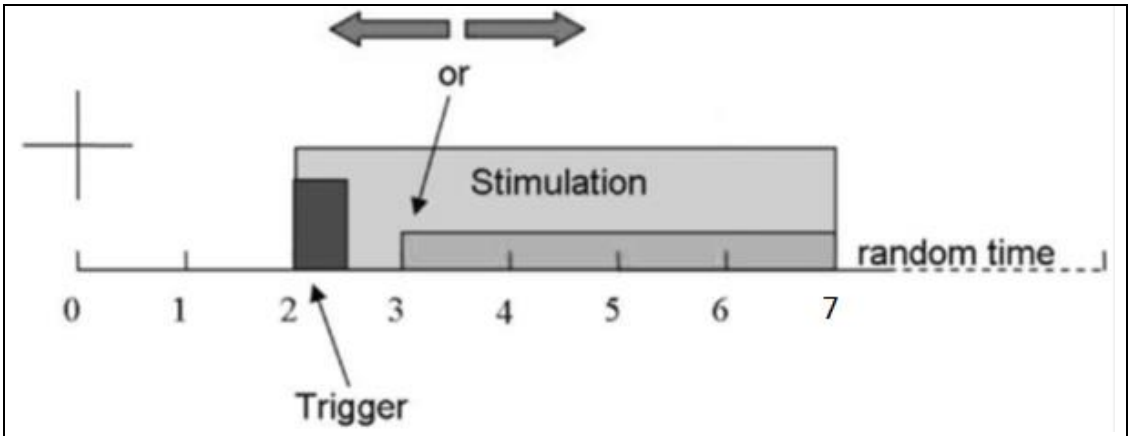

Fig. 5. Each trial starts at 0s with a fixation cross displayed on the computer monitor. After 2s, a trigger occurs and the stimulation of both index fingers begins. At second 3, the cue (indicating where to focus attention) appears on the screen. The trial ends at 7s and the screen is cleared. A randomized time lag is added before a new trial starts.

The novel tactile experiment will be carried out in the same way aside from a few key differences. Both hands will receive the same stimulation frequency. Verillo [6] shows that a user's ATT changes depending on the amount of surface area stimulated. Therefore the stimulation for one hand will be delivered via three motors on three finger tips vs. one motor on one fingertip for the other. A pre-test will be carried out where the amplitude of the oscillations is lowered until the user can only feel the stimulation on the hand with 3 motors. There will be a 3rd option where no cue appears and the fixation cross remains on the screen. This will be for recording true negatives.

A number of different signal processing methods will be applied to the data using Matlab to see which one generates the best classifier. Performance is measured through sensitivity and specificity. Sensitivity is the percentage of results from a stimulus that were correctly classified as such:

$$\frac{no.of\ true\ positives}{no.of\ true\ positives + no.of\ false\ negatives} * 100$$

Specificity is the percentage of results from the other stimuli that do not get wrongly classified as the former stimulus:

$$\frac{no.of\ true\ negatives}{no.of\ true\ negatives + no\ of\ false\ positives} * 100$$

In essence, a classifier with high sensitivity will classify all the elements that belong in its group, but also elements outside its group that happen to be similar. A classifier with high specificity will be much more stringent at classifying elements as belonging to its group, but at the expense that elements that do belong to the group but have minor anomalies are not classified as such. Ideally a classifier should maximise both metrics.

Recruitment

16 test subjects will be recruited from the student and staff population of the University of Warwick. This will be done by email, word of mouth and posters. Participation in this study is completely voluntary and no pressure will be exerted on potential participants to take part. Participants will be over 18 and should suffer from no pre-existing neurological conditions. In extreme cases, those with bushy, plentiful hair will be rejected as it will interfere with the electrodes making contact. The number of participants was reached by viewing what sample sizes were used in the literature for similar BCI tests.

A copy of the advertisement and email used for recruiting is available in the appendix. The poster

will be put up around campus and the email will be sent to WMG, School of Engineering and Psychology departments.

Allowances

Test subjects will be able to withdraw at any time, even after the experiments, and request that their data is deleted.

Informed Consent

Before the experiments each test subject will be given a consent form and participant information leaflet. A verbal summary of the experiment will also be given to them before they start and they will be invited to ask any questions.

Duration

30 minutes preparation will be needed before a session to prepare the electrodes and place them on the test subject. Each session will consist of 100 trials, lasting approximately 20 minutes. A further 15 minutes will then be needed to remove and clean the electrodes.

Ethical considerations – include details of the Research Ethics Committee (REC) which will review the study/project and see end of the document for further guidance

Participant Information Leaflet (see appendices)

Participant Consent Form (see appendices)

Data Protection

Only the subject's sex and age will be mentioned in any published work. Their data will be stored on a password protected network drive for 10 years as per the university's Data Management Policy. The consent forms will be stored in a locked filing cabinet located inside a locked office. Their names will be retained on the consent forms so that they can be identified if they wish to withdraw their consent at a later date.

Right of Withdrawal

Participants have the right to halt their experimental sessions or withdraw completely at any time, even after their EEG data has been collected. The data will be erased and not used in any study.

Safety

All equipment involved is CE certified except for the tactile stimulators that are connected a grounded computer. There is a known illness called Hand-Arm Vibration (HAV) syndrome associated with long-term exposure to vibrating tools. However, according to the UK Health & Safety Executive (HSE), it would take more than 24 hours constant exposure for motors this size to have an effect [7]. Note that the HSE's HAV exposure calculator can only go up to 24 hours when calculating the maximum exposure time.

Benefits & Risk to the Participants

Participants will be offered a selection of snack cakes at the end of each experimental session. There are no potential health risks.

Financing

This project is funded by the WMG as part of my PhD

Dissemination and Implementation

The results of this research study will be submitted to scientific journals/conferences. Participants will have access to such a publication if required

References

[1] J.R. Wolpaw, N. Birbaumer, D.J. McFarland, G. Pfurtscheller, and T.M. Vaughan, "Brain-computer interfaces for communication and control," *Clinical Neurophysiology*, vol. 113, pp. 767-791, March 2002.

[2] K.H. Chiappa, ed. *Evoked potentials in clinical medicine*. Lippincott Williams & Wilkins, 1997.

[3] D. Regan, "Steady-state evoked potentials," *Journal of the Optical Society of America*, vol. 67, pp. 1475-1489, 1977.

[4] G.R. Muller-Putz, R. Scherer, C. Neuper, and G. Pfurtscheller, "Steady-state somatosensory evoked potentials: suitable brain signals for Brain–Computer Interfaces?" *IEEE Trans. on Neural Systems and Rehabilitation Eng.*, vol. 14, pp. 30-37, March 2006.

[5] A.Z. Snyder, "Steady-state vibration evoked potentials: description of technique and characterization of responses," *EEG and clinical Neurophysiology*, vol. 84, pp. 257-268, May 1992.

[6] R.T. Verillo, "Effect of contactor area on the vibrotactile threshold", *Journ. of the Acoustical Society of America*, vol. 35, pp. 1962-1966, September 1963.

[7] "Hand-Arm Vibration: Employer's responsibilities – legal duties", *Health & Safety Executive*, Web. 23 June 2014.

Appendices (e.g. questionnaire(s), patient information leaflet(s), consent form(s), interview schedule(s), interview topic guide(s))

Participant Information Leaflet – see attachment "bsrec_participant_information_leaflet_davies_v2.doc"

Participant Consent Form – see attachment "Consent Form_davies_v2.doc"

Recruitment Poster – see attachment "recruitPoster.doc"

Recruitment Email – see attachment "recruitEmail.doc **"**

APPENDIX C

Participant Information Leaflet for SSSEP BCI Paradigm Study

PARTICIPANT INFORMATION LEAFLET

Study Title: **Exploiting the absolute threshold of vibrotactile stimulation to generate evoked potentials in EEG**

Investigator(s): **Simon Davies**

Introduction

You are invited to take part in a research study. Before you decide, you need to understand why the research is being done and what it would involve for you. Please take the time to read the following information carefully. Talk to others about the study if you wish.

(Part 1 tells you the purpose of the study and what will happen to you if you take part. Part 2 gives you more detailed information about the conduct of the study)

Please ask us if there is anything that is not clear or if you would like more information. Take time to decide whether or not you wish to take part.

PART 1

What is the study about?

This study is evaluating the performance of a novel Brain-Computer Interface (BCI). A BCI lets you control a computer with your mind. Surface electrodes on your scalp will detect brain activity and try to interpret if you are focusing on your left or right hand. A tiny motor on each hand, identical to that of a mobile phone's, will vibrate at precise frequencies. We will then look for those frequencies' presence in your brain activity.

Do I have to take part?

It is entirely up to you to decide. We will describe the study and go through this information sheet, which we will give you to keep. If you choose to participate, we will ask you to sign a consent form to confirm that you have agreed to take part (if part of this study is an online or postal questionnaire/survey, by returning a completed questionnaire/survey, you are giving your consent for the information that you have supplied to be used in this study and formal signed consent will not be collected where postal or online questionnaires/surveys are concerned). You will be free to withdraw at any time, without giving a reason and this will not affect you or your circumstances in any way.

What will happen to me if I take part?

The experiment will take place in Room A408C in the School of Engineering. Approximately 30 minutes will be needed to apply the EEG cap to your head. Firstly a cloth cap will be placed on your head. 64 electrodes (small metal discs) will be placed inside pre-made holes in the cap. Then a water-soluble, non-irritant, non-corrosive conductive gel will be inserted into the holes to fill the gap between your skin and the electrodes.

Next a tiny vibrating motor will be secured to each of your index fingers using a Velcro strap.

For the experiment, a computer monitor in front of you will generate an audio cue before showing an arrow pointing randomly either left, right or not appearing at all as the motors activate. You must then focus on the hand that corresponds to the direction of the arrow. In the case of no arrow being presented, a fixation cross will be displayed on the screen and the motors will not activate. This process lasts around 9 seconds and will be repeated 100 times with short breaks in between each block of 25. After 50 trials the motors will be swapped round to your opposing hands.

During the experiment, white noise will be played through speakers at a 50dB level to prevent any unwanted auditory stimulus. This is as loud as a normal conversation.

The next experiment will be very similar except that ***three*** motors will be secured to one of your hands instead of one. Once each session is finished the cap will be removed and any excess gel wiped off. Though the gel will not be visible, if your hair still feels uncomfortable you will be able to make use of the showers in the International Digital Laboratory.

What are the possible disadvantages, side effects, risks, and/or discomforts of taking part in this study?

Extensive touching of the scalp is needed in order to place the electrodes and the cap. The gel used is completely non-corrosive or irritable, but even after all visible traces are wiped off your hair will still feel slightly sticky until you next have a shower.

What are the possible benefits of taking part in this study?

This study may lead to the creation of a more efficient BCI that allows patients with

severe paralysis some degree of communication.

Expenses and payments

We cannot offer any financial compensation but you can help yourself to a selection of snack cakes after the session.

What will happen when the study ends?

The results of this research study will be incorporated into a PhD thesis and may also be submitted to a peer reviewed scientific journals or conferences. Your personal information will not be identified in any publication. You will have access to such a publication if required.

Will my taking part be kept confidential?

Yes. We will follow strict ethical and legal practice and all information about you will be handled in confidence. Further details are included in Part 2.

What if there is a problem?

Any complaint about the way you have been dealt with during the study or any possible harm that you might suffer will be addressed. Detailed information is given in Part 2.

This concludes Part 1.

If the information in Part 1 has interested you and you are considering participation, please read the additional information in Part 2 before making any decision.

PART 2

Who is organising and funding the study?

This study is conducted by Simon Davies for his PhD project, under supervision by Professor Christopher James. The funding will come from the WMG department.

What will happen if I don't want to carry on being part of the study?

Participation in this study is entirely voluntary. Refusal to participate will not affect you in any way. If you decide to take part in the study, you will need to sign a consent form, which states that you have given your consent to participate.

If you agree to participate, you may nevertheless withdraw from the study at any time without affecting you in any way.

You have the right to withdraw from the study completely and decline any further contact by study staff after you withdraw.

What if there is a problem?

This study is covered by the University of Warwick's insurance and indemnity cover. If you have an issue, please contact Jo Horsburgh (details below).

Who should I contact if I wish to make a complaint?

Any complaint about the way you have been dealt with during the study or any possible harm you might have suffered will be addressed. Please address your complaint to the person below, who is a Senior University of Warwick official entirely independent of this study:

Jo Horsburgh
Deputy Registrar
Deputy Registrar's Office
University of Warwick
Coventry, UK, CV4 8UW.
T: +00 44 (0) 2476 522 713 E: J.Horsburgh@warwick.ac.uk

Will my taking part be kept confidential?

Only your sex and age will be recorded. The data will be stored on a password protected computer's local hard drive located inside a locked office. The consent forms will be stored in a locked filing cabinet located inside the same office.

What will happen to the results of the study?

The results will form part of a PhD thesis which will be publicly available. The data may also be used as part of a conference or journal paper.

Who has reviewed the study?

This study has been reviewed and given favourable opinion by the University of Warwick's Biomedical and Scientific Research Ethics Committee (BSREC): **REGO-2014-880, 28th July 2014**

What if I want more information about the study?

If you have any questions about any aspect of the study or your participation in it not answered by this participant information leaflet, please contact:

Simon Davies
s.r.h.davies@warwick.ac.uk
07935274335

Supervisor:
Prof. Christopher James.
c.james@warwick.ac.uk
02476151261

Thank you for taking the time to read this participant information leaflet.

APPENDIX D

Participants Consent Form for SSSEP BCI Paradigm Study

THE UNIVERSITY OF WARWICK

CONSENT FORM

(Biomedical and Scientific Research Ethics Committee) Study Number:

Patient Identification Number for this study:

Title of Project: Exploiting the absolute threshold of vibrotactile stimulation to generate evoked potentials in EEG

Name of Researcher(s): Simon Davies

Please initial all boxes

1. I confirm that I have read and understand the information sheet dated **DATE** (version **1.0**) for the above study. I have had the opportunity to consider the information, ask questions and have had these answered satisfactorily. ☐
2. I understand that my participation is voluntary and that I am free to withdraw at any time without giving any reason, without my legal rights being affected. ☐
3. I understand that the data collected during the study, may be looked at by individuals from The University of Warwick, where it is relevant to my taking part in this research. I give permission for these individuals to have access to my records. ☐
4. I understand that I will need to wear an EEG cap and that gel will be applied. I agree to this. ☐
5. I agree to take part in the above study. ☐

Name of Participant	Date	Signature
Name of Person taking consent	Date	Signature

APPENDIX E

Programming Code for SSSEP BCI Paradigms

E.1 Standard SSSEP Paradigm

```
int numberTrials = 51;
int pulseFreqLeft = 25;
int pulseFreqRight = 16;

unsigned long previousMillisStim=0;
unsigned long previousMillisPause=0;
unsigned long previousMillisLeft=0;
unsigned long previousMillisRight=0;
unsigned long startTime=0;

int motorPin1 = 3;
int motorPin2 = 5;
int motorPin3 = 6;
int motorPin4 = 9;
int motorL = 0;
int motorR = 0;
int trialNo = 0;
int trialPause = 1;
int randNumber;
int randPause;
String s1 = "Trial ";

void setup()
{
  pinMode(motorPin1, OUTPUT);
  pinMode(motorPin2, OUTPUT);
  pinMode(motorPin3, OUTPUT);
  pinMode(motorPin4, OUTPUT);
  Serial.begin(9600);
  trialPause = 1;
  delay(10000);
}

void loop() {
  unsigned long currentMillis = micros();
  if (trialNo <= numberTrials) {
    if (trialPause == 1) {
      trialNo = trialNo + 1;
      Serial.println(s1 + trialNo);
```

```
      randNumber = random(0,2);
      randPause = random(0,1000);
      randPause = randPause - 500;
      trialPause = 0;
      previousMillisPause = currentMillis;
      while ((unsigned long)(currentMillis -
previousMillisPause) <= (2000000 + (randPause * 1000))) {
        currentMillis = micros();
      }
      Serial.println(randNumber);
    }
    else {
      if ((unsigned long)(currentMillis - previousMillisStim)
<= (7000000 + (randPause*1000))) {  // 5 second stimulation
        if ((unsigned long)(currentMillis -
previousMillisLeft) >= (500000/pulseFreqLeft)) {  // Left
motors
          if (motorL == 0) {
            analogWrite(motorPin1, 255);
            analogWrite(motorPin2, 194);
            motorL = 1;
          }
          else {
            analogWrite(motorPin1, 0);
            analogWrite(motorPin2, 0);
            motorL = 0;
          }
          previousMillisLeft = (unsigned long)currentMillis;
        }
        if ((unsigned long)(currentMillis -
previousMillisRight) >= (500000/pulseFreqRight)) {  // Right
motors
          if (motorR == 0) {
            analogWrite(motorPin3, 227);
            analogWrite(motorPin4, 196);
            motorR = 1;
          }
          else {
            analogWrite(motorPin3, 0);
            analogWrite(motorPin4, 0);
            motorR = 0;
          }
          previousMillisRight = (unsigned long)currentMillis;
        }
      }
      else {
        analogWrite(motorPin1, 0);
        analogWrite(motorPin2, 0);
        analogWrite(motorPin3, 0);
        analogWrite(motorPin4, 0);
        trialPause = 1;
        previousMillisStim = (unsigned long)currentMillis;
      }
    }
  }
  else {
```

```
    delay(100000);
  }
}
```

E.2 Novel SSSEP Paradigm

```
int numberTrials = 51;
int pulseFreqLeft = 25;

unsigned long previousMillisStim=0;
unsigned long previousMillisPause=0;
unsigned long previousMillisLeft=0;
unsigned long startTime=0;

int motorPin1 = 3;
int motorPin2 = 5;
int motorPin3 = 6;
int motorPin4 = 9;
int motorL = 0;
int trialNo = 0;
int trialPause = 1;
int randNumber;
int randPause;
String s1 = "Trial ";

void setup()
{
  pinMode(motorPin1, OUTPUT);
  pinMode(motorPin2, OUTPUT);
  pinMode(motorPin3, OUTPUT);
  pinMode(motorPin4, OUTPUT);
  Serial.begin(9600);
  trialPause = 1;
  delay(10000);
}

void loop() {
  unsigned long currentMillis = micros();
  if (trialNo <= numberTrials) {
    if (trialPause == 1) {
      trialNo = trialNo + 1;
      Serial.println(s1 + trialNo);
      randNumber = random(0,2);
      randPause = random(0,1000);
      randPause = randPause - 500;
      trialPause = 0;
      previousMillisPause = currentMillis;
      while ((unsigned long)(currentMillis -
previousMillisPause) <= (2000000 + (randPause * 1000))) {
        currentMillis = micros();
      }
      Serial.println(randNumber);
    }
    else {
```

```
      if ((unsigned long)(currentMillis - previousMillisStim)
<= (7000000 + (randPause*1000))) {  // 5 second stimulation
        if ((unsigned long)(currentMillis -
previousMillisLeft) >= (500000/pulseFreqLeft)) {  // Left
motors
          if (motorL == 0) {
            analogWrite(motorPin1, 32);
            analogWrite(motorPin2, 194);
            analogWrite(motorPin3, 227);
            analogWrite(motorPin4, 196);
            motorL = 1;
          }
          else {
            analogWrite(motorPin1, 0);
            analogWrite(motorPin2, 0);
            analogWrite(motorPin3, 0);
            analogWrite(motorPin4, 0);
            motorL = 0;
          }
          previousMillisLeft = (unsigned long)currentMillis;
        }
      }
      else {
        analogWrite(motorPin1, 0);
        analogWrite(motorPin2, 0);
        analogWrite(motorPin3, 0);
        analogWrite(motorPin4, 0);
        trialPause = 1;
        previousMillisStim = (unsigned long)currentMillis;
      }
    }
  }
  else {
    delay(100000);
  }
}
```

E.3 Neutral SSSEP Paradigm

```
int numberTrials = 51;
int pulseFreqLeft = 25;

unsigned long previousMillisStim=0;
unsigned long previousMillisPause=0;
unsigned long previousMillisLeft=0;
unsigned long startTime=0;

int motorPin1 = 6;
int motorPin2 = 9;
int motorL = 0;
int trialNo = 0;
int trialPause = 1;
int randNumber;
int randPause;
```

```
String s1 = "Trial ";

void setup()
{
  pinMode(motorPin1, OUTPUT);
  pinMode(motorPin2, OUTPUT);
  Serial.begin(9600);
  trialPause = 1;
  delay(10000);
}

void loop() {
  unsigned long currentMillis = micros();
  if (trialNo <= numberTrials) {
    if (trialPause == 1) {
      trialNo = trialNo + 1;
      Serial.println(s1 + trialNo);
      randNumber = random(0,2);
      randPause = random(0,1000);
      randPause = randPause - 500;
      trialPause = 0;
      previousMillisPause = currentMillis;
      while ((unsigned long)(currentMillis -
previousMillisPause) <= (2000000 + (randPause * 1000))) {
        currentMillis = micros();
      }
      Serial.println(randNumber);
    }
    else {
      if ((unsigned long)(currentMillis - previousMillisStim)
<= (7000000 + (randPause*1000))) {  // 5 second stimulation
        if ((unsigned long)(currentMillis -
previousMillisLeft) >= (500000/pulseFreqLeft)) {  // Left
motors
          if (motorL == 0) {
            analogWrite(motorPin1, 227);
            analogWrite(motorPin2, 196);
            motorL = 1;
          }
          else {
            analogWrite(motorPin1, 0);
            analogWrite(motorPin2, 0);
            motorL = 0;
          }
          previousMillisLeft = (unsigned long)currentMillis;
        }
      }
      else {
        analogWrite(motorPin1, 0);
        analogWrite(motorPin2, 0);
        trialPause = 1;
        previousMillisStim = (unsigned long)currentMillis;
      }
    }
  }
  else {
```

```
    delay(100000);
  }
}
```

E.4 Processing IDE Visual Display

```
import processing.serial.*;  /* You need this for Serial
communication*/
import java.awt.AWTException;
import java.awt.Robot;
import java.awt.event.KeyEvent;

/* Global Variables------------------------------- */
Serial comPort;
String [] comPortList;
String comPortString;

PFont font;
String [] myFontList;
int fontNumber;
String fontString;
Robot robot;

/*-------------------------------------------------*/

void setup() {

  //size(displayWidth, displayHeight);
/* set the size of the screen, 500x500 */
  size(1920, 980);                                    /* set
the size of the screen, 500x500 */
  background(0);                                     /* change
the background of the screen to black */

  comPortList=Serial.list();                         /* Get
Available COM ports             */
  myFontList = PFont.list();
  try {
    robot = new Robot();
  }
  catch (AWTException e) {
    e.printStackTrace();
    exit();
  }



  comPort=new Serial(this, "COM23", 9600); /* Open the first
COM port in the list  */

  /* which will generate a serialEvent    */
}
/*-------------------------------------------------*/
```

```
void draw() {
  // The serialEvent will control the display
}

/*-------------------------------------------------*/

void serialEvent(Serial cPort) {
  comPortString = cPort.readStringUntil('\n');
  if (comPortString != null) {
    comPortString=trim(comPortString);
    background(0);
    /* Map the Arduino value to the number of fonts */
    //  fontNumber =
int(map(Integer.parseInt(comPortString),1,1000,1,myFontList.le
ngth));

    /* Select the font based on the Arduino Value */
    fontString = comPortString;

    /* Set the font */
    font=createFont(fontString, 200);
    textFont(font);

    // background(0);   //Undo the comment for a different
effect

    /* Choose a random Earthy colour for the font */
    fill(255, 128, 0);

    /* Display the font on the screen in a random position */
    if (fontString.length() > 5) {
      text(fontString, (1920*0.5)-300, 980*0.5);
      robot.keyPress(KeyEvent.VK_M);
    } else if (fontString.equals("0") == true) {
      text("Left", (1920*0.5), 980*0.5);
      robot.keyPress(KeyEvent.VK_J);
    } else if (fontString.equals("1") == true) {
      text("Right", (1920*0.5), 980*0.5);
      robot.keyPress(KeyEvent.VK_K);
    }
    robot.keyRelease(KeyEvent.VK_M);
    robot.keyRelease(KeyEvent.VK_J);
    robot.keyRelease(KeyEvent.VK_K);
    robot.keyRelease(KeyEvent.VK_L);
  }
}
```